



**HAL**  
open science

## **A monoclonal antibody targeting nonjunctional claudin-1 inhibits fibrosis in patient-derived models by modulating cell plasticity**

Natascha Roehlen, Antonio Saviano, Houssein El Saghire, Emilie Crouchet, Zeina Nehme, Fabio del Zompo, Frank Juehling, Marine Oudot, Sarah C. Durand, François Ht Duong, et al.

### ► To cite this version:

Natascha Roehlen, Antonio Saviano, Houssein El Saghire, Emilie Crouchet, Zeina Nehme, et al.. A monoclonal antibody targeting nonjunctional claudin-1 inhibits fibrosis in patient-derived models by modulating cell plasticity. *Science Translational Medicine*, 2022, 14 (676), 10.1126/scitranslmed.abj4221 . hal-04045641

**HAL Id: hal-04045641**

**<https://hal.science/hal-04045641>**

Submitted on 24 Mar 2023

**HAL** is a multi-disciplinary open access archive for the deposit and dissemination of scientific research documents, whether they are published or not. The documents may come from teaching and research institutions in France or abroad, or from public or private research centers.

L'archive ouverte pluridisciplinaire **HAL**, est destinée au dépôt et à la diffusion de documents scientifiques de niveau recherche, publiés ou non, émanant des établissements d'enseignement et de recherche français ou étrangers, des laboratoires publics ou privés.

1 A monoclonal antibody targeting non-junctional Claudin-1 inhibits fibrosis in  
2 patient-derived models by modulating cell plasticity

3

4 **Authors:** Natascha Roehlen<sup>1†</sup>, Antonio Saviano<sup>1,2†</sup>, Houssein El Saghire<sup>1</sup>, Emilie Crouchet<sup>1</sup>,  
5 Zeina Nehme<sup>1</sup>, Fabio Del Zompo<sup>1</sup>, Frank Jühling<sup>1</sup>, Marine A. Oudot<sup>1</sup>, Sarah C. Durand<sup>1</sup>, François  
6 H.T. Duong<sup>1</sup>, Sara Cherradi<sup>1</sup>, Victor Gonzalez Motos<sup>1</sup>, Nuno Almeida<sup>1</sup>, Clara Ponsolles<sup>1</sup>, Laura  
7 Heydmann<sup>1</sup>, Tessa Ostyn<sup>3</sup>, Antonin Lallement<sup>1,4</sup>, Patrick Pessaux<sup>1,2</sup>, Emanuele Felli<sup>1,2</sup>, Andrea  
8 Cavalli<sup>5</sup>, Jacopo Sgrignani<sup>5</sup>, Christine Thumann<sup>1</sup>, Olga Koutsopoulos<sup>1</sup>, Bryan C. Fuchs<sup>6#</sup>, Yujin  
9 Hoshida<sup>7</sup>, Maike Hofmann<sup>8</sup>, Mogens Vyberg<sup>9</sup>, Birgitte Martine Viuff<sup>10</sup>, Elisabeth D. Galsgaard<sup>10</sup>,  
10 Greg Elson<sup>11</sup>, Alberto Toso<sup>11</sup>, Markus Meyer<sup>11</sup>, Roberto Iacone<sup>11</sup>, Tamas Schweighoffer<sup>11</sup>,  
11 Geoffrey Teixeira<sup>11</sup>, Solange Moll<sup>12</sup>, Claudio De Vito<sup>12</sup>, Tania Roskams<sup>3</sup>, Irwin Davidson<sup>4</sup>,  
12 Danijela Heide<sup>13</sup>, Mathias Heikenwälder<sup>13</sup>, Mirjam B. Zeisel<sup>1§</sup>, Joachim Lupberger<sup>1</sup>, Laurent  
13 Maily<sup>1</sup>, Catherine Schuster<sup>1</sup>, Thomas F. Baumert<sup>1,2,15\*</sup>

14

15 **Affiliations:**

16 <sup>1</sup>Université de Strasbourg, Inserm, Institut de Recherche sur les Maladies Virales et Hépatiques  
17 UMR-S1110, 67000 Strasbourg, France.

18 <sup>2</sup>Service d'hépatogastroentérologie, Hôpitaux Universitaires de Strasbourg, 67000 Strasbourg,  
19 France.

20 <sup>3</sup>Department of Imaging and Pathology, University of Leuven, 3000 Leuven, Belgium.

21 <sup>4</sup>Department of Functional Genomics and Cancer, Institut de Génétique et de Biologie Moléculaire  
22 et Cellulaire, CNRS/INSERM/UNISTRA, 67400 Illkirch Cedex, France.

23 <sup>5</sup>Institute for Research in Biomedicine, Università della Svizzera Italiana, 6500 Bellinzona,  
24 Switzerland.

25 <sup>6</sup>Division of Gastrointestinal and Oncologic Surgery, Massachusetts General Hospital Cancer  
26 Center, Harvard Medical School, Boston, MA 02215, USA.

27 <sup>7</sup>Liver Tumor Translational Research Program, Harold C. Simmons Comprehensive Cancer  
28 Center, Division of Digestive and Liver Diseases, University of Texas Southwestern Medical  
29 Center, Dallas, TX 75390, USA.

30 <sup>8</sup>Department of Medicine II (Gastroenterology, Hepatology, Endocrinology and Infectious  
31 Diseases), Freiburg University Medical Center, Faculty of Medicine, University of Freiburg,  
32 79106 Freiburg, Germany.

33 <sup>9</sup>Center of RNA Medicine, Department of Clinical Medicine, Aalborg University Copenhagen,  
34 2450 København, Denmark, and Department of Pathology, Copenhagen University Hospital  
35 Hvidovre, 2650 Hvidovre, Denmark.

36 <sup>10</sup>Novo Nordisk A/S, 2760 Måløv, Denmark.

37 <sup>11</sup>Alentis Therapeutics, 4123 Allschwil, Switzerland.

38 <sup>12</sup>Department of Pathology, University Hospital of Geneva, 1205 Geneva, Switzerland.

39 <sup>13</sup>Division of Chronic Inflammation and Cancer, German Cancer Research Center, 69120  
40 Heidelberg, Germany.

41 <sup>14</sup>Institut Universitaire de France, 75006 Paris, France.

42 † These authors contributed equally to this work and share first authorship.

43

44 #Present address: Ferring Research Institute 4245 Sorrento Valley Boulevard San Diego, CA  
45 92121, USA.

46 §Present address: Cancer Research Center of Lyon (CRCL), UMR Inserm 1052 CNRS 5286 Mixte  
47 CLB, Université de Lyon 1 (UCBL1), 69008 Lyon, France.

48

49 \*Corresponding author. E-mail: thomas.baumert@unistra.fr.

50

51 Overline: FIBROSIS

52 **One Sentence Summary:** Claudin-1 is a mediator of and therapeutic target for organ  
53 fibrosis.

54

55

56 **Abstract:** Tissue fibrosis is a key driver of end-stage organ failure and cancer, overall accounting  
57 for up to 45% of deaths in developed countries. There is a large unmet medical need for anti-  
58 fibrotic therapies. Claudin-1 (CLDN1) is a member of the tight junction protein family. Although  
59 the role of CLDN1 incorporated in tight junctions is well established, the function of non-  
60 junctional CLDN1 (njCLDN1) is largely unknown. Using highly specific monoclonal antibodies  
61 targeting a conformation-dependent epitope of exposed njCLDN1, we show in patient-derived  
62 liver 3D fibrosis and human liver chimeric mouse models that CLDN1 is a previously unknown  
63 mediator and target for liver fibrosis. Targeting CLDN1 reverted inflammation-induced hepatocyte  
64 pro-fibrogenic signaling and cell fate and suppressed the myofibroblast differentiation of hepatic  
65 stellate cells. Safety studies of a fully humanized antibody in non-human primates did not reveal  
66 any serious adverse events even at high steady-state concentrations. Our results provide preclinical  
67 proof-of-concept for CLDN1-specific mAbs for treatment of advanced liver fibrosis and cancer  
68 prevention. Antifibrotic effects in lung and kidney fibrosis models further indicate a role of  
69 CLDN1 as a therapeutic target for tissue fibrosis across organs. In conclusion, our data pave the  
70 way for further therapeutic exploration of CLDN1-targeting therapies for fibrotic diseases in  
71 patients.

72

73

74 **INTRODUCTION**

75 Organ fibrosis is the result of excessive accumulation of extracellular matrix (ECM) that  
76 results from a wound healing response to repeated and chronic tissue injury. Organ fibrosis  
77 accounts for up to 45% of deaths in developed countries(1) and is a major risk factor for tumor  
78 development. Yet, approved therapies that aim to treat fibrosis are either absent, as for the liver,  
79 or show limited efficacy and safety as for the lung(2-4). Importantly, several key features and  
80 cellular drivers appear to be similar across different organs suggesting common pathways in the  
81 development of end-stage organ fibrosis(1).

82 The major causes of liver fibrosis are chronic hepatitis B (HBV) and C (HCV), alcoholic  
83 liver disease (ALD) and non-alcoholic steatohepatitis (NASH). Hepatocellular carcinoma (HCC)  
84 nearly always arises in the context of advanced liver fibrosis. Thus, direct anti-fibrotic agents are  
85 urgently needed to improve patient survival and outcome in advanced fibrosis by preventing liver  
86 disease progression, cancer risk and mortality(2).

87 Claudin-1 (CLDN1) is a member of the tight junction protein family(5) which is expressed  
88 in a junctional and non-junctional (nj) form. In the liver, njCLDN1 serves as a cell entry factor of  
89 HCV(5, 6), a major cause of liver fibrosis and cancer. Previous studies demonstrated that CLDN1  
90 expression is upregulated in liver cirrhosis and HCC(7). Furthermore, CLDN1 overexpression  
91 induces epithelial-mesenchymal transition in liver cells(8), a pathogenic mechanism implicated in  
92 fibrosis and cancer.

93 Although its function within tight junctions for cell-cell-adhesion is well established, the  
94 role of njCLDN1 in disease biology and as a therapeutic target is largely unknown. We have  
95 previously developed monoclonal antibodies (mAbs) targeting the extracellular loop 1 of CLDN1  
96 expressed on the hepatocyte basolateral membrane outside the tight junctions which potently

97 inhibit HCV cell entry into hepatocytes. Using a panel of mAbs targeting the ECL1 of CLDN1  
98 combined with patient-derived models, we investigated the role of CLDN1 as a mediator and target  
99 for liver fibrosis.

100

101 **RESULTS**

102 **CLDN1 expression is associated with liver fibrosis and disease progression**

103 We first analyzed *CLDN1* gene expression in liver tissues of patients with chronic liver  
104 disease (HBV, HCV, or NASH) in several independent cohorts from Gene Expression Omnibus  
105 (GEO) and in a NASH cohort from the University of Strasbourg (table S1). *CLDN1* is upregulated  
106 in liver tissue of patients with liver disease of all major etiologies (**Fig. 1A**). *CLDN1* expression is  
107 associated with fibrotic disease progression in patients with NASH and HCV-infected individuals  
108 post transplantation(12) (**Fig. 1B**). Corroborating a pathogenetic role of CLDN1 for liver fibrosis,  
109 *CLDN1* is the most highly expressed *CLDN* family member in fibrotic liver (fig. S1A) and the  
110 only family member significantly upregulated in fibrosis (fig. S1B,  $p < 0.0001$ ).

111 We next investigated *CLDN1* expression in the liver at the single-cell level. Comprehensive  
112 expression studies including analysis of single cell (sc) and single nucleus (sn) RNA-seq data (**Fig.**  
113 **1C-E**, fig. S2A-D) showed that *CLDN1* was highly expressed by hepatocytes and cholangiocytes  
114 ( $p < 0.0001$ , U-test, respectively) with increasing expression towards liver bipotent progenitor  
115 cells(17) (**Fig. 1D**).

116 Within the liver microenvironment, activated hepatic stellate cells (aHSCs)/human liver  
117 myofibroblasts (HLMFs) robustly expressed *CLDN1* (**Fig. 1C**, fig. S2C). In contrast, *CDLNI*  
118 abundance in liver endothelial cells, monocytes/macrophages and lymphocytes appeared low or  
119 absent (**Fig. 1C, E**, fig. S2A-E). *CLDN1* expression in hepatocytes, cholangiocytes, progenitor  
120 cells and fibroblasts was confirmed at the protein level by in situ hybridization (ISH),  
121 immunohistochemistry (IHC) and double color immunofluorescence (**Fig. 1F-H** and fig. S2E).

122 In the fibrotic liver, scRNA analyses revealed that *CLDN1* was differentially expressed in  
123 a subpopulation of diseased hepatocytes at the epithelial-stromal interface (**Fig. 1E-F**) and



124 correlated with grade of de-differentiation towards a progenitor or bile-duct like cell type(16)  
125 ( $p=3.75 \times 10^{-8}$ , fig. S2F). Within the mesenchymal cell compartment in fibrotic liver, *CLDN1* was  
126 highly expressed by mesothelial cells ( $p<0.0001$ , U-test, GSE136103, **Fig. 1E** and S2G) that have  
127 previously been described as fibrosis-associated fibroblast progenitor cells(18, 19) (fig. S2H).  
128 Taken together, our studies show that *CLDN1* is robustly expressed in hepatocytes, liver progenitor  
129 cells, cholangiocytes, mesenchymal cells including aHSCs/HLMFs and mesothelial cells. The up-  
130 regulation of *CLDN1* expression in fibrotic liver and its association with disease progression  
131 among different etiologies suggests a functional role in liver fibrosis.

132 To study the expression of njCLDN1 protein in human healthy and fibrotic liver, we used  
133 our well characterized panel of humanized CLDN1-specific antibodies specifically targeting a  
134 conformation-dependent epitope in the EL1 of CLDN1(9-11). Structural modeling revealed that  
135 this epitope is only accessible outside tight junctions (**Fig. 1I**). A subsequent genome-wide protein  
136 array demonstrated that these antibodies selectively bound CLDN1 without any cross-reactivity  
137 (fig. S3). Non-fibrotic or healthy liver tissues showed low or non-detectable njCLDN1 expression.  
138 In contrast, njCLDN1 was specifically upregulated in advanced fibrosis compared to total CLDN1  
139 detected by an antibody targeting the intracellular CLDN1 C-terminal domain (**Fig. 1J**). Consistent  
140 with scRNASeq analyses (**Fig. 1E-F**), CLDN1 upregulation in cirrhosis was associated with  
141 epithelial cellular adhesion molecule (EPCAM) expression, corroborating a role of non-junctional  
142 CLDN1 for hepatocyte-cholangiocyte plasticity that is frequently observable as ductular  
143 reaction(20) (**Fig. 1K**). Immunofluorescence and confocal microscopy of aHSCs/HLMFs isolated  
144 from patients with non-alcoholic fatty liver disease (NAFLD) validated the presence of  
145 homogenous membranous CLDN1 expression in these stromal cells (fig. S4A-B).

146 We next aimed to elucidate drivers of *CLDN1* upregulation in chronic liver disease. TNF-  
147  $\alpha$ -NF $\kappa$ B signaling is a key pathway upregulated in chronic inflammatory liver tissue, liver  
148 fibrogenesis and carcinogenesis(2). Treatment of aHSCs with TNF- $\alpha$  significantly enhanced  
149 *CLDN1* expression (**Fig. 1L**,  $p < 0.0001$ ). A similar upregulation was observed in TNF- $\alpha$ -treated  
150 primary human hepatocytes, albeit to a lower magnitude (**Fig. 1L**). TNF- $\alpha$ -mediated upregulation  
151 was reduced after pharmacological inhibition of NF $\kappa$ B signaling in both aHSCs and primary  
152 human hepatocytes (**Fig. 1L**). To determine whether TNF- $\alpha$  treatment directly induced *CLDN1*  
153 expression via recruitment of NF $\kappa$ B to the *CLDN1* locus, we performed CUT&Tag and ChIP-seq  
154 using antibodies against the p65 subunit of NF $\kappa$ B in LX2 stellate cells with or without 24 hours  
155 treatment with TNF- $\alpha$ . Two previously defined ENCODE cis-regulatory elements upstream and  
156 downstream of *CLDN1* showed robust TNF- $\alpha$ -dependent p65 recruitment (**Fig. 1M**). These sites,  
157 previously identified as bound by NF $\kappa$ B in the ReMAP2022 data set, were validated by ChIP-seq  
158 and CUT&Tag (**Fig. 1M**). These data show that *CLDN1* is a direct target gene of TNF- $\alpha$ -NF $\kappa$ B  
159 pathway. Collectively, these results suggest TNF- $\alpha$ -NF $\kappa$ B signaling drives *CLDN1* upregulation  
160 in chronic inflammatory liver disease.

161

### 162 **In vivo knockdown of CLDN1 using GalNAc siRNA technology reduces liver fibrosis**

163 We next assessed the effect of in vivo CLDN1 knockdown in a patient-derived human liver  
164 chimeric mouse model that expresses human CLDN1 and closely recapitulates key features of  
165 clinical liver fibrosis based on *Fah<sup>-/-</sup>/Rag2<sup>-/-</sup>/Il2rg<sup>-/-</sup> (FRG)-NOD* mice robustly repopulated  
166 with primary human hepatocytes (21). To model NASH-induced advanced fibrosis, we applied a  
167 well-established long-term choline-deficient, L-amino acid-defined, high fat diet (CDA-HFD)(22)  
168 (**Fig. 2A**). For hepatocyte-specific *in vivo* knockdown of human CLDN1 we designed *CLDN1*

169 specific siRNAs covalently linked to a ligand containing three *N*-acetylgalactosamine (GalNAc)  
170 residues(23). After 12 weeks of diet, mice were randomized to 2 groups receiving either siRNA  
171 targeting *CLDN1* or control siRNA at 3mg/kg/week for 8 weeks. GalNAc siRNAs reduced  
172 *CLDN1* protein expression in Huh7 liver cells and in vivo (fig. S5A, fig. S2B, C). Mice treated  
173 with *CLDN1*-targeting GalNAc siRNA showed significantly reduced fibrosis compared to mice  
174 treated with GalNAc control siRNA (**Fig. 2B, C**, table S2, p=0.045). Moreover, mice in the *CLDN1*  
175 knockdown group developed significantly fewer liver nodules (**Fig. 2B, C**, table S2, p=0.044).  
176 Taken together, these data suggest that *CLDN1* plays a functional role in diet-induced liver  
177 fibrosis.

178

### 179 **Targeting non-junctional *CLDN1* reduces fibrosis in a human liver chimeric mouse model**

180 We next evaluated the therapeutic effect of the humanized anti-human *CLDN1* mAb H3L3  
181 in the humanized mouse model of NASH-associated liver fibrosis (21). After 16 weeks of CDA-  
182 HFD diet, mice were randomized to 2 groups and received a weekly intraperitoneal (i.p.) injection  
183 of either the humanized *CLDN1* mAb or an equivalent vehicle control for 8 weeks (**Fig. 2D**) while  
184 the diet was continued. Sirius red staining and fibronectin-1 (FN1) staining analysis revealed  
185 reduced liver fibrosis in independently performed studies (**Fig. 2E-H**, table S3). The anti-fibrotic  
186 effects were independent from the degree of human engraftment as shown by an absent correlation  
187 between human albumin (quantifying the humanization extent of the mice(21)) and fibrosis (fig.  
188 S5B). Humanized mice treated with *CLDN1* mAb H3L3 showed downregulated hepatic gene  
189 expression of fibrosis markers, including tissue metalloproteinase inhibitor 1 (*Timp1*) and collagen  
190 type I alpha 1 chain (*Colla1*) (**Fig. 2H**). Last, *CLDN1* mAb-treated mice exhibited strongly

191 reduced plasma concentrations of C-reactive protein (CRP), a secreted inflammatory biomarker  
192 (fig. S5C).

193         Macroscopic examination of humanized livers revealed significantly reduced liver nodules  
194 in CLDN1 mAb-treated mice in both experiments (**Fig. 2G-H**, fig. S6 and table S3,  $p < 0.05$  and  
195  $p = 0.009$  respectively in experiments 1 and 2). Detailed histopathology analyses revealed that the  
196 expansive nodules consisted of nodular growing mouse hepatocytes, reactive ductules, and human  
197 hepatocytes (fig. S6). Improvement of liver disease was associated with a marked effect on the  
198 expression of a clinical prognostic liver signature (PLS) predicting liver disease progression,  
199 outcome, and survival in patients with chronic liver disease including NASH(25). mAb treatment  
200 significantly reverted the poor-prognosis status of the PLS in the livers of humanized mice (fig.  
201 S5D).

202

### 203 **A CLDN1-specific mAb reduces fibrosis and hepatocarcinogenesis in a mouse model of** 204 **NASH fibrosis and HCC**

205         To further validate anti-fibrotic and cancer-preventive effects of targeting CLDN1 in a fully  
206 immunocompetent mouse model, we engineered a murinized version of our previously established  
207 rat anti-human CLDN1 mAb(9). Despite lower affinity of these antibodies to mouse CLDN1  
208 compared to the human one(10), the murinized CLDN1 mAb showed satisfactory target-  
209 engagement (fig. S7A-G).

210         In addition to CDA-HFD to induce NASH and fibrosis, we injected one dose of  
211 diethylnitrosamine (DEN) to accelerate hepatocarcinogenesis(22). At week 9, the mice were  
212 randomized in 2 groups and received a weekly i.p. injection of either the murinized CLDN1 mAb  
213 or an equivalent vehicle control for 16 weeks (**Fig. 3A**). Two mice in the control group died during

214 the experiment of unknown causes; no deaths occurred in the CLDN1 mAb-treated mice. Sirius  
215 red staining and automated analysis of the collagen proportional area revealed significantly  
216 reduced fibrosis in the CLDN1 mAb group with a relative median fibrosis improvement of 28.4%  
217 (**Fig. 3B-C**, table S4, p=0.003). Furthermore, CLDN1 mAb-treated mice showed significantly  
218 reduced abundance of FN1 (**Fig. 3B-C**, p=0.01) and *Colla1* (**Fig. 3D**, p=0.004), two major  
219 components of the fibrotic ECM(2). Reduced expression of *Acta2* and  $\alpha$ -smooth muscle actin ( $\alpha$ -  
220 SMA) in a subset of the treated mice (**Fig. 3D**, fig. S8A-B) suggested reduced prevalence or  
221 activity of HLMFs.

222 We observed a significant improvement of liver steatosis and NAFLD activity score in  
223 CLDN1 mAb-treated animals (**Fig. 3E**, fig. S8A, respectively p=0.047 and p=0.0098). Similarly,  
224 administration of the mAb was accompanied by a significant reduction of ALT concentrations  
225 (p=0.033) whereas total bilirubin and alkaline phosphatase concentrations remained unchanged  
226 (table S5). Staining for immune cell subpopulations revealed a moderately reduced infiltration of  
227 CD4<sup>+</sup> T cells with no changes in the other main immune cell types in CLDN1 mAb-treated mice  
228 (**Fig. 3F** and fig. S8C-D). In situ hybridization in paraffin-embedded tissues of inflammatory  
229 cytokines demonstrated a reduction of *Ccl2* (fig. S8E), a cytokine involved in liver inflammation  
230 and fibrosis and recruitment of circulating monocytes(24). In contrast, there was no effect on in  
231 situ expression of *Ccl20* and *Cxcl10*.

232 Similarly to the humanized mouse model, we observed a robust reversion of the poor  
233 prognosis status of the clinical PLS which predicts survival, fibrosis progression and HCC risk in  
234 patients with chronic liver disease (fig. S8F). Macroscopic and microscopic examination of mouse  
235 livers showed a marked difference in liver tumor development and burden (**Fig. 3G-I**, table S4).  
236 Histopathological analyses revealed that the tumor nodules consisted of preneoplastic lesions or

237 well-differentiated HCC (fig. S9), confirming the validity of this model for HCC prevention  
238 studies as well as a robust inhibition of hepatocarcinogenesis by the antibody. Extensive safety  
239 studies including histopathology of major organs, complete serum chemistry, and renal and liver  
240 function tests did not show any detectable adverse effects (fig. S10, table S5).

241

### 242 **Treatment with CLDN1-specific mAb inhibits fibrosis progression in a mouse model of** 243 **biliary fibrosis**

244 To validate the anti-fibrotic efficacy of the CLDN1 mAb in another mouse model of  
245 fibrosis, we assessed the effects of CLDN1 mAb in the 3,5-diethoxycarbonyl-1,4-dihydrocollidine  
246 (DDC) model, a widely accepted animal model for biliary fibrosis modeling obstructive cholestasis  
247 and fibrosis(27). Seven-week-old C57BL/6J were fed a 0.1% DDC-supplemented diet and after 1  
248 week, when peri-biliary fibrosis was established, they were randomized into groups receiving  
249 weekly i.p. injection of CLDN1 mAb or vehicle control for 3 weeks (**Fig. 3J**). Sirius red staining  
250 and automated analysis of collagen proportional area revealed significantly reduced fibrosis and  
251 total FN1 (**Fig. 3L-K**, table S6, respectively  $p < 0.0001$  and  $p = 0.001$ ) as well as reduced Ishak score  
252 (**Fig. 3M**, table S6).

253

### 254 **Validation of the profibrogenic role of CLDN1 in patient-derived 3D liver fibrosis and NASH** 255 **models**

256 We next validated the antifibrotic effects of the CLDN1 mAb in patient-derived *ex vivo*  
257 models. The 3D ExVivo Human Liver Tissue model (Organovo) mimics distinct features of NASH  
258 and fibrosis and allows the assessment of liver disease therapeutics(28) (**Fig. 4A**). In this human  
259 NASH model, mAb treatment reduced hepatocyte ballooning and macro- and micro-steatosis in

260 three out of four tissue preparations (**Fig. 4B**). Image-based quantification of the collagen  
261 proportional area revealed that median fibrosis in CLDN1 mAb-treated ExVivo tissues was  
262 significantly reduced compared to control mAb-treated tissues (2.69% vs. 6.14%, **Fig. 4C**,  
263  $p < 0.0001$ ).

264 We studied effects of CLDN1 on fibrosis in patient-derived human liver spheroids, 3D  
265 micro-tissues recapitulating the liver microenvironment(29). Liver tissues from patients with and  
266 without chronic liver disease and fibrosis (table S7) were dissociated and cultured in ultra-low  
267 attachment plates (**Fig. 4D**). This protocol allows the formation of patient-derived spheroids  
268 harboring original liver cell populations (**Fig. 4E**). Treatment with a profibrogenic medium  
269 containing transforming growth factor beta (TGF- $\beta$ ), free fatty acids (FFA) and  
270 lipopolysaccharides (LPS) induced the expression of *COL1A1*, *COL3A1*, *COL4A1*, and *CTGF*  
271 (**Fig. 4F**). Treatment of patient spheroids with CLDN1 mAb reduced the induction of these pro-  
272 fibrogenic markers (**Fig. 4F**). Moreover, CLDN1 mAb treatment decreased collagen deposition  
273 compared to resmetirom, a NASH compound having reached late-stage clinical development (30)  
274 (**Fig. 4G**).

275 Last, we aimed to validate the effect of CLDN1 on the PLS predicting liver disease  
276 progression, survival and HCC risk in liver tissues from patients with advanced fibrosis(31). Liver  
277 slices of NASH patients with NASH with different stages of fibrosis (table S8) were incubated  
278 with CLDN1 mAb or control and analyzed for expression of the clinical PLS (**Fig. 4H**). Treatment  
279 with CLDN1 mAb significantly reverted the PLS from poor to good prognosis for samples of  
280 patients #1-4 (NASH fibrosis #1-#5, poor prognosis genes: false discovery rate (FDR) = 0.16,  
281 0.16, 0.09, 0.17 and 0.28, respectively; good prognosis genes: FDR= 0.50, 0.004, 0.09, 0.20, 0.80,  
282 respectively, **Fig. 4I**).

283 **Targeting CLDN1 reverses inflammation-induced perturbation of cell plasticity in**  
284 **hepatocytes, progenitor cells, and myofibroblasts**

285 We next aimed to evaluate the molecular mechanism of the antifibrotic effect of the  
286 CLDN1-specific mAb. Given the association of CLDN1 expression with cell state, we assessed  
287 scRNA-seq-derived cell lineage marker genes in human liver chimeric mice side-by-side with  
288 transcriptomic data derived from a clinical cohort of NASH patients with mild or advanced fibrosis  
289 (**Fig. 5A**). Gene sets encompassing marker genes of the EPCAM<sup>+</sup> progenitor compartment were  
290 significantly enriched in patients with NASH and advanced fibrosis (Cell cluster maker genes C4,  
291 C39, C24, C7: NES=1.99, 2.05, 2.07, 2.19, FDR<0.001), whereas genes characterizing healthy  
292 mature hepatocytes were strongly downregulated (C30, C17, C14, C11: NES=-1.39, -1.71, -2.21,  
293 -2.23, FDR<0.02) (**Fig. 5B**). Similar results were obtained in fibrotic livers derived from two  
294 NASH fibrosis mouse models compared to corresponding regular diet mice (fig. S11A-B).  
295 Treatment with CLDN1 mAb considerably reverted the hepatocyte-progenitor cell plasticity in  
296 both mouse models (**Fig. 5C**, fig. S11C, D) suggesting that CLDN1-specific mAb treatment  
297 reverts the disease-induced immature progenitor phenotype of hepatocytes back to a mature  
298 phenotype.

299 We next examined the effect of CLDN1 on cell plasticity of mesenchymal cells in the DEN-  
300 CDAHFD mouse model. Expression of marker genes of PDGFRA<sup>+</sup> scar-associated myofibroblasts  
301 (table S9, markers from(16)) was induced both in livers of NASH patients with NASH with  
302 advanced fibrosis as well as fibrotic mouse livers (**Fig. 5D**, fig. S11E). CLDN1 mAb treatment  
303 significantly suppressed expression of these scar-associated myofibroblast gene signatures in the  
304 immunocompetent NASH fibrosis mouse model (FDR<0.001, **Fig. 5E**). Similarly, examining cell  
305 circuit modules driving cirrhosis in patients, we found reduced gene expression related to



306 myofibroblast differentiation and ECM production (module 1 and 24) as well as restoration of  
307 physiological hepatocyte metabolism (module 9, 22 and 23) (**Fig. 5F**, upper panel) in mice treated  
308 with CLDN1-specific mAb.

309 Collectively, our integrative analyses in patient liver tissues and patient-derived mouse  
310 models suggest that treatment with CLDN1 mAb reverses fibrosis-associated cell fate and  
311 plasticity in hepatocytes and fibroblasts.

312

### 313 **Targeting CLDN1 reverses perturbation of liver cell circuits and signaling mediating chronic** 314 **inflammation and fibrosis**

315 To unravel the specific cell circuits and signaling pathways involved in liver disease  
316 progression in vivo and restored by mAb treatment, we analyzed transcriptional signatures of  
317 fibrosis- and carcinogenesis-related signaling in the mouse models (fig. S12A). Fibrotic mouse  
318 NASH livers exhibited upregulated fibrosis-associated pathways similar to NASH patients with  
319 NASH with advanced fibrosis (**Fig. 5F**). Treatment with CLDN1 mAb reversed the induction of  
320 these fibrogenic circuits, with the most pronounced effects on TNF- $\alpha$ -NF $\kappa$ B signaling (**Fig. 5F**).  
321 Similarly, carcinogenesis-associated pathways were upregulated in NASH patients with advanced  
322 fibrosis but suppressed by CLDN1 mAb treatment in both animal models (**Fig. 5F**). Similar results  
323 were obtained by unbiased GSEA of hallmark gene sets in both mouse models (fig. S12B). The  
324 suppression of key target pathways such as NF $\kappa$ B (RELA and RELB) and MAPK (p-p38) was  
325 confirmed by immunohistochemistry in the DEN-CDAHFD NASH fibrosis mouse model (**Fig.**  
326 **5G**, fig. S12C-E).

327

328 **CLDN1-specific mAb inhibits pro-fibrotic signaling and modulates cell-matrix interaction**  
329 **and plasticity in hepatocytes**

330 Next, we investigated the specific effects of CLDN1 mAb on signaling and plasticity in the  
331 cell types identified in the expression and binding studies. Using stable CLDN1 knockout (KO)  
332 and pharmacological intervention, we found that CLDN1 is a driver of the poor prognosis status  
333 of the PLS in cell-based models(25) (fig. S13A-C). Reversal of the poor prognosis status was  
334 CLDN1 mAb dose-dependent (fig. S13C). RNA-seq and GSEA further confirmed mAb-mediated  
335 suppression of hepatocyte-progenitor cell plasticity (fig. S13D) as well as pro-fibrogenic and  
336 carcinogenic signaling (fig. S13E) in cell culture models of both viral and metabolic liver disease.

337 To study the molecular events after CLDN1 mAb target engagement, we identified the  
338 molecular partners of CLDN1 at the membrane of epithelial cells using Huh7 cells with high  
339 CLDN1 expression as a tractable model for immature liver epithelial cells. Co-  
340 immunoprecipitation of CLDN1 identified more than 300 proteins as potential CLDN1 interactants  
341 (data file S2). String analysis with clustering revealed 3 clusters of proteins interacting with  
342 CLDN1 (**Fig. 6A**): cell adhesion proteins, integrins and ECM proteins as well as proteins related  
343 to cell proliferation and fate. Epithelial growth factor receptor (EGFR), EPCAM, the ECM  
344 receptor integrin alpha 5 (ITGA5), and ECM component laminin 5 (LAMA5) were confirmed as  
345 molecular partners by Western blot analyses (**Fig. 6B**). Next, we investigated the consequences of  
346 these cell membrane molecular interactions on pro-fibrotic and pro-carcinogenic signaling  
347 mediated by these pathways. CLDN1 mAb treatment suppressed EGFR and extracellular signal-  
348 regulated kinases (ERK) phosphorylation (**Fig. 6C-D**) and inhibited SRC proto-oncogene, non-  
349 receptor tyrosine kinase (SRC) signaling, a key downstream pathway of cell-ECM  
350 mechanoreceptors(32). Plasma membrane isolation showed a decrease of SRC recruitment at the

351 cell membrane after treatment (**Fig. 6E**). Moreover, CLDN1 mAb inhibited SRC activation by  
352 phosphorylation in a 3D Huh7 spheroid model (**Fig. 6F**). Unbiased proteomic assessment of  
353 signaling in a Huh7-LX2 co-culture model using phospho-specific antibody capture arrays  
354 validated CLDN1 mAb-induced suppression of SRC family and MAPK kinase (p38) activation  
355 and revealed downregulation of other known profibrotic and pro-carcinogenic downstream  
356 effectors including CREB5 and TOR(33)(**Fig. 6G**). The effects of CLDN1 mAb on EGFR-MAPK  
357 and ITGA5-SRC signaling were further validated in precision cut liver slices (PCLS) of patient-  
358 derived tissues (fig. S14A) as well as in patient-derived multicellular spheroids exposed to  
359 profibrogenic injury (**Fig. 6H**). Besides SRC and EGFR, we detected reduced kinase activity of  
360 other kinases known to mediate fibrosis progression, such as IGF1R and IKK-E as well as reduced  
361 activity of kinases involved in carcinogenesis, including ARG, ABL, AKT1/2, and HER2 (**Fig.**  
362 **6H**). A comparative analysis with a liver fibrosis kinome atlas suggests that CLDN1 mAb  
363 treatment in patient spheroids reverts the profibrogenic signaling cascade identified in patients  
364 with advanced liver fibrosis (fig. S14B)(34).

365 Collectively, our data indicate that CLDN1 interacts with EPCAM, EGFR, ITGA5,  
366 laminin, and other proteins at the cell membrane of liver epithelial cells. Target engagement of  
367 CLDN1 mAb with cell surface CLDN1 inhibits downstream profibrogenic and pro-carcinogenic  
368 signaling mediating cell plasticity, fibrogenesis, and carcinogenesis (fig. S14C).

369

### 370 **Treatment with CLDN1-specific mAb modulates liver progenitor cell phenotype and** 371 **plasticity**

372 Given the high abundance of CLDN1 expression in liver progenitor cells and  
373 cholangiocytes, effects on liver cell plasticity might also be mediated via direct effects of CLDN1

374 mAb on ductal cells which play a role in fibrotic liver disease(35). The “ductular reaction”, a  
375 regenerative cholangiocyte and liver progenitor cell proliferation, has been reported as a potential  
376 anti-fibrotic target(35). We generated intrahepatic bile duct-derived organoids from human  
377 cirrhotic liver tissue and treated these cells with CLDN1 mAb or control mAb for 4 days. These  
378 organoids showed high expression of CLDN1 and progenitor markers (fig. S15A). CLDN1 mAb  
379 treatment modulated the phenotype of the organoids with an altered morphology, such as thinner  
380 walls and cystic deformation (**Fig. 7A, left panel**). Computational analysis of the organoid size  
381 further confirmed functional effects on organoid growth (**Fig. 7A, right panel**). Transcriptomic  
382 profiling of organoids by RNA-seq revealed pronounced effects of the antibody on liver organoid  
383 gene expression (**Fig. 7B**). Computational assessment indicated enrichment of upregulated genes  
384 into developmental pathways and downregulated genes into proliferative biological processes  
385 (**Fig. 7C**, fig. S15B-C) suggesting functional effects on cell proliferation and plasticity of CLDN1  
386 mAb on progenitor cells and cholangiocytes. Validation of significant downregulation of the  
387 expression of liver progenitor cell marker TACSTD2/TROP2(*15*) in mAb-treated organoids  
388 confirmed the functional effect of treatment on cell plasticity (p=0.04, **Fig. 7D**).

389

### 390 **CLDN1-specific mAb inhibits profibrogenic differentiation in aHSCs by interfering with** 391 **TNF- $\alpha$ -NF $\kappa$ B signaling**

392 We evaluated direct effects of CLDN1 mAb on mesenchymal cells by RNA-seq analysis  
393 of CLDN1 mAb-treated patient-derived aHSCs/HLMFs (**Fig. 7E**). Marker genes of scar-  
394 associated myofibroblasts type A (table S10), the major phenotype of fibrotic  
395 myofibroblasts(*16*), were significantly inhibited in CLDN1-mAb treated HLMFs (FDR<0.08, **Fig.**  
396 **7E**). Moreover, CLDN1 mAb strongly suppressed TNF- $\alpha$ -NF $\kappa$ B signaling in HLMFs as validated

397 by Western Blot analyses of the TNF- $\alpha$  canonical pathway (**Fig. 7F-H**). Assessment of TGF- $\beta$   
398 signaling did not reveal major effects of the antibody on the TGF- $\beta$  canonical SMAD2/3 signaling  
399 pathway, but showed inhibition of TGF- $\beta$  induced non-canonical pathways, such as pAKT, p-P38  
400 and pERK signaling (**Fig. 7H, I**). Last, we confirmed direct downstream effects on myofibroblast  
401 effector functions. Indeed, CLDN1 mAb treatment of HLMFs from different donors (table S12)  
402 markedly inhibited key activation markers, including *ACTA2*, *COL1A1* and *FNI* (**Fig. 7J**).

403

#### 404 **CLDN1 is a candidate target for treatment of lung and kidney fibrosis**

405 The mechanistic role of CLDN1 during fibrosis is not necessarily limited to the liver.  
406 Several studies have suggested a role of CLDN1 in the pathogenesis of chronic kidney disease(37).  
407 Upregulation of *CLDN1* expression in patients with glomerulonephritis as well as murine fibrotic  
408 kidneys(38) (**Fig. 8A**) suggests the involvement of *CLDN1* in the pathogenesis of renal fibrotic  
409 disease. Furthermore, *CLDN1* was significantly overexpressed in patients with idiopathic  
410 pulmonary fibrosis (IPF) with increasing expression along disease progression (p=0.03, **Fig. 8B**).

411 To investigate the role of CLDN1 as a therapeutic target in other organs, we used two state-  
412 of-the-art mouse models for kidney and lung fibrosis (**Fig. 8C**). Treatment with the murinized  
413 CLDN1-specific mAb (fig. S2) resulted in robust anti-fibrotic effects in the unilateral ureteral  
414 obstruction (UUO) mouse model of kidney fibrosis(40) (**Fig. 8D-E**, table S13). Moreover,  
415 histological assessment of mouse kidneys revealed suppression of macrophage infiltration by  
416 CLDN1 mAb (**Fig. 8F**).

417 We studied the effects of CLDN1 mAb in a bleomycin-induced pulmonary fibrosis mouse  
418 model and compared to dexamethasone, an off-label used drug with protective effects in patients

419 with lung fibrosis(3) (**Fig. 8C**). Treatment with CLDN1 mAb suppressed lung fibrosis in these  
420 animals (**Fig. 8G-H**, table S14). Similar to the liver, CLDN1 was expressed and regulated via  
421 TNF- $\alpha$ -NF $\kappa$ B signaling in both lung (**Fig. 8I-J**) and kidney fibroblasts (**Fig. 8J**). In line with the  
422 role of CLDN1 in liver cell fate and differentiation, treatment of IPF patient-derived  
423 myofibroblasts resulted in reversal of pro-fibrogenic lung fibroblast differentiation states(41)  
424 (**Fig. 8K**). CLDN1 mAb strongly suppressed expression of marker genes of ACTA2<sup>+</sup>  
425 myofibroblasts, PLIN2<sup>+</sup> lipomyofibroblasts, and HAS1<sup>hi</sup> fibroblasts (table S15-17). As observed  
426 in HLMFs, CLDN1 mAb-treatment suppressed TNF $\alpha$ -NF $\kappa$ B signaling in primary lung fibroblasts  
427 (**Fig. 8L**). These findings suggest CLDN1 as a candidate target for kidney and lung fibrosis which  
428 warrants further investigation.

429

430 **ALE.F02, an CLDN1 therapeutic candidate antibody for treating human fibrotic diseases, is**  
431 **safe in cynomolgus monkeys**

432 To ensure the safety of CLDN1 mAbs in a species with full human target homology and  
433 equivalent antibody affinity, we expanded toxicity studies to non-human primates (table S18). As  
434 a candidate for future human therapeutic applications, we chose a fully humanized variant which  
435 we designated ALE.F02. Differently from H3L3, the Fc region of the ALE.F02 molecule contains  
436 three mutations (L234F, L235E, and P331S) which have been introduced to reduce binding to Fc  
437 gamma receptors. In cynomolgus monkeys (*M. fascicularis*), the sequence of human CLDN1 and  
438 the antibody's binding epitope is 100% conserved. A rapid escalation protocol achieved safe,  
439 multiple weekly dosing up to the highest tested dose of 150 mg/kg. No major clinical changes were  
440 observed. Notably, there was no indication of NISCH syndrome in the animals, a condition caused  
441 by genetic CLDN1 deficiency in humans. These studies confirmed that CLDN1-targeting therapies

442 are safe *in vivo* and that ALE.F02 did not affect the integrity or barrier function of tight junctions.  
443 Serum analysis indicated a dose-dependent, sustainable and effective antibody concentration in  
444 macaques (fig. S16A). Simulations using the macaque data predicted that PK profiles in humans  
445 with a single dose of ~3-10 mg/kg ALE-F02 would saturate CLDN1 for about 2 weeks (fig. S16B).  
446  
447

448 **DISCUSSION**

449           In this study we uncovered CLDN1 as a mediator and therapeutic target for tissue fibrosis.  
450 Using the liver as a model of chronic inflammation-associated fibrogenesis and carcinogenesis we  
451 show that targeting CLDN1 by highly specific mAbs robustly reduced fibrosis and tumor  
452 development in mouse models for NASH and biliary fibrosis; strongly reduces liver fibrosis in *ex*  
453 *vivo* patient-derived model; and reversed transcriptomic liver disease signatures predictive of liver  
454 fibrosis progression and HCC risk. A key strength of our study is its focus on authentic patient-  
455 derived model systems, the consistency of results across complementary model systems, different  
456 organs and patient cohorts supporting its validity and translatability into the clinic.

457           Our comprehensive analyses provide the following model for the molecular mechanism of  
458 CLDN1 mAb mediated anti-fibrotic effects: hepatocytes and their progenitors are the primary  
459 target cells of CLDN1 mAb antifibrotic effect. Our detailed gene expression analyses *in vivo* and  
460 in patients revealed that mAb treatment restores the hepatocyte fate by suppressing hepatocyte de-  
461 differentiation following epithelial liver injury. Target engagement at the hepatocyte cell  
462 membrane interferes with the interaction of CLDN1 with EPCAM, EGFR, ITGA5 as well as the  
463 ECM, resulting in inhibition of downstream signaling of well-established pro-fibrotic and pro-  
464 carcinogenic signaling pathways across organs, such as SRC and MAPK signaling.

465           The second cell type mediating the anti-fibrotic properties of the mAb are likely  
466 aHSCs/HLMFs which express CLDN1 in patients. CLDN1 mAb inhibits TNF- $\alpha$ -NF $\kappa$ B as well  
467 as non-canonical TGF- $\beta$  signaling resulting in inhibition of myofibroblast activation and  
468 differentiation across organs. Cross-talk between liver epithelial cells and fibroblasts modulate the  
469 ECM with decreased collagen and fibronectin production. The reprogramming of hepatocytes and  
470 its microenvironment ultimately results in the attenuation of tissue fibrosis.



471 Our study has some limitations: First, we can not exclude that other signaling pathways or  
472 additional mechanistic events are at play mediating the anti-fibrotic effect of the antibodies.  
473 Second, while we used a large panel of complementary model systems including patient-derived  
474 models, any model system only partially recapitulates pathogenesis of fibrosis in patients.

475 The large majority of liver disease therapeutics target metabolism, inflammation or cell  
476 death, which are relevant in the early stage of disease(42, 43). A key differentiator of CLDN1-  
477 specific mAb is the combination of robust anti-fibrotic and HCC preventive effect, which  
478 addresses the key unmet medical need in advanced liver fibrosis.

479 Our study also provides the opportunity to develop companion biomarkers such as TIMP1 ,  
480 a clinically applied read-out for liver fibrosis as part of the ELF score, or CTGF, a biomarker  
481 candidate for fibrosis across organs(44, 45). Furthermore, the potent effect on the PLS may enable  
482 to stratify patients at high risk for HCC and the highest need for treatment.

483 Our data demonstrate that the administration of the antibody is safe without detectable  
484 adverse and off-target effects. Safety studies in non-human primates demonstrate that even  
485 repeated high dose administration does not induce any major adverse effects and support further  
486 clinical development in humans.

487 Beyond the liver, our *in vivo* data suggest that CLDN1 is also a candidate target for kidney  
488 and lung fibrosis(3, 4). Our functional studies suggest common mechanisms across organs as  
489 demonstrated by similar inhibition profiles of lung fibroblast differentiation by CLDN1 mAb via  
490 interference with TNF- $\alpha$ -NF $\kappa$ B signaling. However, given the expression of CLDN1 in organ-  
491 specific cell types in the kidney(37) or lung(46), it is likely that also additional organ-specific  
492 mechanisms are at play.

493           Collectively, the development of CLDN1-specific mAb provides an opportunity for the  
494 clinical development of a first-in-class compound for treatment of organ fibrosis, a major and  
495 rapidly growing unmet medical need world-wide.

496

497 **MATERIAL AND METHODS**

498 ***Study design.*** Computational transcriptomic analyses were conducted in publicly available  
499 and own patient cohorts of chronic liver disease. Overall and cell-type specific target expression  
500 was characterized by immunohistochemistry, immunofluorescence and in situ hybridization of  
501 multiple non-fibrotic and fibrotic tissues of different patient cohorts. *In vivo* genetic knockdown  
502 studies using siRNA were performed to validate CLDN1 as a driver of liver fibrosis. NjCLDN1  
503 targeted by highly specific mAbs was evaluated as a target to treat fibrosis in a large set of *in vivo*  
504 and *ex vivo* models. The molecular mechanism of action was studied by co-immunoprecipitation  
505 studies, transcriptomic and proteomic analyses in cell-based models of chronic liver disease,  
506 including patient-derived 3D *ex vivo* models, such as spheroids and liver organoids. Finally, in  
507 preparation for clinical translation, the pharmacological and safety properties of a humanized  
508 CLDN1 antibody was validated in non-human primates. Experiments were partially blinded and  
509 performed in triplicates in at least three independent experiments, unless otherwise stated. Patient  
510 tissues for *ex vivo* and *in vitro* studies were randomly assigned. Additional methods are available  
511 in the supplementary materials.

512 ***Human subjects and patient cohorts.*** For transcriptomic analyses and *ex vivo* perturbation  
513 studies human liver tissue samples were obtained from patients who had undergone liver resections  
514 for HCC, colorectal cancer metastasis, or cholangiocellular carcinoma between 2014 and 2022 at  
515 Strasbourg University Hospitals, France (DC-2016-2616 and RIPH2 LivMod IDRCB 2019-  
516 A00738-49, ClinicalTrial NCT04690972). All patients provided written informed consent and the  
517 protocol followed the ethical principles of the declaration of Helsinki and was approved by the  
518 local independent ethics committees. For CLDN1 expression analysis, liver tissues were obtained  
519 from local biobanks of the Department of Imaging & Pathology, KU Leuven, the University

520 Hospital Geneva, Pathology at Hvidovre University Hospital, Denmark or Indivumed, Hamburg.  
521 Demographic data and clinical characteristics of patients enrolled are summarized in table S1-S2  
522 and S5-S6, respectively. Datasets of clinical cohorts with chronic liver disease (GSE34798,  
523 GSE83148, GSE49541), chronic kidney disease (GSE11585 and GSE60685), IPF (GSE2052,  
524 GSE53845, GSE24206) were selected following comprehensive database analysis, where we  
525 identified CLDN1 as part of the microarray data. GSE34798, GSE83148, GSE49541, GSE34798,  
526 GSE115857, GSE53845 and GSE24206 were analysed using *shinyGEO*(47) with expression  
527 values shown as log<sub>2</sub> expression. All other microarray data were analysed using signal intensity  
528 values. Liver scRNA-seq data (GSE124395 and GSE136103) and snRNA-seq data (GSE185477)  
529 were obtained as Seurat objects and investigated.

530 ***Bioinformatic and statistical analyses.*** Human RNA-seq data was mapped using HISAT2  
531 to the human genome hg19. Mouse RNA-seq data was mapped to the mouse genome mm10 and  
532 annotated using the Gencode vM15 gene annotation. Data from humanized mice were mapped  
533 similarly, but to an artificial genome consisting of all human (hg19) and mouse (mm10)  
534 chromosomes, and only reads mapping to human chromosomes were kept for further analysis as  
535 described(48). Reads were counted with htseq-count, and a differentially expression analysis was  
536 performed with DESeq2 applying GENCODE 19. Gene Set Enrichment Analysis (GSEA) was  
537 used for unbiased pathway analysis using Molecular Signature Database (MSigDB)(49). Unbiased  
538 assessment of HALLMARK(49), gene ontology and curated gene sets(49) were used for primary  
539 screening of clinically relevant signaling pathways and cell circuits in NASH liver tissue  
540 microarray data (GSE49541), that were then subsequently analyzed in RNA-seq data of our NASH  
541 mouse models. HALLMARK pathways were further analysed in an unbiased way in RNA-seq  
542 data from two NASH mouse models. GSEA of hepatocyte and EPCAM<sup>+</sup> bile duct cell signature

543 gene sets (C8, MSigDB, derived from scRNA-seq studies in human liver(15)) were used for  
544 evaluation of hepatocyte cell fate. Results from GSEA were adjusted for the false discovery rate  
545 (FDR). FDR<0.25 or FDR<0.05 was considered statistically significant. All other data was  
546 compared using Student's t-test when normally distributed (Shapiro-Wilk test) or non-parametric  
547 tests (U-test, Kruskal-Wallis test) when non-normally distributed. Functional results in patient-  
548 derived cells were compared using Wilcoxon matched paired test. P <0.05 and FDR<0.25 were  
549 considered statistically significant.

550

551

552

553

554

555 **ACKNOWLEDGMENTS**

556           The authors acknowledge the proteomics platform of IGBMC, where mass spectrometry  
557 analysis was performed supported by an ARC foundation grant (Orbitrap) and a Canceropôle  
558 Grand Est foundation grant. The authors thank the CRB (Centre de Ressources Biologiques-  
559 Biological Resource Centre) of the Strasbourg University Hospitals for the management of patient-  
560 derived liver tissue. The authors thank Dr. R. Bartenschlager (University of Heidelberg, Germany),  
561 Dr. C. Rice (Rockefeller University, New York, NY) for providing plasmids for production of  
562 HCVcc Jc1 strains, Dr. M. Evans (Mount Sinai Hospital, New York, NY) for providing mouse  
563 and human CLDN1 expression plasmids, Dr. F. Chisari (The Scripps Research Institute, La Jolla,  
564 CA) for the gift of Huh7.5.1 cells, Prof. G. Christofori (University of Basel) for the gift of Huh7  
565 cell line, Dr. S. Friedman (Mount Sinai Hospital, New York) for the gift of the LX2 stellate cell  
566 line, Dr. F. Habersetzer (Strasbourg University Hospitals) for patient serum samples for isolation  
567 of infectious HBV and Dr. D. Root (Broad Institute of MIT and Harvard, Cambridge, MA) for  
568 providing expression plasmids for lentiviruses and sgRNAs for CLDN1 KO. We thank Marie  
569 Parnot (Inserm U1110, University of Strasbourg) for help with proteomic studies, Miriam  
570 Fernandez-Vaquero and Jenny Hetzer (German Cancer Research Center, Heidelberg, Germany) for  
571 help in histopathology staining, Thomas Cagarelli (Dept. of Pathology, University of Geneva) and  
572 Dr. H. Jacobs (ICS Mouse Clinic, IGBMC, Illkirch) for histopathology analyses of part of the  
573 animal and human tissues, Prof. A. Schmitt-Graeff (Dept. of Pathology, University Hospital  
574 Freiburg), Prof. Antje Prasse (Hannover Medical School) for advice in histopathology analyses  
575 of liver and lung tissues, Mikhail Gromak (Department of Medicine II, University Freiburg) for  
576 the contribution to organoid studies, Dr. Meritxell Huch (Max Planck Institute, Dresden) for  
577 critical input in analysis of organoid studies and Dr. Lynda Audjehane (Human HepCell, Faculté

578 de Médecine Pierre et Marie Curie, Site Saint-Antoine, Paris, France) for providing human  
579 myofibroblasts for pilot staining experiments in the initial phase of the study.

580

## 581 **FUNDING**

582 Funding was obtained from the following grants: European Union ERC-AdG-2014 *HEPCIR*  
583 *#671231* (T.F.B.), European Union ERC-AdG-2020 *FIBCAN #101021417* (T.F.B.) ,European  
584 Union ERC-PoC-2016 *PRELICAN #7555460* (T.F.B.), European Union ERC-PoC-2018  
585 *HEPCAN #862551* (T.F.B.), European Union ERC Consolidator grant *HepatoMetabopath*  
586 *#683000* (M.H.), European Union H2020 *HEPCAR #667273* (T.F.B. and M.H.), Fondation ARC  
587 [www.fondation-arc.org](http://www.fondation-arc.org) *TheraHCC2.0 IHU201901299* (T.F.B.), ANRS Grant *ECTZ103701*  
588 *CLAUDIN-1* (T.F.B.), SATT Conectus, University of Strasbourg (CANCLAU) (T.F.B.), French  
589 National Research Agency LABEX ANR-10-LABX-0028\_ *HEPSYS* (T.F.B.), German Research  
590 Foundation (DFG) RO 5983/1-1 (N.R.), C1 KU Leuven grant (C14/20/097) (T.R.), DFG-SFB-  
591 1479 OncoEscape (TP 10) to M.H., RHU DELIVER ANR-21-RHUS-0001 (T. F. B.), Minor  
592 operating expenses were covered by Norvo Nordisk A/S.

593

594

595 **AUTHOR CONTRIBUTIONS**

596 T.F.B. initiated and coordinated the study. H.E.S., N.R., A.S., E.C., L.M., C.T, V.G.M.,  
597 M.A.O., S.C., F.H.T.D., Z.N., N.A., C.P., L.H., S.C.D, M.H., A.L., F.D.Z. C.S., J.L., M.B.Z. and  
598 T.F.B. designed or performed experiments and analyzed data. A.S., D.H. and S.C.D. analyzed  
599 histopathology of mouse liver tissue. G.T. designed CLDN1 expression analyses and functional  
600 studies. Z.N., A.L., F.J. and I.D. performed or analyzed epigenetic experiments. S.M., T.O., T.R.,  
601 M.V., C.D.V., E.D.G. and B.M.V performed CLDN1 expression analyses by IHC, IF or ISH in  
602 human or mouse liver tissue. Y.H. analyzed gene expression of the prognostic liver signature in  
603 part of the cell lines. F.J., H.E.S. and N.R. performed computational analyses, E.F. and P.P.  
604 prepared liver resections for *ex vivo* models. B.C.F., M.H. and A.T. co-designed animal  
605 experiments and edited the manuscript. A.C. and J.S. performed structural modeling of CLDN1  
606 mAb binding to CLDN1. G.E., M.M., R.I., T.S. designed and conducted the experiments in non-  
607 human primates. G.T. helped generate figures. M.B.Z, C.S., J.L. and O.K. edited the manuscript.  
608 N.R., H.E.S., E.C., A.S. and T.F.B. designed the figures and wrote the manuscript.

609

610 **COMPETING INTERESTS**

611 Inserm, the University of Strasbourg, the Strasbourg University Hospitals and the Institut  
612 Hospitalo-Universitaire have filed patents and patent applications: US62/153,727 (Clinical gene  
613 signature-based human cell culture model and uses thereof; inventors T.F.B., Y.H.), US13/119,233  
614 (Anti-Claudin-1 antibodies for the inhibition of hepatitis C virus infection; C. S., T. F. B.);  
615 US15/979,609 PCT/EP2016/055942 (Anti-Claudin-1 monoclonal antibodies for the prevention  
616 and treatment of HCC; T. F. B., M.B.Z); US16/086,934 PCT/EP2017/056703 (Humanized anti-  
617 Claudin 1 antibodies and uses thereof; T. F. B.) and PCT/EP2020/081941 (Anti-Claudin 1



618 monoclonal antibodies for the prevention and treatment of fibrotic disease; T. F. B., E. C., N. R.,  
619 A. S., R. I., M. M., T. S.), which have all been licensed to Alentis Therapeutics, Basel. G. E., M.  
620 M., A. T., G. T., R. I, T. S., T. F. B, C. S, Y. H. own shares of Alentis. G. E., M. M., A. T., G. T.,  
621 R. I are employees of Alentis, T. F. B. serves as a consultant for Alentis. T. S. was an employee  
622 of Alentis. B.M.V is an employee and minor stock holder of Novo Nordisk. B.C.F is an employee  
623 of Ferring Pharmaceuticals and serves on the Scientific Advisory Board of Mediar Therapeutics.  
624 Any potential conflict of interest is managed independently by the SATT Conectus and Inserm  
625 Transfert for the authors of the University of Strasbourg and Inserm.

626

#### 627 **DATA AND MATERIALS AVAILIBILITY**

628 All data associated with this study are available in the main text or the supplementary  
629 materials. Raw data from figures are in data file S1. Transcriptomic data reported in this paper  
630 have been deposited at the Gene Expression Omnibus database (GEO) with accession numbers  
631 GSE174542, GSE174543, and GSE206581. FRG mice are available under a material transfer  
632 agreement with Yecuris. Recombinant HCV strains and Huh7.5 cell lines for infection studies are  
633 available under a material transfer agreement with Apath LLC.

634

635 **SUPPLEMENTARY MATERIAL**

636 • **Materials and Methods**

637 • **Figure S1-S19**

638 • **Table S1-S18**

639 • **Data File S1-S2**

640 • **References (51-91)**

641

642

643 **REFERENCES and notes**

- 644 1. D. C. Rockey, P. D. Bell, J. A. Hill, Fibrosis--a common pathway to organ injury and  
645 failure. *N Engl J Med* **372** (12), 1138-1149 (2015).
- 646 2. N. Roehlen, E. Crouchet, T. F. Baumert, Liver Fibrosis: Mechanistic Concepts and  
647 Therapeutic Perspectives. *Cells* **9** (4), 875 (2020).
- 648 3. L. Richeldi, F. Varone, M. Bergna, J. de Andrade, J. Falk, R. Hallowell, S. Jouneau, Y.  
649 Kondoh, L. Morrow, W. Randerath, M. Streck, G. Tabaj, Pharmacological management of  
650 progressive-fibrosing interstitial lung diseases: a review of the current evidence. *Eur Respir*  
651 *Rev* **27** (150), 180074 (2018).
- 652 4. M. Ruiz-Ortega, S. Rayego-Mateos, S. Lamas, A. Ortiz, R. R. Rodrigues-Diez, Targeting  
653 the progression of chronic kidney disease. *Nat Rev Nephrol* **16** (5), 269-288 (2020).
- 654 5. M. B. Zeisel, P. Dhawan, T. F. Baumert, Tight junction proteins in gastrointestinal and  
655 liver disease. *Gut* **68** (3), 547-561 (2019).
- 656 6. M. J. Evans, T. von Hahn, D. M. Tscherne, A. J. Syder, M. Panis, B. Wolk, T.  
657 Hatzioannou, J. A. McKeating, P. D. Bieniasz, C. M. Rice, Claudin-1 is a hepatitis C virus  
658 co-receptor required for a late step in entry. *Nature* **446** (7137), 801-805 (2007).
- 659 7. A. Holczbauer, B. Gyongyosi, G. Lotz, P. Torzsok, P. Kaposi-Novak, A. Szijarto, P. Tatrai,  
660 P. Kupcsulik, Z. Schaff, A. Kiss, Increased expression of claudin-1 and claudin-7 in liver  
661 cirrhosis and hepatocellular carcinoma. *Pathol Oncol Res* **20** (3), 493-502 (2014).

- 662 8. Y. Suh, C. H. Yoon, R. K. Kim, E. J. Lim, Y. S. Oh, S. G. Hwang, S. An, G. Yoon, M. C.  
663 Gye, J. M. Yi, M. J. Kim, S. J. Lee, Claudin-1 induces epithelial-mesenchymal transition  
664 through activation of the c-Abl-ERK signaling pathway in human liver cells. *Oncogene* **32**  
665 (41), 4873-4882 (2013).
- 666 9. I. Fofana, S. E. Krieger, F. Grunert, S. Glauben, F. Xiao, S. Fafi-Kremer, E. Soulier, C.  
667 Royer, C. Thumann, C. J. Mee, J. A. McKeating, T. Dragic, P. Pessaux, F. Stoll-Keller, C.  
668 Schuster, J. Thompson, T. F. Baumert, Monoclonal anti-claudin 1 antibodies prevent  
669 hepatitis C virus infection of primary human hepatocytes. *Gastroenterology* **139** (3), 953-  
670 964, 964 e951-954 (2010).
- 671 10. C. C. Colpitts, R. G. Tawar, L. Mailly, C. Thumann, L. Heydmann, S. C. Durand, F. Xiao,  
672 E. Robinet, P. Pessaux, M. B. Zeisel, T. F. Baumert, Humanisation of a claudin-1-specific  
673 monoclonal antibody for clinical prevention and cure of HCV infection without escape.  
674 *Gut* **67** (4), 736-745 (2018).
- 675 11. L. Mailly, F. Xiao, J. Lupberger, G. K. Wilson, P. Aubert, F. H. Duong, D. Calabrese, C.  
676 Leboeuf, I. Fofana, C. Thumann, S. Bandiera, M. Lutgehetmann, T. Volz, C. Davis, H. J.  
677 Harris, C. J. Mee, E. Girardi, B. Chane-Woon-Ming, M. Ericsson, N. Fletcher, R.  
678 Bartenschlager, P. Pessaux, K. Vercauteren, P. Meuleman, P. Villa, L. Kaderali, S. Pfeffer,  
679 M. H. Heim, M. Neunlist, M. B. Zeisel, M. Dandri, J. A. McKeating, E. Robinet, T. F.  
680 Baumert, Clearance of persistent hepatitis C virus infection in humanized mice using a  
681 claudin-1-targeting monoclonal antibody. *Nat Biotechnol* **33** (5), 549-554 (2015).

- 682 12. A. L. Rasmussen, N. Tchitchek, N. J. Susnow, A. L. Krasnoselsky, D. L. Diamond, M. M.  
683 Yeh, S. C. Prohl, M. J. Korth, K. A. Walters, S. Lederer, A. M. Larson, R. L. Carithers, A.  
684 Benecke, M. G. Katze, Early transcriptional programming links progression to hepatitis C  
685 virus-induced severe liver disease in transplant patients. *Hepatology* **56** (1), 17-27 (2012).
- 686 13. W. Zhou, Y. Ma, J. Zhang, J. Hu, M. Zhang, Y. Wang, Y. Li, L. Wu, Y. Pan, Y. Zhang, X.  
687 Zhang, X. Zhang, Z. Zhang, J. Zhang, H. Li, L. Lu, L. Jin, J. Wang, Z. Yuan, J. Liu,  
688 Predictive model for inflammation grades of chronic hepatitis B: Large-scale analysis of  
689 clinical parameters and gene expressions. *Liver Int* **37** (11), 1632-1641 (2017).
- 690 14. C. A. Moylan, H. Pang, A. Dellinger, A. Suzuki, M. E. Garrett, C. D. Guy, S. K. Murphy,  
691 A. E. Ashley-Koch, S. S. Choi, G. A. Michelotti, D. D. Hampton, Y. Chen, H. L. Tillmann,  
692 M. A. Hauser, M. F. Abdelmalek, A. M. Diehl, Hepatic gene expression profiles  
693 differentiate presymptomatic patients with mild versus severe nonalcoholic fatty liver  
694 disease. *Hepatology* **59** (2), 471-482 (2014).
- 695 15. N. Aizarani, A. Saviano, Sagar, L. Mailly, S. Durand, J. S. Herman, P. Pessaux, T. F.  
696 Baumert, D. Grun, A human liver cell atlas reveals heterogeneity and epithelial  
697 progenitors. *Nature* **572** (7768), 199-204 (2019).
- 698 16. P. Ramachandran, R. Dobie, J. R. Wilson-Kanamori, E. F. Dora, B. E. P. Henderson, N. T.  
699 Luu, J. R. Portman, K. P. Matchett, M. Brice, J. A. Marwick, R. S. Taylor, M. Efremova,  
700 R. Vento-Tormo, N. O. Carragher, T. J. Kendall, J. A. Fallowfield, E. M. Harrison, D. J.  
701 Mole, S. J. Wigmore, P. N. Newsome, C. J. Weston, J. P. Iredale, F. Tacke, J. W. Pollard,

- 702 C. P. Ponting, J. C. Marioni, S. A. Teichmann, N. C. Henderson, Resolving the fibrotic  
703 niche of human liver cirrhosis at single-cell level. *Nature* **575** (7783), 512-518 (2019).
- 704 17. T. S. Andrews, J. Atif, J. C. Liu, C. T. Perciani, X. Z. Ma, C. Thoeni, M. Slyper, G. Eraslan,  
705 A. Segerstolpe, J. Manuel, S. Chung, E. Winter, I. Cirlan, N. Khuu, S. Fischer, O.  
706 Rozenblatt-Rosen, A. Regev, I. D. McGilvray, G. D. Bader, S. A. MacParland, Single-Cell,  
707 Single-Nucleus, and Spatial RNA Sequencing of the Human Liver Identifies  
708 Cholangiocyte and Mesenchymal Heterogeneity. *Hepatology* **6** (4), 821-840 (2022).
- 709 18. Y. Li, J. Wang, K. Asahina, Mesothelial cells give rise to hepatic stellate cells and  
710 myofibroblasts via mesothelial-mesenchymal transition in liver injury. *Proc Natl Acad Sci*  
711 *U S A* **110** (6), 2324-2329 (2013).
- 712 19. M. B. Buechler, R. N. Pradhan, A. T. Krishnamurthy, C. Cox, A. K. Calviello, A. W. Wang,  
713 Y. A. Yang, L. Tam, R. Caothien, M. Roose-Girma, Z. Modrusan, J. R. Arron, R. Bourgon,  
714 S. Muller, S. J. Turley, Cross-tissue organization of the fibroblast lineage. *Nature* **593**  
715 (7860), 575-579 (2021).
- 716 20. S. Ko, J. O. Russell, L. M. Molina, S. P. Monga, Liver Progenitors and Adult Cell Plasticity  
717 in Hepatic Injury and Repair: Knowns and Unknowns. *Annu Rev Pathol* **15**, 23-50 (2020).
- 718 21. H. Azuma, N. Paulk, A. Ranade, C. Dorrell, M. Al-Dhalimy, E. Ellis, S. Strom, M. A. Kay,  
719 M. Finegold, M. Grompe, Robust expansion of human hepatocytes in Fah<sup>-/-</sup>/Rag2<sup>-/-</sup>/Il2rg<sup>-</sup>  
720 <sup>-/-</sup> mice. *Nat Biotechnol* **25** (8), 903-910 (2007).

- 721 22. N. Kishida, S. Matsuda, O. Itano, M. Shinoda, M. Kitago, H. Yagi, Y. Abe, T. Hibi, Y.  
722 Masugi, K. Aiura, M. Sakamoto, Y. Kitagawa, Development of a novel mouse model of  
723 hepatocellular carcinoma with nonalcoholic steatohepatitis using a high-fat, choline-  
724 deficient diet and intraperitoneal injection of diethylnitrosamine. *BMC Gastroenterol* **16**  
725 (1), 61 (2016).
- 726 23. A. J. Debacker, J. Voutila, M. Catley, D. Blakey, N. Habib, Delivery of Oligonucleotides  
727 to the Liver with GalNAc: From Research to Registered Therapeutic Drug. *Mol Ther* **28**  
728 (8), 1759-1771 (2020).
- 729 24. C. Baeck, A. Wehr, K. R. Karlmark, F. Heymann, M. Vucur, N. Gassler, S. Huss, S.  
730 Klussmann, D. Eulberg, T. Luedde, C. Trautwein, F. Tacke, Pharmacological inhibition of  
731 the chemokine CCL2 (MCP-1) diminishes liver macrophage infiltration and steatohepatitis  
732 in chronic hepatic injury. *Gut* **61** (3), 416-426 (2012).
- 733 25. E. Crouchet, S. Bandiera, N. Fujiwara, S. Li, H. El Saghire, M. Fernandez-Vaquero, T.  
734 Riedl, X. Sun, H. Hirschfield, F. Juhling, S. Zhu, N. Roehlen, C. Ponsolles, L. Heydmann,  
735 A. Saviano, T. Qian, A. Venkatesh, J. Lupberger, E. R. Verrier, M. Sojoodi, M. A. Oudot,  
736 F. H. T. Duong, R. Masia, L. Wei, C. Thumann, S. C. Durand, V. Gonzalez-Motos, D.  
737 Heide, J. Hetzer, S. Nakagawa, A. Ono, W. M. Song, T. Higashi, R. Sanchez, R. S. Kim,  
738 C. B. Bian, K. Kiani, T. Croonenborghs, A. Subramanian, R. T. Chung, B. K. Straub, D.  
739 Schuppan, M. Ankavay, L. Cocquerel, E. Schaeffer, N. Goossens, A. P. Koh, M. Mahajan,  
740 V. D. Nair, G. Gunasekaran, M. E. Schwartz, N. Bardeesy, A. K. Shalek, O. Rozenblatt-  
741 Rosen, A. Regev, E. Felli, P. Pessaux, K. K. Tanabe, M. Heikenwalder, C. Schuster, N.

- 742 Pochet, M. B. Zeisel, B. C. Fuchs, Y. Hoshida, T. F. Baumert, A human liver cell-based  
743 system modeling a clinical prognostic liver signature for therapeutic discovery. *Nat*  
744 *Commun* **12** (1), 5525 (2021).
- 745 26. D. E. Kleiner, E. M. Brunt, M. Van Natta, C. Behling, M. J. Contos, O. W. Cummings, L.  
746 D. Ferrell, Y. C. Liu, M. S. Torbenson, A. Unalp-Arida, M. Yeh, A. J. McCullough, A. J.  
747 Sanyal, Design and validation of a histological scoring system for nonalcoholic fatty liver  
748 disease. *Hepatology* **41** (6), 1313-1321 (2005).
- 749 27. V. Mariotti, M. Strazzabosco, L. Fabris, D. F. Calvisi, Animal models of biliary injury and  
750 altered bile acid metabolism. *Biochim Biophys Acta Mol Basis Dis* **1864** (4 Pt B), 1254-  
751 1261 (2018).
- 752 28. D. Carter, S. Presnell, B. David, A. Chen, Modeling NAFLD using 3D bioprinted human  
753 liver tissue. *J Hepatol* **68** (S1), S357-S358 (2018).
- 754 29. D. Antoni, H. Burckel, E. Josset, G. Noel, Three-dimensional cell culture: a breakthrough  
755 in vivo. *Int J Mol Sci* **16** (3), 5517-5527 (2015).
- 756 30. S. A. Harrison, M. R. Bashir, C. D. Guy, R. Zhou, C. A. Moylan, J. P. Frias, N. Alkhouri,  
757 M. B. Bansal, S. Baum, B. A. Neuschwander-Tetri, R. Taub, S. E. Moussa, Resmetirom  
758 (MGL-3196) for the treatment of non-alcoholic steatohepatitis: a multicentre, randomised,  
759 double-blind, placebo-controlled, phase 2 trial. *Lancet* **394** (10213), 2012-2024 (2019).



- 760 31. S. Nakagawa, L. Wei, W. M. Song, T. Higashi, S. Ghoshal, R. S. Kim, C. B. Bian, S.  
761 Yamada, X. Sun, A. Venkatesh, N. Goossens, G. Bain, G. Y. Lauwers, A. P. Koh, M. El-  
762 Abtah, N. B. Ahmad, H. Hoshida, D. J. Erstad, G. Gunasekaran, Y. Lee, M. L. Yu, W. L.  
763 Chuang, C. Y. Dai, M. Kobayashi, H. Kumada, T. Beppu, H. Baba, M. Mahajan, V. D.  
764 Nair, M. Lanuti, A. Villanueva, A. Sangiovanni, M. Iavarone, M. Colombo, J. M. Llovet,  
765 A. Subramanian, A. M. Tager, S. L. Friedman, T. F. Baumert, M. E. Schwarz, R. T. Chung,  
766 K. K. Tanabe, B. Zhang, B. C. Fuchs, Y. Hoshida, Molecular Liver Cancer Prevention in  
767 Cirrhosis by Organ Transcriptome Analysis and Lysophosphatidic Acid Pathway  
768 Inhibition. *Cancer Cell* **30** (6), 879-890 (2016).
- 769 32. I. Jang, K. A. Beningo, Integrins, CAFs and Mechanical Forces in the Progression of  
770 Cancer. *Cancers (Basel)* **11** (5), 721 (2019).
- 771 33. S. Wullschleger, R. Loewith, M. N. Hall, TOR signaling in growth and metabolism. *Cell*  
772 **124** (3), 471-484 (2006).
- 773 34. J. F. Creeden, Z. A. Kipp, M. Xu, R. M. Flight, H. N. B. Moseley, G. J. Martinez, W. H.  
774 Lee, K. Alganem, A. S. Imami, M. R. McMullen, S. Roychowdhury, A. M. Nawabi, J. A.  
775 Hipp, S. Softic, S. A. Weinman, R. McCullumsmith, L. E. Nagy, T. D. Hinds, Jr., Hepatic  
776 kinome atlas: An in-depth identification of kinase pathways in liver fibrosis of humans and  
777 rodents. *Hepatology*, (2022).

- 778 35. K. Sato, M. Marzioni, F. Meng, H. Francis, S. Glaser, G. Alpini, Ductular Reaction in Liver  
779 Diseases: Pathological Mechanisms and Translational Significances. *Hepatology* **69** (1),  
780 420-430 (2019).
- 781 36. L. Broutier, A. Andersson-Rolf, C. J. Hindley, S. F. Boj, H. Clevers, B. K. Koo, M. Huch,  
782 Culture and establishment of self-renewing human and mouse adult liver and pancreas 3D  
783 organoids and their genetic manipulation. *Nat Protoc* **11** (9), 1724-1743 (2016).
- 784 37. K. Hasegawa, S. Wakino, P. Simic, Y. Sakamaki, H. Minakuchi, K. Fujimura, K. Hosoya,  
785 M. Komatsu, Y. Kaneko, T. Kanda, E. Kubota, H. Tokuyama, K. Hayashi, L. Guarente, H.  
786 Itoh, Renal tubular Sirt1 attenuates diabetic albuminuria by epigenetically suppressing  
787 Claudin-1 overexpression in podocytes. *Nat Med* **19** (11), 1496-1504 (2013).
- 788 38. S. Lovisa, V. S. LeBleu, B. Tampe, H. Sugimoto, K. Vадnagara, J. L. Carstens, C. C. Wu,  
789 Y. Hagos, B. C. Burckhardt, T. Pentcheva-Hoang, H. Nischal, J. P. Allison, M. Zeisberg,  
790 R. Kalluri, Epithelial-to-mesenchymal transition induces cell cycle arrest and parenchymal  
791 damage in renal fibrosis. *Nat Med* **21** (9), 998-1009 (2015).
- 792 39. A. Pardo, K. Gibson, J. Cisneros, T. J. Richards, Y. Yang, C. Becerril, S. Yousem, I.  
793 Herrera, V. Ruiz, M. Selman, N. Kaminski, Up-regulation and profibrotic role of  
794 osteopontin in human idiopathic pulmonary fibrosis. *PLoS Med* **2** (9), e251 (2005).
- 795 40. R. L. Chevalier, M. S. Forbes, B. A. Thornhill, Ureteral obstruction as a model of renal  
796 interstitial fibrosis and obstructive nephropathy. *Kidney Int* **75** (11), 1145-1152 (2009).

- 797 41. A. C. Habermann, A. J. Gutierrez, L. T. Bui, S. L. Yahn, N. I. Winters, C. L. Calvi, L.  
798 Peter, M. I. Chung, C. J. Taylor, C. Jetter, L. Raju, J. Roberson, G. Ding, L. Wood, J. M.  
799 S. Sucre, B. W. Richmond, A. P. Serezani, W. J. McDonnell, S. B. Mallal, M. J. Bacchetta,  
800 J. E. Loyd, C. M. Shaver, L. B. Ware, R. Bremner, R. Walia, T. S. Blackwell, N. E.  
801 Banovich, J. A. Kropski, Single-cell RNA sequencing reveals profibrotic roles of distinct  
802 epithelial and mesenchymal lineages in pulmonary fibrosis. *Sci Adv* **6** (28), eaba1972  
803 (2020).
- 804 42. A. Mullard, FDA rejects NASH drug. *Nat Rev Drug Discov* **19** (8), 501 (2020).
- 805 43. P. N. Newsome, K. Buchholtz, K. Cusi, M. Linder, T. Okanoue, V. Ratziu, A. J. Sanyal,  
806 A. S. Sejling, S. A. Harrison, N. N. Investigators, A Placebo-Controlled Trial of  
807 Subcutaneous Semaglutide in Nonalcoholic Steatohepatitis. *N Engl J Med* **384** (12), 1113-  
808 1124 (2021).
- 809 44. V. W. Wong, L. A. Adams, V. de Ledinghen, G. L. Wong, S. Sookoian, Noninvasive  
810 biomarkers in NAFLD and NASH - current progress and future promise. *Nat Rev*  
811 *Gastroenterol Hepatol* **15** (8), 461-478 (2018).
- 812 45. S. Robert, T. Gicquel, T. Victoni, S. Valenca, E. Barreto, B. Bailly-Maitre, E. Boichot, V.  
813 Lagente, Involvement of matrix metalloproteinases (MMPs) and inflammasome pathway  
814 in molecular mechanisms of fibrosis. *Biosci Rep* **36** (4), e00360 (2016).

- 815 46. J. Lv, B. Sun, Z. Mai, M. Jiang, J. Du, CLDN-1 promoted the epithelial to migration and  
816 mesenchymal transition (EMT) in human bronchial epithelial cells via Notch pathway. *Mol*  
817 *Cell Biochem* **432** (1-2), 91-98 (2017).
- 818 47. J. Dumas, M. A. Gargano, G. M. Dancik, shinyGEO: a web-based application for analyzing  
819 gene expression omnibus datasets. *Bioinformatics* **32** (23), 3679-3681 (2016).
- 820 48. N. Hamdane, F. Juhling, E. Crouchet, H. El Saghire, C. Thumann, M. A. Oudot, S.  
821 Bandiera, A. Saviano, C. Ponsolles, A. A. Roca Suarez, S. Li, N. Fujiwara, A. Ono, I.  
822 Davidson, N. Bardeesy, C. Schmidl, C. Bock, C. Schuster, J. Lupberger, F. Habersetzer,  
823 M. Doffoel, T. Piardi, D. Sommacale, M. Imamura, T. Uchida, H. Ohdan, H. Aikata, K.  
824 Chayama, T. Boldanova, P. Pessaux, B. C. Fuchs, Y. Hoshida, M. B. Zeisel, F. H. T.  
825 Duong, T. F. Baumert, HCV-Induced Epigenetic Changes Associated With Liver Cancer  
826 Risk Persist After Sustained Virologic Response. *Gastroenterology* **156** (8), 2313-2329  
827 e2317 (2019).
- 828 49. A. Liberzon, C. Birger, H. Thorvaldsdottir, M. Ghandi, J. P. Mesirov, P. Tamayo, The  
829 Molecular Signatures Database (MSigDB) hallmark gene set collection. *Cell Syst* **1** (6),  
830 417-425 (2015).
- 831 50. K. Street, D. Risso, R. B. Fletcher, D. Das, J. Ngai, N. Yosef, E. Purdom, S. Dudoit,  
832 Slingshot: cell lineage and pseudotime inference for single-cell transcriptomics. *BMC*  
833 *Genomics* **19** (1), 477 (2018).

- 834 51. M. Ryaboshapkina, M. Hammar, Human hepatic gene expression signature of non-  
835 alcoholic fatty liver disease progression, a meta-analysis. *Sci Rep* **7** (1), 12361 (2017).
- 836 52. R. H. Hubner, W. Gitter, N. E. El Mokhtari, M. Mathiak, M. Both, H. Bolte, S. Freitag-  
837 Wolf, B. Bewig, Standardized quantification of pulmonary fibrosis in histological samples.  
838 *Biotechniques* **44** (4), 507-511, 514-507 (2008).
- 839 53. M. Boeckh, M. M. Berrey, R. A. Bowden, S. W. Crawford, J. Balsley, L. Corey, Phase 1  
840 evaluation of the respiratory syncytial virus-specific monoclonal antibody palivizumab in  
841 recipients of hematopoietic stem cell transplants. *J. Infect. Dis.* **184** (3), 350-354 (2001).
- 842 54. P. Bankhead, M. B. Loughrey, J. A. Fernandez, Y. Dombrowski, D. G. McArt, P. D.  
843 Dunne, S. McQuaid, R. T. Gray, L. J. Murray, H. G. Coleman, J. A. James, M. Salto-Tellez,  
844 P. W. Hamilton, QuPath: Open source software for digital pathology image analysis. *Sci*  
845 *Rep* **7** (1), 16878 (2017).
- 846 55. H. M. Berman, J. Westbrook, Z. Feng, G. Gilliland, T. N. Bhat, H. Weissig, I. N.  
847 Shindyalov, P. E. Bourne, The Protein Data Bank. *Nucleic Acids Res* **28** (1), 235-242  
848 (2000).
- 849 56. M. P. Jacobson, D. L. Pincus, C. S. Rapp, T. J. Day, B. Honig, D. E. Shaw, R. A. Friesner,  
850 A hierarchical approach to all-atom protein loop prediction. *Proteins* **55** (2), 351-367  
851 (2004).

- 852 57. M. P. Jacobson, R. A. Friesner, Z. Xiang, B. Honig, On the role of the crystal environment  
853 in determining protein side-chain conformations. *J Mol Biol* **320** (3), 597-608 (2002).
- 854 58. K. Zhu, T. Day, D. Warshaviak, C. Murrett, R. Friesner, D. Pearlman, Antibody structure  
855 determination using a combination of homology modeling, energy-based refinement, and  
856 loop prediction. *Proteins* **82** (8), 1646-1655 (2014).
- 857 59. N. K. Salam, M. Adzhigirey, W. Sherman, D. A. Pearlman, Structure-based approach to  
858 the prediction of disulfide bonds in proteins. *Protein Eng Des Sel* **27** (10), 365-374 (2014).
- 859 60. H. Beard, A. Cholleti, D. Pearlman, W. Sherman, K. A. Loving, Applying physics-based  
860 scoring to calculate free energies of binding for single amino acid mutations in protein-  
861 protein complexes. *PLoS One* **8** (12), e82849 (2013).
- 862 61. M. A. Lomize, I. D. Pogozheva, H. Joo, H. I. Mosberg, A. L. Lomize, OPM database and  
863 PPM web server: resources for positioning of proteins in membranes. *Nucleic Acids Res*  
864 **40** (Database issue), D370-376 (2012).
- 865 62. W. L. Jorgensen, J. Chandrasekhar, J. D. Madura, R. W. Impey, L. M. Klein, Comparison  
866 of simple potential functions for simulating liquid water. *J Chem Phys* **79**, 926-935 (1983).
- 867 63. K. Roos, C. Wu, W. Damm, M. Reboul, J. M. Stevenson, C. Lu, M. K. Dahlgren, S.  
868 Mondal, W. Chen, L. Wang, R. Abel, R. A. Friesner, E. D. Harder, OPLS3e: Extending  
869 Force Field Coverage for Drug-Like Small Molecules. *Journal of Chemical Theory and*  
870 *Computation* **15** (3), 1863-1874 (2019).

- 871 64. G. Martyna, D. Tobias, M. Klein, Constant pressure molecular dynamics algorithms. *The*  
872 *Journal of Chemical Physics* **101** (5), 4177-4189 (1994).
- 873 65. G. J. Martyna, M. L. Klein, M. Tuckerman, Nosé–Hoover chains: The canonical ensemble  
874 via continuous dynamics. *The Journal of Chemical Physics* **97** (4), 2635-2643 (1992).
- 875 66. K. J. Bowers, E. Chow, H. Xu, R. O. Dror, M. P. Eastwood, B. A. Gregersen, J. L. Klepeis,  
876 I. Kolossvary, M. A. Moraes, F. D. Sacerdoti, J. K. Salmon, Y. Shan, D. E. Shaw, paper  
877 presented at the Proceedings of the 2006 ACM/IEEE conference on Supercomputing,  
878 Tampa, Florida, 2006.
- 879 67. T. Tubiana, J. C. Carvaillo, Y. Boulard, S. Bressanelli, TTClust: A Versatile Molecular  
880 Simulation Trajectory Clustering Program with Graphical Summaries. *J Chem Inf Model*  
881 **58** (11), 2178-2182 (2018).
- 882 68. R. Tibshirani, G. Walther, T. Hastie, Estimating the number of clusters in a data set via the  
883 gap statistic. *J R Stat Soc Series B Stat Methodol.* **63** (2), 411-423 (2001).
- 884 69. G. C. P. van Zundert, J. Rodrigues, M. Trellet, C. Schmitz, P. L. Kastritis, E. Karaca, A. S.  
885 J. Melquiond, M. van Dijk, S. J. de Vries, A. Bonvin, The HADDOCK2.2 Web Server:  
886 User-Friendly Integrative Modeling of Biomolecular Complexes. *J Mol Biol* **428** (4), 720-  
887 725 (2016).

- 888 70. C. Dominguez, R. Boelens, A. M. Bonvin, HADDOCK: a protein-protein docking  
889 approach based on biochemical or biophysical information. *J Am Chem Soc* **125** (7), 1731-  
890 1737 (2003).
- 891 71. F. Ambrosetti, S. Jandova, A. M. Bonvin, A protocol for information-driven antibody-  
892 antigen modelling with the HADDOCK2.4 webserver. *arXiv:2005.03283*, (2020).
- 893 72. A. Vangone, A. M. Bonvin, Contacts-based prediction of binding affinity in protein-protein  
894 complexes. *Elife* **4**, e07454 (2015).
- 895 73. J. Freeth, J. Soden, New Advances in Cell Microarray Technology to Expand Applications  
896 in Target Deconvolution and Off-Target Screening. *SLAS Discov* **25** (2), 223-230 (2020).
- 897 74. M. Charni-Natan, I. Goldstein, Protocol for Primary Mouse Hepatocyte Isolation. *STAR*  
898 *Protoc* **1** (2), 100086 (2020).
- 899 75. V. Kegel, D. Deharde, E. Pfeiffer, K. Zeilinger, D. Seehofer, G. Damm, Protocol for  
900 Isolation of Primary Human Hepatocytes and Corresponding Major Populations of Non-  
901 parenchymal Liver Cells. *J Vis Exp* (109), e53069 (2016).
- 902 76. L. Aoudjehane, G. Bisch, O. Scatton, C. Granier, J. Gaston, C. Housset, P. Roingeard, F.  
903 L. Cosset, F. Perdigao, P. Balladur, T. Wakita, Y. Calmus, F. Conti, Infection of Human  
904 Liver Myofibroblasts by Hepatitis C Virus: A Direct Mechanism of Liver Fibrosis in  
905 Hepatitis C. *PLoS One* **10** (7), e0134141 (2015).



- 906 77. L. Maily, F. Xiao, J. Lupberger, G. K. Wilson, P. Aubert, F. H. T. Duong, D. Calabrese,  
907 C. Leboeuf, I. Fofana, C. Thumann, S. Bandiera, M. Lutgehetmann, T. Volz, C. Davis, H.  
908 J. Harris, C. J. Mee, E. Girardi, B. Chane-Woon-Ming, M. Ericsson, N. Fletcher, R.  
909 Bartenschlager, P. Pessaux, K. Vercauteren, P. Meuleman, P. Villa, L. Kaderali, S. Pfeffer,  
910 M. H. Heim, M. Neunlist, M. B. Zeisel, M. Dandri, J. A. McKeating, E. Robinet, T. F.  
911 Baumert, Clearance of persistent hepatitis C virus infection in humanized mice using a  
912 claudin-1-targeting monoclonal antibody. *Nat Biotechnol* **33** (5), 549-554 (2015).
- 913 78. C. A. Schneider, W. S. Rasband, K. W. Eliceiri, NIH Image to ImageJ: 25 years of image  
914 analysis. *Nat. Methods* **9** (7), 671-675 (2012).
- 915 79. S. Fafi-Kremer, I. Fofana, E. Soulier, P. Carolla, P. Meuleman, G. Leroux-Roels, A. H.  
916 Patel, F. L. Cosset, P. Pessaux, M. Doffoel, P. Wolf, F. Stoll-Keller, T. F. Baumert, Viral  
917 entry and escape from antibody-mediated neutralization influence hepatitis C virus  
918 reinfection in liver transplantation. *J Exp Med* **207** (9), 2019-2031 (2010).
- 919 80. L. Y. King, C. Canasto-Chibuque, K. B. Johnson, S. Yip, X. Chen, K. Kojima, M.  
920 Deshmukh, A. Venkatesh, P. S. Tan, X. Sun, A. Villanueva, A. Sangiovanni, V. Nair, M.  
921 Mahajan, M. Kobayashi, H. Kumada, M. Iavarone, M. Colombo, M. I. Fiel, S. L. Friedman,  
922 J. M. Llovet, R. T. Chung, Y. Hoshida, A genomic and clinical prognostic index for  
923 hepatitis C-related early-stage cirrhosis that predicts clinical deterioration. *Gut* **64** (8),  
924 1296-1302 (2015).

- 925 81. A. Subramanian, P. Tamayo, V. K. Mootha, S. Mukherjee, B. L. Ebert, M. A. Gillette, A.  
926 Paulovich, S. L. Pomeroy, T. R. Golub, E. S. Lander, J. P. Mesirov, Gene set enrichment  
927 analysis: a knowledge-based approach for interpreting genome-wide expression profiles.  
928 *Proc Natl Acad Sci U S A* **102** (43), 15545-15550 (2005).
- 929 82. M. Nakatsukasa, S. Kawasaki, K. Yamasaki, H. Fukuoka, A. Matsuda, M. Tsujikawa, H.  
930 Tanioka, M. Nagata-Takaoka, J. Hamuro, S. Kinoshita, Tumor-associated calcium signal  
931 transducer 2 is required for the proper subcellular localization of claudin 1 and 7:  
932 implications in the pathogenesis of gelatinous drop-like corneal dystrophy. *Am J Pathol*  
933 **177** (3), 1344-1355 (2010).
- 934 83. K. J. Livak, T. D. Schmittgen, Analysis of relative gene expression data using real-time  
935 quantitative PCR and the 2(-Delta Delta C(T)) Method. *Methods* **25** (4), 402-408 (2001).
- 936 84. J. Lupberger, T. Croonenborghs, A. A. Roca Suarez, N. Van Renne, F. Juhling, M. A.  
937 Oudot, A. Virzi, S. Bandiera, C. Jamey, G. Meszaros, D. Brumaru, A. Mukherji, S. C.  
938 Durand, L. Heydmann, E. R. Verrier, H. El Saghire, N. Hamdane, R. Bartenschlager, S.  
939 Fereshetian, E. Ramberger, R. Sinha, M. Nabian, C. Everaert, M. Jovanovic, P. Mertins, S.  
940 A. Carr, K. Chayama, N. Dali-Youcef, R. Ricci, N. M. Bardeesy, N. Fujiwara, O. Gevaert,  
941 M. B. Zeisel, Y. Hoshida, N. Pochet, T. F. Baumert, Combined Analysis of Metabolomes,  
942 Proteomes, and Transcriptomes of Hepatitis C Virus-Infected Cells and Liver to Identify  
943 Pathways Associated With Disease Development. *Gastroenterology* **157** (2), 537-551 e539  
944 (2019).

- 945 85. O. Bauhofer, A. Ruggieri, B. Schmid, P. Schirmacher, R. Bartenschlager, Persistence of  
946 HCV in quiescent hepatic cells under conditions of an interferon-induced antiviral  
947 response. *Gastroenterology* **143** (2), 429-438 e428 (2012).
- 948 86. S. Bandiera, S. Pernot, H. El Saghire, S. C. Durand, C. Thumann, E. Crouchet, T. Ye, I.  
949 Fofana, M. A. Oudot, J. Barths, C. Schuster, P. Pessaux, M. H. Heim, T. F. Baumert, M.  
950 B. Zeisel, Hepatitis C Virus-Induced Upregulation of MicroRNA miR-146a-5p in  
951 Hepatocytes Promotes Viral Infection and Deregulates Metabolic Pathways Associated  
952 with Liver Disease Pathogenesis. *J Virol* **90** (14), 6387-6400 (2016).
- 953 87. E. R. Verrier, C. C. Colpitts, C. Bach, L. Heydmann, A. Weiss, M. Renaud, S. C. Durand,  
954 F. Habersetzer, D. Durantel, G. Abou-Jaoude, M. M. Lopez Ledesma, D. J. Felmlee, M.  
955 Soumillon, T. Croonenborghs, N. Pochet, M. Nassal, C. Schuster, L. Brino, C. Sureau, M.  
956 B. Zeisel, T. F. Baumert, A targeted functional RNA interference screen uncovers glypican  
957 5 as an entry factor for hepatitis B and D viruses. *Hepatology* **63** (1), 35-48 (2016).
- 958 88. V. J. Barbero-Becerra, P. J. Giraudi, N. C. Chavez-Tapia, M. Uribe, C. Tiribelli, N. Rosso,  
959 The interplay between hepatic stellate cells and hepatocytes in an in vitro model of NASH.  
960 *Toxicol In Vitro* **29** (7), 1753-1758 (2015).
- 961 89. R. Hilhorst, L. Houkes, M. Mommersteeg, J. Musch, A. van den Berg, R. Ruijtenbeek,  
962 Peptide microarrays for profiling of serine/threonine kinase activity of recombinant kinases  
963 and lysates of cells and tissue samples. *Methods Mol Biol* **977**, 259-271 (2013).

964 90. A. Roy, A. Tolone, R. Hilhorst, J. Groten, T. Tomar, F. Paquet-Durand, Kinase activity  
965 profiling identifies putative downstream targets of cGMP/PKG signaling in inherited  
966 retinal neurodegeneration. *Cell Death Discov* **8** (1), 93 (2022).

967 91. K. Muller, H. Honcharova-Biletska, C. Koppe, M. Egger, L. K. Chan, A. T. Schneider, L.  
968 Kusgens, F. Bohm, Y. Boege, M. E. Healy, J. Schmitt, S. Comtesse, M. Castoldi, C.  
969 Preisinger, M. Szydlowska, E. Focaccia, N. T. Gaisa, S. H. Loosen, S. Jors, F. Tacke, C.  
970 Roderburg, V. Keitel, J. G. Bode, P. Boor, R. J. Davis, T. Longerich, F. Geisler, M.  
971 Heikenwalder, A. Weber, M. Vucur, T. Luedde, JNK signaling prevents biliary cyst  
972 formation through a CASPASE-8-dependent function of RIPK1 during aging. *Proc Natl*  
973 *Acad Sci U S A* **118** (12), e2007194118 (2021).

974 92. H. Wickham, *ggplot2: Elegant Graphics for Data Analysis*. Springer-Verlag New York  
975 (2016).

976 93. Y. Hao, S. Hao, E. Andersen-Nissen, W. M. Mauck, 3rd, S. Zheng, A. Butler, M. J. Lee,  
977 A. J. Wilk, C. Darby, M. Zager, P. Hoffman, M. Stoeckius, E. Papalexi, E. P. Mimitou, J.  
978 Jain, A. Srivastava, T. Stuart, L. M. Fleming, B. Yeung, A. J. Rogers, J. M. McElrath, C.  
979 A. Blish, R. Gottardo, P. Smibert, R. Satija, Integrated analysis of multimodal single-cell  
980 data. *Cell* **184** (13), 3573-3587 e3529 (2021).

981  
982  
983

984 **FIGURE LEGENDS**

985 **Figure 1. CLDN1 expression is upregulated in chronic liver disease. A.** *CLDN1*  
986 upregulation in liver tissues of patients with chronic HCV, HBV infection, or NASH. **B.** *CLDN1*  
987 expression in livers of patients with NASH with mild (F0-1) or advanced fibrosis (F3-4) and liver  
988 tissues of transplanted HCV-infected patients with stable or progressive fibrotic disease. **C.**  
989 *CLDN1* expression in healthy liver at the single-nucleus level. ( $p < 0.0001$ , U-test). **D.** *CLDN1*  
990 expression along the cholangiocyte-bipotent progenitor cells-hepatocyte pseudotime trajectory by  
991 Slingshot in a combined scRNA-seq and snRNA-seq dataset(50). **E.** *CLDN1* expression at the  
992 single-cell level in human cirrhotic and healthy liver cells. Differential expression analysis  
993 identified *CLDN1* as a marker of mesothelial cells, hepatocytes and cholangiocytes ( $p < 0.0001$ , U-  
994 test, respectively). **F.** Enhanced *CLDN1* expression in hepatocytes at the stromal-epithelial  
995 interface of HCV cirrhotic nodule. Scale bars=1 mm. **G.** RNA ISH showing *CLDN1* expression in  
996 a subpopulation of *COL3A1*<sup>+</sup> stellate cells in NASH-associated liver cirrhosis. Scale bars=50 $\mu$ m  
997 (low resolution) and 20 $\mu$ m (high resolution image). **H.** Staining of *CLDN1* with  $\alpha$ SMA by  
998 immunofluorescence and CK19 and EPCAM by immunohistochemistry showing *CLDN1*  
999 expression in cholangiocytes, EPCAM<sup>+</sup> bile duct cells and stellate cells. Scale bars=50 $\mu$ m. **I.**  
1000 Upper panel: Computationally predicted structural model of the non-junctional *CLDN1*/*CLDN1*  
1001 mAb complex. Lower panel: Absent accessibility of the epitope targeted by the *CLDN1* mAb in  
1002 tight junctions. **J.** Expression of total *CLDN1* and nj*CLDN1* in mild (F0-2,  $n=8$ ) or advanced liver  
1003 fibrosis (F3-4,  $n=10$ ) using an antibody targeting the C-terminal domain of *CLDN1* (total *CLDN1*)  
1004 or mAb ALE.F02 targeting nj*CLDN1*. **K.** Co-staining of *CLDN1* and EPCAM in ductular  
1005 reactions. Scale bars=65 $\mu$ m (F2) and 100 $\mu$ m (F4). **L.** Regulation of nj*CLDN1* expression by TNF-

1006  $\alpha$ . HLMFs and primary human hepatocytes (PHHs) were treated with TNF- $\alpha$ , IKK-16 or TNF- $\alpha$   
1007 + IKK16 and CLDN1 expression analyzed by flow cytometry using anti-CLDN1 mAb H3L3 ( $n=3$   
1008 independent experiments with 2-4 replicates per condition).  $\Delta$ MFI is shown as fold change  
1009 compared to untreated cells. **M.** The *CLDN1* locus with the indicated CUT&Tag and ChIP-seq  
1010 tracks. Red boxes identify p65-bound sites that coincide with Encode-defined cis-Regulatory  
1011 Elements (cCREs) both upstream and downstream of *CLDN1* with the density of previously  
1012 identified ChIP-seq RELA binding sites (peak regions) as listed in ReMAP2022. \*\*\*\* $p<0.0001$ ,  
1013 \*\*\* $p<0.001$ , \*\* $p<0.01$ , \* $p<0.05$  U-test (**A-B, J**), U-test with Bonferroni correction (C, E), and  
1014 Student's t-test (**L**). MFI=Mean fluorescence intensity; MP=mononuclear phagocyte.  
1015

1016 **Figure 2. Targeting CLDN1 by siRNA or mAbs reduces liver fibrosis in a patient-**  
1017 **derived mouse model. A-C** *CLDN1* knockdown by GalNAc-siRNA reduces liver fibrosis in  
1018 humanized liver fibrosis mouse model. **A.** Illustration of the experimental approach. **B.** CLDN1  
1019 expression, fibrosis assessment in humanized areas, and tumor nodule count according to the  
1020 treatment group (siCTRL *n*=6, siCLDN1 *n*=5). **C.** Representative images of human CLDN1  
1021 staining, Sirius red, fibronectin-1 (FN1) immunostaining and macroscopy of GalNAc siCLDN1  
1022 and siCTRL mice. Scale bar=50μm, 250μm, 50μm respectively. **D-H.** CLDN1 mAb treatment  
1023 reduced liver fibrosis and HCC. **D.** Study protocol of humanized mouse NASH model treated with  
1024 CLDN1 mAb. **E-F.** Fibrosis assessment in the total liver tissue and humanized areas, and tumor  
1025 nodule count of experiment 1 (**E**, Control *n*=3, CLDN1 mAb *n*=4), and experiment 2 (**F**, Control  
1026 *n*=10, CLDN1 mAb *n*=10) which were performed independently. Sample size in FN1 experiment  
1027 2 (Control *n*=8, CLDN1 mAb *n*=7). Control group was treated with i.p. injections of vehicle. **G.**  
1028 Representative images of FAH, Sirius red, FN1 staining and macroscopic images according to  
1029 treatment groups (experiment 1). Scale bars=250μm, 250μm, 50μm, respectively. **H.** Gene  
1030 expression of fibrosis markers *Colla1* and *Timp1* (experiment 1). Bars show mean ±SEM.  
1031 \**p*<0.05, \*\**p*<0.01, U-test (**B**, **E**, **F**), t-test (**H**), respectively. FAH=fumarylacetoacetate hydrolase;  
1032 hCLDN1= human CLDN1.  
1033

1034 **Figure 3. Targeting non-junctional CLDN1 reduces fibrosis and tumor development**  
1035 **in mouse models for liver and biliary fibrosis. A.** Study protocol of DEN-CDA-HFD NASH  
1036 fibrosis mouse model and mAb treatment. **B.** Representative images of Sirius Red and fibronectin-  
1037 1 (FN1) staining in mouse livers. Scale bars=250µm and 50µm, respectively. **C.** Collagen  
1038 proportional area (CPA) (Control *n*=18, CLDN1 mAb *n*=20) and FN1 quantification (Control  
1039 *n*=15, CLDN1 mAb *n*=16) in representative areas according to the treatment group. **D.** Gene  
1040 expression of fibrosis markers *Coll1a1* (Control *n*=5, CLDN1 mAb *n*=5) and *Acta2* (Control *n*=4,  
1041 CLDN1 mAb *n*=5). **E.** Liver fat proportional area and NAFLD activity score according to the  
1042 assigned treatment (Control *n*=18, CLDN1 mAb *n*=20). **F.** Quantification of liver immunostaining  
1043 of CD3<sup>+</sup> T cells, and CD68<sup>+</sup> macrophages (Control *n*=15, CLDN1 mAb *n*=16). **G.** Representative  
1044 images of macroscopy and HSP70<sup>+</sup> areas in mouse livers. Scale bars=500µm. **H.** Macroscopic (left  
1045 panel) and histological (right panel) assessment of tumor occurrence in mouse livers (Control  
1046 *n*=18, CLDN1 mAb *n*=20). **I.** Number and size of tumor nodules and proportion of HSP70<sup>+</sup> tumors  
1047 in mice livers (Control *n*=18, CLDN1 mAb *n*=20). **J.** Study protocol of DDC mouse model for  
1048 biliary fibrosis. **K.** Sirius red and FN1 staining in CLDN1 mAb- or Control-treated DDC mice.  
1049 Representative images are shown. **L.** Quantification of CPA and FN1-positive area in all mice. **M.**  
1050 Ishak score in CLDN1 mAb- or control-treated DDC mice. All control groups were treated with  
1051 i.p. injections of vehicle. \*\*\*\**p*<0.0001, t-test. Bars show mean ±SEM. \**p*<0.05, \*\**p*<0.01,  
1052 \*\*\**p*<0.001, \*\*\*\**p*<0.0001, U-test, respectively. H&E=Haemotoxylin and Eosin; HSP70=Heat-  
1053 shock protein 70; SEM=standard error of the mean.

1054



1055 **Figure 4. CLDN1-specific mAb effects in patient-derived *ex vivo* models of chronic**  
1056 **liver disease. A.** Illustration of Organovo ExVive fibrosis model. **B.** Images of Trichromic Masson  
1057 and H&E staining in Organovo ExVive tissues sections treated with CLDN1 mAb or control mAb  
1058 ( $n=4$  biological and  $N=8$  technical replicates per condition). Macrovascular steatosis is indicated  
1059 by green and microvascular steatosis by red arrows. Scale bars= $40\mu\text{m}$ . **C.** Quantification of  
1060 collagen proportional area in Organovo ExVive tissue. **D.** Illustration of patient-derived liver  
1061 spheroids. **E.** Immunostaining of ASPGR1, CD31, CD68 and  $\alpha$ -SMA in patient-derived liver  
1062 spheroids. Staining with anti-mouse secondary antibodies were used as a control. Spheroids were  
1063 visualized by Celigo imaging cytometer. Scale bar= $500\mu\text{m}$ . **F.** Gene expression of *COL1A1*,  
1064 *CTGF* ( $n=3$  independent experiments with  $n=4$  biological replicates per condition) in liver  
1065 spheroids exposed to a TGF- $\beta$ , FFA and LPS and treated with either CLDN1 mAb or control mAb.  
1066 **G.** Total collagen deposition in patient-derived liver spheroids stimulated with FFA, LPS, and  
1067 TGF- $\beta$  and treated with CLDN1 mAb, control mAb or resmetirom ( $n=8$  different donors with 1-3  
1068 replicates per condition). **H.** Modulation of PLS to good (green) or poor (orange) prognosis status  
1069 (51) in precision cut liver slices. Significance (FDR, Kolmogorov-Smirnov test) of induction (red)  
1070 or suppression (blue) of PLS poor- or good-prognosis genes is shown. Bars show mean  $\pm$ SEM.  
1071 \* $p<0.05$ , \*\*\*\* $p<0.0001$ , t-test (C), U-test (F, G). ECs=Endothelial cells; H&E=Haemotoxylin and  
1072 Eosin; HCs=Hepatocytes; HSCs=Hepatic stellate cells; KCs=Kupffer cells; SEM=standard error  
1073 of the mean.  
1074

1075 **Figure 5. Treatment with CLDN1-specific mAb suppresses liver cell circuits**  
1076 **mediating inflammation, fibrosis, and carcinogenesis.** A. Graphical illustration of  
1077 methodological approach to assess liver fibrosis associated cell plasticity in bulk RNA-seq data  
1078 derived from two fibrosis mouse models. B. Modulation of gene sets characterizing mature  
1079 hepatocytes and immature progenitor cells in patients with NASH with mild or advanced fibrosis.  
1080 C. Effect of CLDN1 mAb on liver progenitor and mature hepatocyte marker gene sets in  
1081 humanized NASH fibrosis mice. D. Differential expression of a gene set characterizing scar-  
1082 associated myofibroblasts(*I6*) in NASH patients with mild compared to advanced fibrosis. E.  
1083 Effect of CLDN1 mAb on expression of scar-associated myofibroblast marker genes in the regular  
1084 NASH fibrosis mouse model. F. Modulation of fibrogenic and carcinogenic signaling pathways  
1085 and human cirrhosis gene modules in NASH patients with NASH with mild or advanced fibrosis,  
1086 humanized NASH fibrosis mice treated with CLDN1 mAb or control and regular NASH fibrosis  
1087 mice treated with CLDN1 mAb or control. Heatmaps illustrate NES of altered gene sets (all  
1088 FDR<0.25 except for induction of fibrogenic, KRas signaling and cirrhosis modules #1, #7, #19,  
1089 #24 and #23 in humanized mice control tissues and reversal of E2F targets, TGF- $\beta$  signaling and  
1090 cirrhosis modules #1, #7 and #24 in CLDN1 mAb treated NASH fibrosis mice, FDR>0.25). G.  
1091 RELA, RELB, and p-P38 positive cells were assessed by immunohistochemistry in DEN-  
1092 CDAHFD mice treated with CLDN1 mAb ( $n= 16$  animals per staining) or control ( $n=15$  animals  
1093 per staining). For the RELB analysis, in case of multiple liver specimen from the same mouse, the  
1094 maximum value per mouse was considered except in case of >5-fold difference between the  
1095 minimum and maximum value where the mean value was used (U-Test). Vertical bars show mean  
1096  $\pm$ SEM and single data points. Horizontal bars indicate NES of significantly (FDR<0.25) altered  
1097 gene sets. \* $p<0.05$ , U-test.

1099 **Figure 6. Targeting CLDN1 inhibits pro-fibrotic signaling mediating cell-matrix**  
1100 **interaction and plasticity in hepatocytes. A.** Co-immunoprecipitation followed by mass-  
1101 spectrometry identified CLDN1 interactants. String analysis with MCL clustering is shown. **B.**  
1102 Validation of the main CLDN1 interactants in Huh7 cells by Western Blot analysis. Negative  
1103 control is the hepatocyte marker ASGR1. **C.** CLDN1 mAb treatment decreases EGFR  
1104 phosphorylation in Huh7 cells (representative results of  $n=3$  independent experiments are shown).  
1105 **D.** CLDN1 mAb inhibits ERK phosphorylation in Huh7 cells (representative results of  $n=4$   
1106 independent experiments are shown). **E.** CLDN1 decreases SRC recruitment at the membrane in  
1107 Huh7 cells (representative results of  $n=2$  independent experiments with  $n=2$  biological replicates  
1108 are shown). **F.** CLDN1 mAb inhibits SRC phosphorylation in Huh7 spheroids (representative  
1109 results of  $n=4$  independent experiments are shown). **G.** Effect of CLDN1 mAb on phosphokinase  
1110 signaling in the patient-derived NASH liver spheroid model shown in Fig. 4. **H.** Kinome assay of  
1111 CLDN1 mAb-treated vs. Control mAb-treated patient-derived spheroids. B-F shows  
1112 representative results out of 3 independent experiments. Full-length Western blots are shown in  
1113 fig. S16. ASGR1: Asialoglycoprotein Receptor 1; CTRL=Control; FT=Flowthrough;  
1114 MCL=Markov clustering.  
1115

1116 **Figure 7. CLDN1 mAb modulates liver progenitor cell phenotype and inhibits**  
1117 **profibrogenic differentiation of activated stellate cells. A.** Left panel: Representative images of  
1118 human cirrhosis-derived primary liver organoids after 4 days of treatment with CLDN1 or Control  
1119 mAb. Scale bars=10 $\mu$ m. Right panel: Size (measured as organoid area) of CLDN1 mAb-treated  
1120 organoids is shown as fold change compared to mean organoid size in Control mAb-treated  
1121 organoids (2 independent experiments with  $n=3$  and  $n=4$  replicates per condition respectively,  
1122  $p=0.03$ , U-test). **B.** Differentially expressed genes in CLDN1 mAb vs. Control mAb-treated liver  
1123 organoids. **C.** Enrichment of gene sets related to epithelial development in CLDN1 mAb and  
1124 enrichment of proliferation associated gene sets versus isotype control mAb treated organoids (all:  
1125  $FDR<0.0001$ , Kolmogorov-Smirnov test). Shown are the most relevant significantly altered  
1126 pathways. **D.** Expression of progenitor marker *TACSTD2* in human cirrhosis-derived primary  
1127 liver organoids treated with CLDN1 mAb or Control mAb ( $n=1$  donor and  $n=3$  independent  
1128 experiments with  $n=3-4$  replicates per condition) is shown as fold change compared to Control  
1129 mAb-treated cells ( $p=0.04$ , U-test). **E.** Effect of CLDN1 mAb on scar-associated myofibroblast  
1130 type A and B marker genes (table S11-S12) in patient-derived HLMFs. **F.** Enrichment plot for  
1131 TNF- $\alpha$ -NF $\kappa$ B signaling (HALLMARK\_TNFA\_SIGNALING\_VIA\_NFKB) in HLMFs treated by  
1132 CLDN1 mAb compared to control mAb. **G.** Representative immunoblots of pS32 I $\kappa$ B $\alpha$ , I $\kappa$ B $\alpha$ ,  
1133 pS536 p65, p65, H3 histone, and beta tubulin in the cytosolic fraction of HLMFs treated with TNF-  
1134  $\alpha$  for 2h ( $n=3-4$  independent experiments with 1 replicate per condition, respectively). **H.**  
1135 Representative immunoblots of pS465/467 SMAD2/ pS423/425 SMAD3, SMAD2/3,  
1136 pThr180/Tyr182 p38, p38, pS473 Akt, Akt, pT202/Y204 ERK1/ pT185/Y187 ERK2, ERK, and  
1137 Actin in HLMFs treated with TGF- $\beta$ . **I.** Quantification of immunoblots of pT202/Y204 ERK1/  
1138 pT185/Y187 ERK2, ERK ( $n= 6$ ), pS473 Akt, Akt ( $n= 4$ ) and pThr180/Tyr182 p38, p38 ( $n= 6$ ) in

1139 HLMFs treated with TGF- $\beta$  (p=0.02, p=0.03 and p=0.03, U-test, respectively). **J.** Expression of  
1140 *ACTA2*, *COL1A1* (n=7 different donors and independent experiments with N=2-4 technical  
1141 replicates per condition), and *FNI* in HLMFs (n=3 different donors and independent experiments  
1142 with N=2-4 technical replicates per condition) treated with CLDN1 mAb or control is shown as  
1143 fold change compared to untreated cells (p=0.003, p=0.01 and p=0.02, Wilcoxon-matched paired  
1144 test, respectively). Original Western blots are shown in figs. S18-S19. \*p<0.05, \*\*p<0.01.  
1145

1146 **Figure 8. CLDN1 as therapeutic target in fibrotic kidney and lung diseases. A.** *CLDN1*  
1147 gene expression in membranous glomerulonephritis renal tissues(14) and fibrotic kidney tissue  
1148 (38) compared to respective healthy kidneys. **B.** *CLDN1* gene expression in pulmonary tissues of  
1149 patients with IPF(39). **C.** Illustration of the UUO and bleomycin mouse models of kidney and lung  
1150 fibrosis. **D.** Representative images of Sirius-red in kidneys from vehicle and CLDN1 mAb-treated  
1151 animals. **E.** Quantification of collagen proportional area in UUO mice treated with vehicle control,  
1152 telmisartan or CLDN1 mAb (*n*=8 mice per group). **F.** Representative images of F4/80  
1153 immunostaining in kidney tissues of CLDN1 mAb- or control-treated animals. Arrows show  
1154 macrophage infiltration. **G.** Representative images of Trichrome masson staining of lung tissue  
1155 from vehicle and CLDN1 mAb-treated animals. **H.** Evaluation of pulmonary fibrosis by Ashcroft  
1156 score (52) in vehicle- (*n*=14), CLDN1 mAb- (*n*=13) and dexamethasone- (*n*=8) treated animals. **I.**  
1157 Representative images of CLDN1 mAb binding to CLDN1 on lung fibroblasts. Scale bar=100µm.  
1158 **J.** Kidney fibroblasts and lung fibroblasts were treated with TNF- $\alpha$  (10 ng/mL), IKK-16 (1 µM),  
1159 TNF- $\alpha$  + IKK16, or vehicle control and subjected to fluorocytometric analysis of CLDN1 mAb  
1160 H3L3 binding, respectively (3 independent experiments with *n*=3 biological replicates per  
1161 condition).  $\Delta$ MFI is shown as fold change compared to untreated cells. **K.** Modulation of gene sets  
1162 characterizing lung fibrosis-associated fibroblast differentiation states in CLDN1 mAb- or control  
1163 mAb-treated IPF patient-derived fibroblasts. **L.** Enrichment plot for TNF- $\alpha$ -NF $\kappa$ B signaling  
1164 (HALLMARK\_TNFA\_SIGNALING\_VIA\_NFKB) in IPF fibroblasts treated by CLDN1 mAb  
1165 compared to control mAb. Vertical bars show mean  $\pm$ SEM and single data points. Horizontal bars  
1166 indicate NES of significantly (FDR<0.25) altered gene sets. \**p*<0.05, \*\*\**p*<0.001, \*\*\*\**p*<0.0001,  
1167 t-test (**A, E, G, J**) or U-test (**B**), respectively. IPF=idiopathic pulmonary fibrosis; MFI=Mean  
1168 fluorescence intensity; UUO=unilateral ureteral obstruction.

## MATERIALS AND METHODS

*Reagents and antibodies.* The following reagents were used for *in vitro* experiments in this study: DMSO, oleic acid and palmitic acid (#D8418, #O1383 and P0500, Sigma-Aldrich), IL6 (Sigma-Aldrich), TGF- $\beta$  (R&D Systems), IFN $\gamma$  (Thermo Fisher Scientific), PMA (Sigma-Aldrich). Humanized CLDN1 specific mAb H3L3 has been described(10) and was produced by Evitria, Schlieren. Murinized CLDN1 specific mAb (TAR-Rm) was generated by co-transfecting chinese hamster ovary (CHO) cells with plasmids containing appropriate heavy and light chain variants as described(10) by Evitria. For proteomic studies, a fully humanized variant derived from the same original OM-7D3-B3 rat anti-human CLDN1 antibody clone (ALE.F02) was used. Differently from H3L3, the Fc region of the ALE.F02 molecule contains three mutations (L234F, L235E and P331S) that have been introduced to reduce binding to Fc gamma receptors whilst maintaining binding to the neonatal Fc receptor. The isotype control antibodies used were palivizumab IgG4(53) (RRID: AB 2910861, Evitria) and motavizumab (RRID: AB 2910856, Evitria).

*CLDN1 expression analysis in liver tissue by immunohistochemistry, immunofluorescence, and in-situ-hybridization.* Immunohistochemistry (total CLDN1): For colocalization experiments, double immunostainings were performed on serial sections (3  $\mu$ m thick) using Claudin1 antibody (#E-AB-30939, Elabscience) and each of the following 5 different antibodies: rabbit polyclonal anti-human CK19 (RRID: AB 2281020, #ab52625, Abcam) at a 1:400 dilution, rabbit polyclonal anti-human EPCAM (RRID: AB 10984102, #PA5-19832, Invitrogen) at a 1:250 dilution, mouse monoclonal anti-human CD34 (RRID: AB 2074356,

1191 #343607, DakoCytomation) at a 1:600 dilution and mouse monoclonal anti-human CD68 (RRID:  
1192 AB\_2314148, #M0814, DakoCytomation) at a 1:800 dilution. Briefly, 3 µm serial sections of  
1193 paraffin-embedded livers were submitted to the appropriate antigen retrieval and incubated with  
1194 rabbit polyclonal anti-human Claudin1 antibody (#E-AB-30939, Elabscience,) at a 1:250 dilution  
1195 1 h at room temperature followed by an anti-rabbit antibody (RRID: AB\_10015288, #111-006-  
1196 045, Jackson Immuno Research) for 30 min (room temperature) and then liquid diaminobenzidine  
1197 substrate–chromogen system (DakoCytomation,). Sections were then incubated with the  
1198 corresponding second primary antibody for 1 h at room temperature followed by the appropriate  
1199 second antibody for 30 min and then by phosphatase alkaline-fast red enzyme system  
1200 (DakoCytomation). Counterstaining was performed using Mayer hematoxylin.  
1201 Immunohistochemistry (non-junctional CLDN1): Frozen liver sections were air-dried for at least  
1202 45 minutes at room temperature (RT) and fixed in zinc formalin for 2 minutes. After rinsing the  
1203 sections in Millipore water for at least 3 minutes, endogenous peroxidase activity was blocked in  
1204 a solution of PBS supplemented with 0.3% H<sub>2</sub>O<sub>2</sub> for 20 minutes. The sections were washed in PBS  
1205 tween for 3 min and then blocked with avidin and then biotin for each 30 minutes. After 3 washes  
1206 in PBS tween, CLDN1 mAb Ale-F02 targeting njCLDN1 was diluted in antibody diluent (Ventana  
1207 antibody diluent, #06440002001, Roche) supplemented with 10% human serum, and incubated for  
1208 1 hour at room temperature. For co-staining with EPCAM, anti-EPCAM antibody (RRID:  
1209 AB\_10984102, #PA5-19832, Thermo Fisher) was added at 5 µg/mL. After 3 washes the  
1210 streptavidin complex was applied for 20 minutes at RT. After 3 washes, slices were incubated with  
1211 DAB for 5 minutes at room temperature and then washed in Millipore water for 2 minutes.  
1212 Counterstaining was performed with hematoxylin (dilution 1/16) for 15 seconds. Slides were  
1213 thoroughly washed in running tap water for at least 2 minutes. The sections were dehydrated and



1214 all slides were mounted. Immunofluorescence: Multicolor immunofluorescent staining was  
1215 performed on formalin-fixed paraffin-embedded sections cut at a thickness of 3 μm. First, slides  
1216 were dewaxed and antigen retrieval was performed in Tris-EDTA buffer (pH8) for 30 minutes at  
1217 99°C followed by bleaching to remove autofluorescence. Slides were incubated with primary  
1218 antibody mixture of anti-alpha-SMA antibody (RRID: AB\_2223500, #M0851, Dako, 1/200), anti-  
1219 CLDN1 antibody targeting total CLDN1 (E-AB-30939, 1/600, Elabscience) and anti-CD68  
1220 (RRID: AB\_2616797, # 916104, Biolegend, 1/150) for 4 hours, followed by incubation with  
1221 fluorescence-labelled secondary antibody mixture for 30 minutes. Slides were mounted with  
1222 mounting medium containing DAPI and images were taken using the Zeiss Axioscan.Z1 slide  
1223 scanner. In-situ hybridization: RNAscope duplex ISH was performed on the Leica Biosystems  
1224 BOND RX platform, 4.5 μm sections were baked and deparaffinized on the instrument, followed  
1225 by target retrieval (30 min at 95°C using Leica Epitope Retrieval Buffer 2) and 5 min protease  
1226 treatment (Advanced Cell Diagnostics (ACD)). RNAscope probes (ACD) directed against human  
1227 CLDN1 and human COL3A1 were hybridized for 2 h at 42°C using RNAscope 2.5 LS Duplex  
1228 Reagent Kit (ACD) followed by RNAscope amplification. Fast red chromogenic detection for  
1229 detection of COL3A1 was performed first, followed by green chromogenic detection (ACD) for  
1230 detection of CLDN1. Dihydrodipicolinate reductase (dapB), a bacterial gene, was used as a  
1231 negative control probe. Sections were counterstained with haematoxylin. Images were acquired  
1232 using Olympus UC90 camera and Olympus cellSense Entry 2.3 imaging software. Staining  
1233 quantification was performed using QuPath version 0.3.2(54).

1234

1235 *Modeling of the claudin-1/antibody complex.* Generation of a CLDN1 structural model:

1236 To date the structure of CLDN1 has not been solved and no structure is available in the protein  
1237 data bank (PDB)(55). We therefore generated an atomistic model by homology modeling.  
1238 Sequence analysis revealed that claudin-19 (CLDN19) has a sequence similarity of 57% with  
1239 CLDN1 and was therefore selected as a template. A structural model of CLDN1 was generated  
1240 and optimized using PRIME, a dedicated pipeline implemented in the Schrodinger suite for  
1241 molecular modeling(56, 57). Generation of the antibody model: The structure of the antibody was  
1242 generated using the antibody modelling pipeline implemented in the Schrodinger suite for  
1243 molecular modeling(58-60). Molecular dynamics simulations: To explore conformational  
1244 variability and dynamics of CLDN1, we performed extensive molecular dynamics simulations. An  
1245 atomistic model of CLDN1 in a membrane was build using the OPM webserver(61). In particular  
1246 CLDN1 was immersed in a POPC lipid bilayer with a concentration of 0.15M NaCl. Furthermore,  
1247 the TIP3P model(62) was used to describe the water molecules whereas all other parts of the  
1248 system were described by the OPLS3e force field(63). The full system was then equilibrated using  
1249 the following protocol: 1. Brownian Dynamics was run for 100 ps in an NVT ensemble (T=10 K)  
1250 applying harmonic restraints on solute heavy atoms (force constant 50 kcal/mol/Å<sup>2</sup>); 2. NVT  
1251 (T=10K) MD simulation of 12 ps in NVT ensemble conserving the same restraints applied in 1.;  
1252 3. NPT (T=300K and P=1atm) MD simulation (12 ps) conserving the same restraints applied in  
1253 1.; 4. NPT (T=300K and P=1atm) MD simulation (24 ps) without restraints. Pressure and the  
1254 temperature were fixed at 300 K and 1 atm by the Martyna-Tobias-Klein barostat(64) and the  
1255 Nose-Hoover chain thermostat(65), respectively. Three independent production runs of 1 μs were  
1256 performed. The DESMOND software in its GPU implementation was used as simulations  
1257 engine(66). Last, a cluster analysis was run to extract the most relevant conformations from the

1258 MD trajectories. This analysis was carried out with the tclust program(67). The CLDN1 backbone  
1259 atoms were considered for both alignment and clustering, the optimal number of clusters was  
1260 automatically determined using the “elbow” method with kmeans(68). Modeling of  
1261 CLDN1/antibody complex: Cluster analysis identified six different clusters. However, only two  
1262 included more than 20% of the conformations sampled during molecular dynamics. The centers of  
1263 these two clusters were, therefore, used for the modelling of the structure of the Claudin-1/antibody  
1264 complex. CLDN1/antibody docking was simulated using the Haddock v2.4 webserver(69, 70) as  
1265 described by and the definition of the epitope given in(9). Two complex structures, one for each  
1266 representative CLDN1 structure, were selected for further investigation. Next, to optimize the  
1267 CLDN1/antibody interface and account for induced-fit effects on the proteins, two complexes were  
1268 simulated by MD for 500ns using the same set-up described before, and the trajectories analyzed  
1269 by cluster analysis. Last, the interaction free energy ( $\Delta G$ ) for the most representative structure  
1270 from the two largest clusters were computed using the PRODIGY software(72) and the model with  
1271 the best (more negative)  $\Delta G$  was selected as the final model of the Claudin-1/Antibody complex.

1272  
1273 **Retrogenix study.** Retrogenix’s cell microarray technology was performed as  
1274 described(73). Briefly, 5484 expression vectors, encoding both ZsGreen1 and a full-length human  
1275 plasma membrane protein or a cell-surface tethered human secreted protein were arrayed in  
1276 duplicate across 16 microarray slides (‘slide-sets’) for a primary screen. An expression vector  
1277 (pIRES-hEGFR-IRES-ZsGreen1) was spotted in quadruplicate on every slide and was used to  
1278 ensure that a minimal threshold of transfection efficiency had been achieved or exceeded on every  
1279 slide. Human HEK293 cells (RRID: CVCL\_0045) were used for reverse transfection/expression.

1280 The test antibody was added to each slide after cell fixation, giving a final concentration of 2  
1281 µg/mL. Detection of binding was performed by using AlexaFluor 647 labelled anti-human IgG Fc  
1282 detection antibody (RRID: AB 2563330, #409320, BioLegend). Fluorescent images were  
1283 analyzed and quantitated (for transfection) using ImageQuant software. A protein ‘hit’ was defined  
1284 as a duplicate spot showing a raised signal compared to background. Hits were classified as  
1285 ‘strong, medium, weak, or very weak’, depending on the intensity of the duplicate spots. To  
1286 confirm the hits and assess specificity, vectors encoding all hits identified in the primary screens,  
1287 plus vectors encoding CD20 and EGFR, were arrayed and expressed in HEK293 cells (RRID:  
1288 CVCL\_0045) on new slides. Confirmation/specificity screens and analyses were carried out as for  
1289 primary screening except that identical slides were treated, after cell fixation, with the test antibody  
1290 individually at the same concentration as before (2 µg/mL), 1 µg/mL Rituximab biosimilar, or no  
1291 test antibody/secondary only (n=2 slides per treatment).

1292

1293 *Isolation of primary liver cells.* Mouse: Primary Mouse Hepatocytes (PMH) were isolated  
1294 from fresh non-diseased mouse liver tissue, as described(74). Human: Isolation of PHH and non-  
1295 parenchymal cells from patients’ liver tissue (table S12) was performed as previously  
1296 described(75). Briefly, human liver tissue samples from surgical interventions were digested using  
1297 a two-step EGTA/collagenase perfusion technique. PHH were depleted by initial centrifugation at  
1298 50xg and nonparenchymal cells were further purified by serial centrifugation at different speed  
1299 and density gradient centrifugation. Fast attachment of Kupffer cells to culture plates as well as  
1300 magnetic separation of endothelial cells using CD31 microbeads (CD31 MicroBead Kit, human,  
1301 Miltenyi) further allowed separation and cultivation of HSCs(75).

1302

**Binding studies of murinized and humanized CLDN1 specific mAbs by flow cytometry.**

Binding of murinized and humanized CLDN1 mAb to cells was analyzed by flow cytometry with  $\sim 1 \times 10^5$  cells in triplicate per condition. PHH and PMH (primary antibody staining): Isolated PHH and PMH were incubated with increasing concentrations of humanized CLDN1 mAb H3L3 or murinized mAb CLDN1 TAR-Rm (0.01-100  $\mu\text{g}/\text{mL}$ ), respectively. 293-T cells (primary antibody staining): 293-T cells (RRID: CVCL\_4U22) were transfected with plasmids encoding for human or mouse CLDN1 fused with cerulean fluorescent protein or empty plasmid fused with cerulean fluorescent protein (kindly provided by M. Evans, Mount Sinai Hospital, New York). Transfected cells were incubated with increasing concentrations of humanized CLDN1 mAb H3L3, murinized CLDN1 mAb TAR-Rm or the respective isotype control antibodies. Activated hepatic stellate cells (primary antibody staining): Isolated HSCs were differentiated into activated HSCs (aHSCs) within 10 days of culture on plastic (76). Phenotypic identity was subsequently confirmed by  $\alpha$ -SMA-positive staining using immunofluorescence (see below). For flowcytometric analysis of CLDN1 mAb binding under conditions of inflammation, transdifferentiated aHSCs were treated with TNF- $\alpha$  (10 ng/mL), IKK-16 (1  $\mu\text{M}$ ) or TNF- $\alpha$  (10 ng/mL) + IKK-16 (1  $\mu\text{M}$ ) for 24 h before incubation with humanized CLDN1 mAb H3L3 or isotype control mAb at 10  $\mu\text{g}/\text{mL}$ . Secondary antibody staining (all cell types): After incubation with the respective mAbs concentrations for 1h, all cells were washed and incubated with phycoerythrin (PE)-conjugated species-specific (human or mouse) secondary antibodies (RRID: AB\_2337676, #109-116-088 or RRID: AB\_2338629, #115-116-146, Jackson Immuno Research) at 4  $^{\circ}\text{C}$  for 45 min to allow detection of binding. Cells were subsequently washed and fixed with 2% paraformaldehyde (PFA). Data were acquired using Cytoflex B2R2V0 (Beckman Coulter) and analyzed using CytExpert 2.1 and FlowJo v10 (Beckman Coulter). All experiments were repeated in at least 3 independent experiments in

1326 triplicate. In case of studies with patients' material, independent experiments with cells derived  
1327 from at least 3 different donors were performed in triplicate. CLDN1 expression was calculated  
1328 as the difference of the mean fluorescence intensities of cells stained with CLDN1 mAb and cells  
1329 stained with the isotype control mAbs. The kinetics of the interaction between humanized or  
1330 murinized mAb against human or mouse CLDN1, respectively, were determined by gating in  
1331 cerulean-positive cells using FlowJo and the Michaelis-Menten mathematical model using R 3.5.1  
1332 (<http://www.R-project.org/>).

1333

1334 *Liver fibrosis mouse models.* All experiments were performed at the animal facility of  
1335 Inserm U1110 according to local laws and ethics committee approval (institutional protocol  
1336 approval number APAFiS #3559, #7216 and #32429). The mice were housed in individually  
1337 ventilated cages with 12h/12h light/dark cycles and *ad libitum* access to food and water.  
1338 *Pharmacokinetics studies.* Three C3H male mice (RRID:MGI:6197584, 6-8 weeks old) were i.p.  
1339 injected with 500 µg of murinized CLDN1 specific mAb TAR-R-mIgG. At day 1, 3, 8, and 15  
1340 after injection, 100 µL blood was harvested under general anesthesia (isoflurane 3%) by retro-  
1341 orbital puncture with dry capillaries. Serum concentrations of the murinized CLDN1 specific mAb  
1342 were quantified by flow cytometry as described(77). Briefly, 3x10<sup>4</sup> CLDN1-overexpressing  
1343 Huh7.5.1 cells were incubated for 30 min at 4 °C with 20 µL of 1/50-diluted serum or serial  
1344 concentrations (0, 0.1, 0.3, 1, 3, 10, and 30 µg/mL) of CLDN1-specific mAb TAR-R-mIgG in  
1345 1:50-diluted serum from an untreated C3H mouse. After extensive washing, cells were labelled  
1346 with PE-conjugated goat-anti-mouse Abs (RRID: AB 2338629, #115-116-146, Jackson  
1347 ImmunoResearch Laboratories) and fixed with 2% paraformaldehyde. Cells were analyzed on a  
1348 BD LSRII FACS. To determine the mAb concentration at each time point, the PE mean

1349 fluorescence intensity (MFI) of all viable cells in experimental samples were compared with that  
1350 of the titration curve. The mAb serum concentrations were then plotted against time and the half-  
1351 life was calculated for each mouse using its regression curve. *DEN-CDA-HFD model*: Forty 7-  
1352 week old male C57BL/6J mice (RRID: IMSR\_JAX:000664, Charles River Laboratories) received  
1353 a single i.p. injection of DEN (100 mg/kg, Sigma-Aldrich) and were subsequently fed with the  
1354 CDA-HFD (A06071302, Research Diet) after 3 weeks. After 6 weeks of diet, the mice were  
1355 randomized in 2 groups, receiving weekly i.p. injections of 500 µg of either CLDN1 specific mAb  
1356 or vehicle control for 16 weeks. After 16 weeks of treatment, all mice were sacrificed, the blood  
1357 was sampled and the liver as well as other major organs (brain, heart, lung, kidney, stomach,  
1358 intestine, spleen, bladder and skin) were harvested and underwent macroscopic and microscopic  
1359 examination (fig. S8). *Humanized liver NASH mouse model*: *Fah<sup>-/-</sup>/Rag2<sup>-/-</sup>/Il2rg<sup>-/-</sup> (FRG) –*  
1360 *NOD* (RRID: IMSR\_JAX:018454) breeding mice were kept at the Inserm Unit 1110 SPF animal  
1361 facility and maintained with 16 mg/L of 2-(2-nitro-4-trifluoro-methyl-benzoyl)-1,3  
1362 cyclohexanedione (NTBC; Swedish Orphan Biovitrum) in drinking water. Six-week-old mice  
1363 were intravenously injected with 1.5 x 10<sup>9</sup> plaque forming units (pfu) of an adenoviral vector  
1364 encoding the secreted form of the human urokinase-like plasminogen activator (Ad-uPA)(21).  
1365 Forty-eight hours later, 10<sup>6</sup> PHH were injected intrasplenically via a 27-gauge needle. For the  
1366 procedure, the mice were kept under gaseous isoflurane anesthesia and received a subcutaneous  
1367 injection of buprenorphine at the dose of 0.1 mg/kg. After transplantation, NTBC administration  
1368 was gradually decreased and completely withdrawn in 7 d. Transplant success was evaluated 2  
1369 months after the procedure by dosing human albumin in mouse serum as previously described(77).  
1370 The mice successfully transplanted were fed with CDA-HFD for 16 weeks and then treated with  
1371 humanized CLDN1-specific mAb 500 µg or vehicle for additional 8 weeks. For the *GalNAc*

1372 siRNA *in vivo* knockdown study, mice successfully transplanted with PHH were fed with CDA-  
1373 HFD for 12 weeks followed by subsequent subcutaneous injections of *in vitro* validated siRNA  
1374 targeting the human *CLDN1* or siCTRL (3 mg/kg/week) for 8 weeks. DDC (3,5-  
1375 Diethoxycarbonyl-1,4-Dihydrocollidine) mouse model: Seven-week-old C57BL/6J male mice  
1376 (RRID: IMSR JAX:000664, Charles River Laboratories) were fed a 0.1% DDC-supplemented  
1377 diet (R03-25, Safe). One week after beginning the 0.1% DDC diet, the mice were randomly  
1378 assigned to either the treatment group (IP injection of 25 mg/kg/week of H3L3 anti-CLDN1 mAb)  
1379 or control group (PBS) for three weeks. Mice were sacrificed after 4 weeks of 0.1% DDC diet and  
1380 plasma and livers were harvested for subsequent analyses. *ELISAs on mouse serum*. CRP was  
1381 measured in collected plasma of the humanized mice using Human C-Reactive Protein/CRP  
1382 Quantikine ELISA Kit (#DCRP00, R&D Systems) according to the manufacturer's instructions.

1383

#### 1384 **Mouse liver tissue staining analysis**

1385 *Histological analysis*. All organs were immediately fixed in a 10% formalin solution after  
1386 harvesting and subsequently included in paraffin. Liver slices stained with hematoxylin & eosin  
1387 (H&E) and Sirius Red were obtained for all mice. For immunohistochemistry staining, the  
1388 following antibodies were used: CD11c (RRID: AB\_2800282, #97585, Cell Signaling), CD3  
1389 (RRID: AB\_1956722, #MA1-90582, Invitrogen), CD4 (RRID: AB\_2573008, #14-9766-82,  
1390 eBioscience), CD8a (RRID: AB\_2572861, #14-0808-82, Invitrogen), CLEC4F (RRID:  
1391 AB\_2081339, #AF2784, R&D Systems), Fibronectin-1 (RRID: AB\_732380, #ab45688, Abcam),  
1392 LY6C (RRID: AB\_302004, #ab15627, Abcam), MHC II (RRID: AB\_10006678, #NBP1-43312,  
1393 Novus Biologicals), MPO (RRID: AB\_307322, #ab9535, Abcam), REL A (RRID: AB\_535932,  
1394 #NB\_100-2176, Novus Biologicals), REL B (RRID: AB\_632341, #sc-226, Santa Cruz), pP38



1395 (RRID: AB 2139682, #4511, Cell Signaling), HSP70 (RRID: AB 1150514, #IMG-80181,  
1396 IMGENEX), FAH (RRID: AB\_2678806, #HPA044093, Sigma),  $\alpha$ -SMA (RRID: AB\_476701,  
1397 #A2547, Sigma). Staining quantification was performed on entire histological slide or on 5 to 10  
1398 consecutive images at 10x or 20x magnification per staining Images were analyzed using ImageJ  
1399 software v1.51j8 (Rasband W, National Institutes of Health, USA) or QuPath version 0.3.2(54).

1400 For the collagen proportional area quantification in humanized areas, two consecutive liver  
1401 cuts were stained with FAH and Sirius Red. The corresponding FAH-positive area in the Sirius  
1402 Red histological slide was selected as region of interest and then the collagen proportional area  
1403 quantified using ImageJ software(78). For quantification of other immunostaining in  
1404 representative humanized area, the humanized areas were selected from the hematoxylin staining  
1405 based on the phenotype of human hepatocytes showing a brighter cytoplasm and different nucleus  
1406 and cytoplasm size compared to mouse ones(21). All the available tissue slides were analyzed with  
1407 two exceptions: for  $\alpha$ -SMA staining in the DEN-CDAHFD model samples were selected on  
1408 fibrosis phenotype, for fibronectin-1 analyses of CLDN1 mAb-treated humanized NASH mice of  
1409 experiment 2, outliers were excluded according to the Rosner test.

1410 In situ hybridization of mouse liver tissues: RNAscope ISH was performed on the Leica  
1411 BOND III platform, 5  $\mu$ m sections were baked and deparaffinized on the instrument, followed by  
1412 target retrieval (30 min at 95°C using EDTA Buffer) and 15 min protease treatment. RNAscope  
1413 probes (ACD) directed against mouse and *Ccl2*, *Ccl20*, *Cxcl10* were hybridized for 2 h at 42°C.  
1414 Staining was performed using BOND RNAscope Brown Detection (DS981) and slides were  
1415 counterstained with haematoxylin. Staining quantification was performed using QuPath version  
1416 0.3.2(54).

1417

1418 *Kidney fibrosis (unilateral ureteral obstruction model, UUO) mouse model:* The  
1419 experiment was conducted by SMC laboratories (Japan) according to local laws and following  
1420 ethics committee approval (SLMC053-1906-8 (UUO): U015). Seven-week-old female C57BL/6J  
1421 mice (RRID: IMSR\_JAX:000664) were obtained from Japan SLC, Inc. and housed and cared for  
1422 in accordance with the Japanese Pharmacological Society Guidelines for Animal Use at SMC  
1423 laboratories, Japan. Animals were housed and fed with a normal diet (CE-2; CLEA Japan) under  
1424 controlled conditions. On day 0, UUO surgery was performed under mixed anesthetic agents  
1425 (medetomidine, midazolam, butorphanol). Mice were randomized to receive CLDN1 mAb  
1426 (500 µg in 100 µL/mouse, n=8) or vehicle (100 µL, n=8) which were administered  
1427 intraperitoneally of twice weekly for 14 days. Telmisartan (30 mg/kg, n=8) was administered  
1428 orally once daily for 14 days. The animals were sacrificed by exsanguination through direct cardiac  
1429 puncture under isoflurane anesthesia (Pfizer Inc.) at day 14. For plasma biochemistry, non-fasting  
1430 blood was collected in polypropylene tubes with anticoagulant (Novo-Heparin, Mochida  
1431 Pharmaceutical Co. Ltd.) and centrifuged at 1,000xg for 15 min. at 4 °C. The supernatant was  
1432 collected and stored at -80 °C until use. Plasma urea nitrogen was measured by FUJI DRI-CHEM  
1433 7000 (Fujifilm). *Histological and image analysis.* To visualize collagen deposition, kidney  
1434 sections were stained using picro-Sirius red solution (Waldeck). For quantification of interstitial  
1435 fibrosis area, bright field images in the corticomedullary region were captured using a digital  
1436 camera (DFC295) at 200-fold magnification, and the positive areas in 5 fields/section were  
1437 measured using ImageJ software. For immunohistochemistry, sections were cut from paraffin  
1438 blocks and deparaffinized and rehydrated. Endogenous peroxidase activity was blocked using  
1439 0.3% H<sub>2</sub>O<sub>2</sub> for 5 min., followed by incubation with Block Ace (Dainippon Sumitomo Pharma Co.  
1440 Ltd.) for 10 min. The sections were incubated with a 100-fold dilution of anti-F4/80 antibody

1441 (RRID: AB 1227368, #T-2006, BMA Biomedicals) at room temperature for 1 hour. After  
1442 incubation with secondary antibody (#31470, HRP-Goat anti-rat antibody, Invitrogen), enzyme-  
1443 substrate reactions were performed using 3, 3'-diaminobenzidine/H<sub>2</sub>O<sub>2</sub> solution (Nichirei  
1444 Bioscience Inc., Japan). For quantitative analysis of inflammation areas, bright field images of  
1445 F4/80-immunostained sections were captured using a digital camera (DFC295) at 200- and 400-  
1446 fold magnifications.

1447

1448 *Lung fibrosis (Bleomycin-induced) mouse model.* The experiment was conducted by  
1449 SMC laboratories (Japan) according to local laws and following ethics committee approval  
1450 (SLMP052-1906-7 (IPF): B048). Six-week-old female C57BL/6J mice (RRID:  
1451 IMSR JAX:000664) were obtained from Japan SLC, Inc. and housed and cared in accordance  
1452 with the Japanese Pharmacological Society Guidelines for Animal Use at SMC laboratories.  
1453 Animals were housed and fed with normal diet (CE-2; CLEA Japan) under controlled conditions.  
1454 On day 0, mice were anesthetized with a mixture of medetomidine (Nippon Zenyaku Kogyo),  
1455 midazolam (Sandoz K.K.) and butorphanol (Meiji Seika Pharma) anesthesia and intratracheally  
1456 administered BLM (Nippon Kayaku) in saline at a dose of 3 mg/kg, in a volume of 50  $\mu$ L per  
1457 animal using a Microsprayer (Penn-Century). Mice were randomized to receive CLDN1 mAb  
1458 (500  $\mu$ g/mouse and 5 mL/kg,  $n=9$ ) or vehicle (5 mL/kg,  $n=9$ ) which were administered  
1459 intraperitoneally twice weekly from day 0 to 20. Dexamethasone (0.25 mg/kg,  $n=9$ ) was  
1460 administered orally once daily from day 0 to 20. The animals were sacrificed at day 21 by  
1461 exsanguination through the abdominal aorta under a mixture of medetomidine, midazolam and  
1462 butorphanol anesthesia. *Histological and image analysis.* Right lung tissues prefixed in 10%  
1463 neutral buffered formalin were embedded in paraffin and sectioned at 4  $\mu$ m. For Masson's

1464 Trichrome staining, the sections were stained with Masson's Trichrome staining Kit (Sigma)  
1465 according to the manufacturer's instructions. The degree of pulmonary fibrosis was evaluated  
1466 using the Ashcroft score(52).

1467  
1468 *Non-human primate study.* The experiment was performed by Charles River Laboratories  
1469 from February to April 2020 according to local laws and following ethics committee approval  
1470 under study number CRL 20229915. The animals were housed in the Charles River Laboratories  
1471 France Safety Assessment SAS test facility (France). This dose-ascending study was performed  
1472 with the fully humanized variant Ale-F02. Five groups of cynomolgus monkey aged from 29 to 33  
1473 month were included in the study. Groups 1 to 3 included 1 animal while groups 4 and 5 two  
1474 animals per group. Animals in group 1 were treated with an intravenous CLDN1-specific mAb  
1475 injection at 0.3 mg/kg, in group 2 at 3 mg/kg, in group 3 at 15 mg/kg, in group 4 at 60 mg/kg, in  
1476 group 5 at 150 mg/kg. The groups 1 to 3 received a single administration, while groups 4 and 5, a  
1477 weekly injection for a total of 4 doses (Day 1, 8, 15 and 22). The animals were observed for 6  
1478 weeks. Parameters monitored included morbidity/mortality, clinical signs, injection site  
1479 observations, body weights, food consumption and clinical pathology parameters (hematology,  
1480 coagulation, clinical chemistry and urinalysis). All animals were sampled for toxicokinetic on Day  
1481 1, before and at various time points after dosing and on Days 7, 14, 21 and 29 as well as Day 42  
1482 for animal 1 to 3 only.

1483 Pharmacokinetic modeling was performed by LYO-X (Allschwil); in brief, for parameter  
1484 estimation and diagnostic plots, Monolix Suite 2019R2, and for the human PK-binding  
1485 simulations, Simulx (Monolix Suite 2019R2), mlxR 4.1.0 (Lavielle 2019) and R 3.6.0 (R  
1486 Development Core Team 2008) were used.

1487  
1488  
1489  
1490  
1491  
1492  
1493  
1494  
1495  
1496  
1497  
1498  
1499  
1500  
1501  
1502  
1503  
1504  
1505  
1506  
1507  
1508  
1509

*Functional assessment of the murinized CLDN1-specific mAb.* Mouse CLDN1-transfected 293-T cells were pre-incubated with murinized CLDN1 mAb or its corresponding murinized isotype control mAb (100 µg/mL) for 1 h at 37 °C and subsequently exposed to HCV pseudoparticles (HCVpp) for 4 h at 37 °C, as described(79). HCVpp entry was analyzed by measuring intracellular luciferase activity after 72 h (relative light units, RLU). Inhibition was expressed as a percentage relative to cells treated with the corresponding murinized isotype control mAb as described(77).

*RNA extraction from human and murine liver tissue.* Liver cells were lysed in TRI-reagent (Molecular Research Center) using GentleMACS Octo Dissociator, and RNA was purified using Direct-zol RNA MiniPrep (Zymo Research) according to the manufacturer’s instructions. RNA quantity and quality were assessed using NanoDrop (ThermoScientific). Gene expression profiling was performed using 250-500 ng total RNA.

*Prognostic liver signature expression analyses.* Profiling of the prognostic liver signature (PLS) was performed using Nanostring nCounter assay as described(80). Induction or suppression of the PLS in gene expression data was determined as previously reported using the Gene Set Enrichment Analysis (GSEA)(81), implemented in GenePattern genomic analysis toolkits. False discovery rate (FDR) <0.25 was regarded as statistically significant(81). PLS was always determined by using control cells, control animals, or control patient-derived tissues as references. Results are presented as simplified heatmaps showing the classification of PLS global status as poor or good prognosis and the significance of induction/suppression of PLS genes (log10 of FDR

1510 values). Global status corresponds to the difference between low-risk and high-risk gene  
1511 enrichments.

1512  
1513 *ChIPseq and CUT&TAG assay.* LX2 cells (RRID: CVCL\_5792) were incubated 24h with  
1514 or without 100 ng/mL TNF- $\alpha$  (Peprotech, #300-01A) and scraped. The CUT&Tag assay against  
1515 H3K27ac (RRID: AB\_2561016, #39133, Active motif) or NF- $\kappa$ B p65 subunit (RRID:  
1516 AB\_10828935, #6956, Cell Signaling Technology) were performed following the manufacturer's  
1517 instructions (Active motif CUT&Tag-IT Assay Kit, #53165, #53160). Briefly,  $1 \times 10^6$  cells per  
1518 conditions were used. The cells were washed 2 times before binding on Concavalin A beads and  
1519 then incubated overnight with primary antibody at the recommended dilution (1:50) or no primary  
1520 antibody (negative control). The next day the corresponding secondary antibody, guinea pig anti-  
1521 rabbit antibody or rabbit anti-mouse antibody (RRID: AB\_11024108, NBP1-72763, Novus  
1522 Biologicals or AB\_228419, #31188, Thermo Fisher) were used at 1:100 dilution in digitonin buffer  
1523 and incubated at room temperature for 1 hour. The CUT&Tag-IT Assembled pA-Tn5  
1524 Transposomes were incubated for 1 hour at room temperature before tagmentation. Cells were  
1525 resuspended in tagmentation buffer and incubated at 37°C for 1 hour, then the tagmentation  
1526 process was stopped by addition of EDTA and SDS. Protein digestion was performed by the  
1527 addition of 80  $\mu$ g/mL of proteinase K and incubated at 55°C for 60 minutes. DNA was retrieved  
1528 using DNA purification columns following the manufacturer's instruction. Library preparation and  
1529 PCR amplification were done using the Kit primers and purified by 2 successive washes with SPRI  
1530 beads (1.1  $\mu$ L/sample volume). Samples were subjected to paired-end sequencing by the  
1531 GenomEast platform on Illumina HiSeq 4000 instrument. The reads were mapped to the HG38  
1532 genome by BWA and peak-calling was performed by MACS2. For H3K27ac 48741 and 61571

1533 peaks were detected in absence and presence of TNF- $\alpha$ , respectively, whereas for p65, 16391 and  
1534 50160 peaks were detected in absence and presence of TNF- $\alpha$ , respectively. RSAT analyses  
1535 ([http://rsat.sb-roscoff.fr/peak-motifs\\_form.cgi](http://rsat.sb-roscoff.fr/peak-motifs_form.cgi)) of the 100 bp surrounding the top p65 1000 peaks  
1536 in absence and presence of TNF- $\alpha$  confirmed a strong enrichment of the RelA/NF- $\kappa$ B recognition  
1537 motifs in the TNF- $\alpha$ -treated sample.

1538

1539 *Organovo ExVivo Human Liver Tissue NASH fibrosis model.* The study was conducted  
1540 by Organovo. PHHs and nonparenchymal cell populations (LECs, HSCs and Kupffer cells)  
1541 cultured in conditioned medium (sugars, free fatty acids and inflammatory inducers) were  
1542 bioprinted in 3D using the NovoGen Bioprinter platform as described(28). Four NASH induced  
1543 ExVivo Human Liver Tissues with Kupffer cells per condition were exposed to Vehicle, CLDN1  
1544 mAb H3L3 or isotype control mAb at 10 or 100  $\mu$ g/mL daily for 21 days. After 21 days, tissues  
1545 were stained with hematoxylin and eosin and Trichromic Masson. Eight sections of each tissue  
1546 replicate underwent histological quantification. One image per each of the eight sections for the  
1547 four tissue replicates stained with Trichromic Masson underwent fibrosis quantification (total 32  
1548 images). Samples treated with isotype and CLDN1 mAbs (10  $\mu$ g/mL) were selected for  
1549 comparative quantitative analyses. Image analysis was performed using ImageJ software.

1550

1551 *Patient-derived liver spheroids and tumorspheres.* Liver tissues from patients with or without  
1552 chronic liver disease (table S7) were gently digested using a two-step digestion method as  
1553 described(25, 75). The sample was then washed with PBS 1x and loaded on a 70  $\mu$ m cell strainer.  
1554 Digested tissue was gently smashed, and the cell strainer washed with up to 10 mL PBS 1x.

1555 Collected cell clusters were further filtered through a 0.45  $\mu$ m filter and centrifuged for 5 min at  
1556 800xg. The cell pellet containing all liver cell types was then re-suspended in Mammocult basal  
1557 medium (StemCell), supplemented with human proliferation supplement (3.4%), hydrocortisone  
1558 (0.056%) and heparin (0.011%) and cultured in 96-well ultra-low attachment plates (Corning,  
1559 Sigma Aldrich). Cell characterization in spheroids by immunofluorescence: Spheroids were fixed  
1560 with formaldehyde (4% for 2 hours), permeabilized with Triton 0,5%, blocked with 5% FBS, and  
1561 incubated with ASGPR1- PE (REA608, Miltenyi, 1:50),  $\alpha$ SMA (RRID: AB\_2223021, #ab5694,  
1562 Abcam, 1:50), CD68 (RRID: AB\_1089059, #333801, Biolegend, 1:50) or CD31-FITC (RRID:  
1563 AB\_2160882, #3528, Cell signaling, 1:50) overnight. Respective species-specific secondary  
1564 antibodies (RRID: AB\_2338078, #111-605-144 or AB\_2338840, #115-545-003, Jackson Immuno  
1565 Research) were added for 1h, followed by washing steps. Spheroids were visualized by Celigo  
1566 imaging cytometer. Spheroid fibrosis model: 150.000-200.000 cells per well were suspended in  
1567 Mammocult complete medium (STEMCELL Technologies) supplemented with 20% donor-  
1568 derived serum (or 20% FBS if donor-derived serum was not available) and seeded on a 96-well  
1569 low-attachment plate (Corning), then spun at 300g for 5 minutes and incubated overnight. The day  
1570 after, spheroids were treated with Mammocult complete medium plus 20% serum supplemented  
1571 with a 2-fold concentrated mixture of oleic acid, palmitic acid, TGF- $\beta$ , LPS, and either CLDN1  
1572 monoclonal antibody or isotype control antibody to reach the final concentrations of 800  $\mu$ M, 400  
1573  $\mu$ M, 10 ng/mL, 100 ng/mL, and 10  $\mu$ g/mL, respectively. Vehicle-treated spheroids served as  
1574 control. Seventy-two hours later, spheroids were lysed, and RNA was extracted using Arcturus  
1575 PicoPure RNA Isolation Kit (Applied Biosystems). Subsequently, total RNA was reverse  
1576 transcribed (H Minus First Strand cDNA synthesis Mix, ThermoScientific) on a Thermocycler



1577 (Bio-Rad T100, Bio-Rad, Hercules). Quantitative PCR was performed on the CFX96 Touch Real-  
1578 Time PCR Detection system with 10  $\mu$ L reaction volumes containing 5  $\mu$ L SYBR Green 2x mix  
1579 (Bio-Rad), 2  $\mu$ L of RNase-free water and 250 nM gene specific sense and antisense primers. For  
1580 qPCR analyses Prime PCR SYBR Green Assays for *COL1A1*, *COL3A1* and *COL4A1* (Biorad)  
1581 were applied according to the manufacturer's instructions. qPCR for *CTGF* and *TACSTD2* was  
1582 analysed with the following primer sequences: *CTGF*: Fw: 5'-ACC GAC TGG AAG ACA CGT  
1583 TTG, Rv: 5'-CCA GGT CAG CTT CGC AAG G; *TACSTD2*: Fw: 5'-CCT GAA CGC AGT TTG  
1584 GAT GTC-3', Rv: 5'-GTA AGG GCA AGC TGA AGA ATA AAT AGA (82). Gene expression  
1585 were normalized to the housekeeping gene *HPRT1* (Fw: 5'-CTG GAA AGA ATG TCT TGA TTG  
1586 TGG, Rv: 5'-TTT GGA TTA TAC TGC CTG ACC AAG) using the  $\Delta\Delta$ Ct method (83).  
1587 Assessment of collagen deposition in spheroids: Healthy liver tissue (**table S7**) was processed into  
1588 multicellular spheroids, stimulated with FFA (100 ng/ml), LPS (100 ng/mL), and TGF- $\beta$  (10  
1589 ng/mL) and then treated with resmetirom (10  $\mu$ M), isotype control antibody (10  $\mu$ g/mL), or  
1590 CLDN1 mAb (10  $\mu$ g/mL) for 4 days. Total collagen deposition was quantified using Total  
1591 Collagen Assay Kit perchlorate-free (Abcam), according to the manufacturer's instructions.

1592

1593 ***Patient-derived liver organoids:*** Organoid establishment and expansion: Organoids were  
1594 established from non-tumorous cirrhotic liver tissue from a patient undergoing liver resection for  
1595 HCC as described(36). Briefly, liver tissue was dissociated using Tumor dissociation kit, human  
1596 (#130-095-929, Miltenyi Biotec) and the gentleMACS Octo Dissociator (Miltenyi) according to  
1597 the manufacturer's instructions. Total cell population was passed through a 75  $\mu$ m cell filter and  
1598 washed 2 times with PBS and centrifuged at 500g, 5 min, 4°C. 10 x 10<sup>3</sup> cells were then re-

1599 suspended in 50  $\mu$ L Corning Matrigel Growth Factor Reduced Basement Membrane Matrix  
1600 (#354230, Corning) and seeded as domes onto 24 well plates. Following incubation for 15 min at  
1601 37°C, 500  $\mu$ L prewarmed initiation medium was added to each well. Once formation of organoids  
1602 was microscopically detected, initiation medium was refreshed by pre-warmed expansion medium  
1603 and medium was replaced every 2-3 days. Organoids were passaged every 1-2 weeks and cells of  
1604 passage 4 were used for perturbation studies. Organoid perturbation study (3 independent  
1605 experiments): Organoids from passage 3 were harvested and washed. Pre-washed organoid cell  
1606 pellet was pre-incubated with 10  $\mu$ g/ml CLDN1 mAb or isotype control mAb in PBS for 1h at  
1607 room temperature. The cell pellet was then washed once with PBS and resuspended in Matrigel  
1608 and seeded as 25  $\mu$ L domes onto 48-well plates. After solidification of Matrigel for 15 minutes at  
1609 37°C, 500  $\mu$ L prewarmed initiation medium supplemented by 10  $\mu$ g/ml CLDN1 mAb or isotype  
1610 control was added to each well. The experiment was performed with 3-4 replicates per condition.  
1611 Organoids were incubated for 4 days at 37°C, representative microscopic images were collected  
1612 and organoids were harvested for RNA extraction using Qiagen RNeasy Mini extraction kit  
1613 (#4106, Qiagen) according to the manufacturer's instructions. Organoid size diameter was  
1614 measured in representative microscopic images at 50-100x magnification using ImageJ.

1615  
1616 *Precision cut ex vivo liver slice culture.* Liver tissue slices (200-500  $\mu$ m-thick) were  
1617 prepared from surgically resected non-tumorous liver tissues from patients with NASH who  
1618 underwent liver resection for HCC (**Fig. 4H-I**) (table S7) and from patients without liver disease  
1619 undergoing liver resection for metastasis of colorectal cancer (fig. S12D) (table S8). The slices  
1620 derived from adjacent non-tumorous tissue were cultured with CLDN1 specific mAb or isotype

1621 control mAb (10 µg/mL) for 24 h and harvested for gene expression analysis, as described above.  
1622 Gene expression data from non-diseased liver tissues (University Strasbourg NASH cohort,  
1623 table S1) were used as reference controls to verify the induction of the PLS in the studied NASH  
1624 patients. For non-diseased tissues, the PCLS were cultured in William's E complete medium  
1625 supplemented with 20% patient serum and were subjected to LPS treatment (100 ng/mL) to induce  
1626 inflammation and to treatment with control (palivizumab IgG4(53)) or CLDN1 mAb (50 µg/mL).  
1627 After 3 days, the tissues were harvested and proteins extracted to assess effect of the treatment on  
1628 EGFR and SRC phosphorylation.

1629  
1630 *Genome wide RNA-seq analyses.* RNA-Seq libraries were generated from 300 ng of total  
1631 RNA using TruSeq Stranded mRNA Sample Preparation Kit (Illumina, Part Number RS-122-  
1632 2101). Briefly, following purification with poly-T oligo attached magnetic beads, the mRNA was  
1633 fragmented using divalent cations at 94 °C for 2 min. The cleaved RNA fragments were copied  
1634 into first strand cDNA using reverse transcriptase and random primers. Strand specificity was  
1635 achieved by replacing dTTP with dUTP during second strand cDNA synthesis using DNA  
1636 Polymerase I and RNase H. Following addition of a single 'A' base and subsequent ligation of the  
1637 adapter on double stranded cDNA fragments, the products were purified and enriched with PCR  
1638 (30 sec at 98 °C; [10 sec at 98 °C, 30 sec at 60 °C, 30 sec at 72°C] x 12 cycles; 5 min at 72°C) to  
1639 create the cDNA library. Surplus PCR primers were further removed by purification using  
1640 AMPure XP beads (Beckman Coulter) and the final cDNA libraries were checked for quality and  
1641 quantified using 2100 Bioanalyzer (Agilent). Libraries were sequenced on the Illumina HiSeq  
1642 4000 as Single-Read 50 base reads following Illumina's instructions. Image analysis and base  
1643 calling were performed using RTA v2.7.3 and bcl2fastq v2.17.1.14.

1644  
1645  
1646  
1647  
1648  
1649  
1650  
1651  
1652  
1653  
1654  
1655  
1656  
1657  
1658  
1659  
1660  
1661  
1662  
1663  
1664  
1665

*In vitro perturbation studies on human activated stellate cells (aHSCs).* Isolated human hepatic stellate cells (HSCs) (75) were seeded at a density of  $5 \times 10^4$  cells/cm<sup>2</sup> in DMEM with 10% FBS on collagen-coated 12-well plates. After 10 days of cultivation on plastic, all cells showed a myofibroblast-like phenotype consistent with an activated stage (76). At this stage (10d of culture), identity and purity of aHSCs were validated by expression of  $\alpha$ -SMA (RRID: AB\_2223021, Abcam), as assessed by immunofluorescence (see below). For analysis of CLDN1 mAb effects on aHSCs activation markers, primary aHSCs were seeded at  $5 \times 10^4$  cells/cm<sup>2</sup> in 12-well plates and treated with CLDN1 mAb (50  $\mu$ g/mL) or vehicle control for 3 days. aHSCs were derived from n=7 different donors (table S12) and experiments were performed in triplicate per condition and donor.

*Immunofluorescence on isolated cells.* Cells were seeded onto 8-chamber cover glasses (Lab-Tek II #1.5, Sigma-Aldrich). The next day, cells were washed twice with PBS and fixed with 4% PFA for 15 min at room temperature, followed by permeabilization with 0.1% Triton-X for 10 min. After two washing steps, cells were blocked for 30 min with 10% FBS. Primary antibody staining with anti- $\alpha$ -SMA Ab (RRID: AB\_2223021, #ab5694, Abcam, 1:100) or anti-CD68 (#CSB-PA282654, CUSABIO, 1:100) and CLDN1 mAb H3L3 or control mAb (10  $\mu$ g/mL, respectively) was performed overnight at 4 °C. Cells were washed with PBS and incubated with goat anti-human Alexa Fluor 488 and/or goat anti-rabbit Alexa Fluor 647 secondary antibodies (RRID: AB\_2337831, #109-515-003 or AB\_2338078, #111-605-144, Jackson Immuno Research) at a dilution of 1:200. Nuclear staining was done using DAPI (1  $\mu$ g/mL) and cells were visualized

1666 using epi-fluorescence and confocal microscopy. Results were confirmed in at least 3 independent  
1667 experiments.

1668  
1669 *Gene expression analyses in 2D cell culture experiments.* Total RNA extraction from 2D  
1670 cell cultures was performed using RNAeasy Mini Kit (Quiagen) according to the manufacturer's  
1671 instructions. Subsequently, 100-500 ng RNA was reverse-transcribed (H Minus First Strand cDNA  
1672 synthesis Mix, ThermoScientific) on a Thermocycler (Bio-Rad T100, Bio-Rad, Hercules).  
1673 Quantitative PCR was performed on the CFX96 Touch Real-Time PCR Detection system with 20  
1674 μL reaction volumes containing 10 μL SYBR Green 2x mix (Bio-Rad), 4 μL of RNase-free water  
1675 and 250 nM gene specific sense and antisense primers. The primer sequences were as follows:  
1676 *ACTA2* Fw: 5'-TGA AGA GCA TCC CAC CCT, Rv: 5'-ACG AAG GAA TAG CCA CGC;  
1677 *COL1A1*: Fw: 5'-CCT CAA GGG CTC CAA CGA G, Rv: 5'-TCA ATC ACT GTC TTG CCC  
1678 *CA*; *TNFA*: Fw: 5'-GAG GCC AAG CCC TGG TAT G, Rv: 5'-CGG GCC GAT TGA TCT  
1679 *CAG C*; *IL6*: Fw: 5'-ACT CAC CTC TTC AGA ACG AAT TG, Rv: 5'-CCA TCT TTG GAA  
1680 *GGT TCA GGT TG*; *TIMP1*: Fw: 5'-GCC CAG AGA GAC ACC AGA GAA C, Rv: 5'-CTA  
1681 *TCA GCC ACA GCA ACA AC AGG*. All gene abundances were normalized to housekeeping  
1682 genes *HPRT1* (Fw: 5'-CTG GAA AGA ATG TCT TGA TTG TGG, Rv: 5'-TTT GGA TTA TAC  
1683 *TGC CTG ACC AAG* in HLMFs) and *GAPDH* (Fw: 5'-GTC TCC TCT GAC TTC AAC AGC G,  
1684 Rv: 5'-ACC ACC CTG TTG CTG TAG CCA A) using the  $\Delta\Delta C_t$  method(83).

1685  
1686 *Western blot analyses of signaling in 2D culture.* TNF- $\alpha$  signaling:  $1 \times 10^6$  aHSCs were  
1687 treated with CLDN1 mAb (10 μg/mL) or control mAb (10 μg/mL) for 3 days in serum free media.  
1688 At day 3 post-treatment, aHSCs were treated again with CLDN1 mAb (10 μg/mL) or control mAb

1689 (10 µg/mL) for an additional 6h, followed by TNF-α stimulation (10 ng/mL) for 2 hours.  
1690 Cytoplasmic and nuclear cell fractions were then isolated using the Cell Fractionation Kit (Abcam,  
1691 ab109719) according to the manufacturer's instructions. Briefly, cells were collected, resuspended  
1692 in buffer A and permeabilized with detergent I. Following incubation for 7 minutes on a rotator at  
1693 RT and centrifugation at 10,000 x g for 1 min, the resultant supernatant fraction was collected and  
1694 considered the cytosol fraction. Following resuspension in buffer A and solubilization with  
1695 detergent II, the cytosol-depleted pellet was centrifuged at 10,000 x g for 1 minutes. Supernatant  
1696 was discarded and cell pellet was resuspended in buffer A and considered the nuclear fraction.  
1697 Protein expression in each fraction was assessed by immunoblotting, with histone H3 (RRID:  
1698 AB 302613, #ab1791, Abcam) and tubulin (RRID: AB 1952434, #GTX101279, GeneTex)  
1699 antibodies being used as markers for nuclear and cytoplasmic fraction, respectively. For  
1700 immunoblotting, the following primary antibodies were used: p65 (RRID: AB\_628017, #sc-8008,  
1701 Santa Cruz Biotechnology), P-p65 (RRID: AB 331284, #3033, Cell Signaling technology), IκB  
1702 (RRID: AB 390781, #4814, Cell Signaling technology), and P-IκB alpha (RRID: AB 561111,  
1703 #2859, Cell Signaling technology). TGF-β signaling: 1x10<sup>5</sup> aHSCs were treated with CLDN1  
1704 mAb (10 µg/mL) or control mAb (10 µg/mL) for 3 days in serum free media. At day 3 post-  
1705 treatment, aHSCs were stimulated with TGF-β (10 ng/mL) for 1 hour to assess SMAD2/3, p38 and  
1706 ERK pathways, or 2 hours to assess Akt pathway. RepSox (2 µM, ab142139, Abcam), SML0543  
1707 (10 µM, Sigma Aldrich), U0126 (10 µM, Sigma Aldrich) or Wortmannin (10 µM, W3144, Sigma  
1708 Aldrich) were used as inhibitors of SMAD2/3, p38, ERK and Akt signaling, respectively. The  
1709 following primary antibodies were used: SMAD 2/3 (RRID: AB 10889933, #8685, Cell Signaling  
1710 technology), P-SMAD 2/3 (RRID: AB\_2631089, #8828, Cell Signaling technology), p38 (RRID:  
1711 AB 330713, #9212, Cell Signaling technology), P-p38 (RRID: AB 2139682, #4511, Cell

1712 Signaling technology), ERK1/ERK2 (RRID: AB\_2140121, #MAB1576, R&D Systems), P-  
1713 ERK1/ERK2 (RRID: AB\_354539, #AF1018, R&D Systems), Akt (RRID: AB\_915783, #4691,  
1714 Cell Signaling technology) and P-Akt (RRID: AB\_2315049, #4060, Cell Signaling technology).  
1715 EGFR signaling: 1x10<sup>5</sup> Huh7 were treated with CLDN1 mAb (10 µg/mL) or control mAb (10  
1716 µg/mL) for 2 days. Medium was then changed to a serum free one, and cultures were treated for 1  
1717 additional day with CLDN1 mAb (10 µg/mL) or control mAb (10 µg/mL). Huh7 were stimulated  
1718 with EGF (10 ng/mL) for 6 hours. Erlotinib (50 nM) was used as inhibitor of EGFR signaling. The  
1719 following primary antibodies were used: EGFR (RRID: AB\_331707, #2232, Cell Signaling  
1720 technology) and p-EGFR (RRID: AB\_2096270, #3777, Cell Signaling technology). SRC (RRID:  
1721 AB\_2106059, #2109, Cell signaling technology), P-SRC (Tyr416) Antibody (RRID: AB\_331697,  
1722 #2101, Cell Signaling technology). Secondary antibodies used were peroxidase AffiniPure goat  
1723 anti-rabbit IgG (H+L) mAb (RRID: AB\_2307391, #111-035-144, Jackson ImmunoResearch) or  
1724 ECL mouse IgG, HRP-linked whole Ab (RRID: AB\_772210, #NA931, Amersham). Protein  
1725 immunodetection of the membranes was performed with Clarity ECL Western Blot Substrate  
1726 (Biorad) in a ChemiDoc MP Imaging System (Biorad).

1727  
1728 *Cell-based models for chronic liver disease.* Huh7.5.1 (RRID: CVCL\_E049) and LX2  
1729 stellate cells (RRID: CVCL\_5792) were cultured in Dulbecco's Modified Eagle Medium (DMEM)  
1730 containing 10% fetal bovine serum (FBS) and 1% DMSO for differentiation (Huh7.5.1<sup>dif</sup> cells) as  
1731 described(84-86). NTCP-overexpressing HepG2 (HepG2-NTCP, RRID: CVCL\_JY40) cells were  
1732 selected using puromycin and cultured in DMEM with 10% FBS as previously described(87).  
1733 HCV: DMSO-differentiated Huh7.5.1<sup>dif</sup> cells were plated in 6-well plates and infected with  
1734 HCVcc Jc1 (genotype 2a/2a) as described (86). HCV infection was assessed at day 10 by qRT-

1735 PCR of intracellular RNA as described (86). CLDN1 mAb or control mAb (palivizumab  
1736 IgG4(53)) (10 µg/mL, respectively) were added for 3 days after HCV infection. HBV: HepG2-  
1737 NTCP cells (RRID: CVCL JY40) were plated in 12-well plates and infected with HBV purified  
1738 from patient serum(87) in presence of CLDN1 mAb or control mAb (10 µg/mL, respectively).  
1739 HBV infection was assessed at day 7 post-infection by qRT-PCR quantification of HBV pre-  
1740 genomic RNA (pgRNA)(87). FFA-NASH model: DMSO-differentiated Huh7.5.1<sup>dif</sup> cells co-  
1741 cultured with LX2 cells (20%) were plated in 12-well plates and exposed to FFA (800 µM oleic  
1742 acid and 400 µM palmitic acid) for 48 hours as described(88). CLDN1 mAb or control mAb  
1743 (10 µg/mL, respectively) were added for 3 days after FFA treatment. Ethanol-ALD model:  
1744 DMSO-differentiated Huh7.5.1<sup>dif</sup> cells were plated in 6-well plates and exposed to ethanol (40  
1745 mM) in presence of CLDN1 mAb or control mAb (10 µg/mL, respectively) for 10 days. Fresh  
1746 medium containing ethanol and mAbs was replenished daily. Each cell culture model was assessed  
1747 in at least three independent experiments, performed in triplicate.

1748  
1749 *Analysis of phosphokinase phosphorylation.* Phosphokinase phosphorylation was  
1750 assessed in cell lysates derived from the NASH *in vitro* model using the Proteome Profiler Human  
1751 Phosphokinase Array Kit (R&D Systems Inc.), according to the manufacturer's instructions.  
1752 Phosphokinases were assessed using biotinylated detection antibodies followed by  
1753 chemiluminescence detection.

1754  
1755 *Pamgene kinase activity profiling in patient-derived spheroids.* Protein tyrosine kinase  
1756 (PTK) and serine-threonine kinase (STK) activities in the patient-derived 3D model of fibrosis  
1757 were assessed by PamGene Assay (PamGene International BV). Patient-derived spheroids were



1758 established and treated with a profibrogenic cocktail as described above. After the 72h treatment,  
1759 4 spheroids were pooled in each biological quadruplicate and proteins were extracted using M-  
1760 PER Mammalian Protein Extraction Reagent (ThermoFisher Scientific). Samples were then spun  
1761 at 16000g for 15 minutes to remove debris. One  $\mu$ g protein were applied on PamChip4 arrays  
1762 containing 196 (PTK) or 144 (PTK) peptides harboring kinase targets/substrates. Fluorescence-  
1763 labelled antibodies against phosphoresidues were used to measure kinase activity in the samples.  
1764 Phosphosites were selected for subsequent analyses if their signals were statistically significantly  
1765 different between conditions (by t-test or ANOVA). The signal per phosphosite is the result of the  
1766 net phosphorylation attributed to the activity of one or more kinases (89, 90). Instrument operation  
1767 and imaging were controlled by the EVOLVE 2.0 software and quantified using BioNavigator 6.3  
1768 (BN6; PamGene International BV). Signal intensities at multiple exposure times were integrated  
1769 by linear regression (S100), Log2-transformed, and normalized using a Combat correction model  
1770 for batch correction where the scaling parameters (mean and sd) were estimated using an empirical  
1771 Bayesian approach. By interpreting kinase activity at multiple phosphosites, an Upstream Kinase  
1772 Analysis (UKA) was performed. Exploiting knowledge on specific kinase-to-substrate  
1773 relationships from publicly available databases, UKA algorithm predicts differential kinase  
1774 activity in the test condition compared to the control. Kinase statistic represents the change in  
1775 kinase activity, indicating inhibition if  $<0$  and activation if  $>0$ . Mean specificity score represents  
1776 the specificity of the change in kinase activity, higher scores highlighting a lower chance of  
1777 observations descending from random set of peptides(91). The hits of our PamGene assay were  
1778 then ordered by Median Final Score, a synthetic measure of both target robustness and  
1779 significance. The 20 top hits were plotted in a heatmap comparing Mean Kinase Statistics of our

1780 model vs those of a recently published liver kinome atlas, established with the same technique  
1781 (34).

1782  
1783 *CLDN1 knockout using CRISPR-Cas9 technology.* Huh7.5.1 stably expressing Cas-9  
1784 endonuclease (Huh7.5.1-Cas9) were DMSO-differentiated for 7 days (Huh7.5.1-Cas9<sup>diff</sup>), and then  
1785 either co-cultured with LX-2 stellate cells (RRID: CVCL 5792, 20%) and treated with free fatty  
1786 acids (FFA; 800  $\mu$ M oleic acid and 400  $\mu$ M palmitic acid) or infected using HCV Jc1. After 3  
1787 (FFA treatment) or 7 days (HCV Jc1 infection), cells were transduced with lentiviruses expressing  
1788 control single guide RNA (sgRNA) or sgRNA targeting *CLDN1* gene expression (sgCLDN1).  
1789 Expression plasmids were provided by Dr. David Root (Broad Institute of Harvard and MIT,  
1790 Cambridge, USA). Transduced cells were selected under hygromycin treatment (500  $\mu$ g/mL) for  
1791 3 days and lysed using iScript RT-qPCR sample preparation reagent. The HCV- or FFA-induced  
1792 PLS was analyzed using nCounter Nanostring technology in cell lysates. In parallel, cells were  
1793 used to analyze *CLDN1* abundance by flow cytometry using a *CLDN1*-specific mAb (H3L3,  
1794 10  $\mu$ g/mL).

1795  
1796 *CLDN1 knockdown using GalNac technology.* The following siRNA sequences were  
1797 designed to target human *CLDN1* or used as non-targeting siRNA (CTRL): *siRNA CLDN1*: 5'-  
1798 UAACAUUAGGACCUUAGAAUU-3' *siRNA CTRL*: 5'-UAAGGCUAUGAAGAGAUAC-3'.  
1799 siRNA were then coupled to GalNac group (Creative Biogene Inc.) for *in vivo* delivery. To validate  
1800 the efficacy of GalNac siRNA, Huh7 cells were transfected with 12 pmol of regular siRNA or  
1801 GalNac siRNA and the corresponding CTRLs by using lipofectamine RNAi Max (Invitrogen,

1802 Cat#13778-150) following the manufacturer's instructions. Knock-down was validated by  
1803 detecting CLDN1 at the cell surface by flow cytometry (see above).

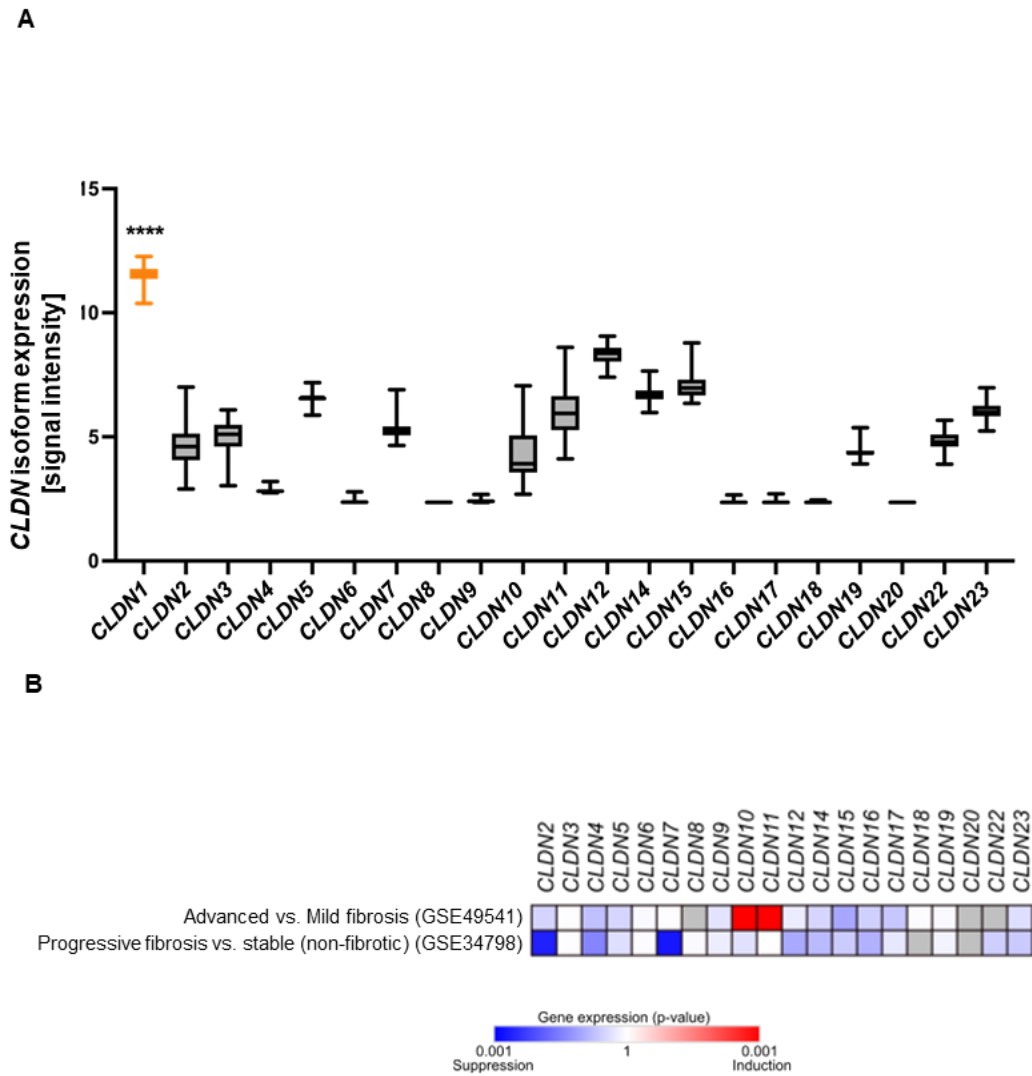
1804  
1805 **CLDN1 co-immunoprecipitation.** For co-immunoprecipitation (co-IP), 5.10<sup>8</sup> Huh7 cells  
1806 (RRID: CVCL-0336) were harvested by scraping in cold PBS<sup>-/-</sup> and plasma membranes were  
1807 extracted by using "Plasma Membrane Protein Extraction Kit (Abcam ab65400) according to  
1808 manufacturers' instructions. Approximately 100 µg of plasma membranes were resuspended in  
1809 250 µL of co-IP buffer (10 mM Tris HCl pH 7.4, .15 M NaCl, 1 mM EDTA, 1 mM EGTA pH 8,  
1810 0.1 % NP40, glycerol 10 % in H2O milliQ water supplemented with protease inhibitors). For WB  
1811 analysis, 50 µL of the total plasma membrane proteins were conserved and used as "Input" control.  
1812 In parallel, 50 µL of magnetic Dynabeads (ThermoFisher) were coupled to 2 µg of CLDN1  
1813 antibody targeting the C-terminus part of the protein to capture membrane interactants (rabbit anti-  
1814 human CLDN1 antibody, ab211737, Abcam) or CTRL antibody (Recombinant Rabbit IgG,  
1815 monoclonal Isotype Control, RRID: AB\_2687931, ab172730, Abcam) 10 min at RT. Dynabeads  
1816 were then mixed with 150 µL of co-IP buffer and 100 µL of plasma membranes and incubated at  
1817 4°C on an orbital shaker. Lasst, Dynabeads were harvested using a magnet (the "Flow-through"  
1818 was conserved for WB analysis) and washed 3 times with cold PBS<sup>-/-</sup>. CLDN1 interactants were  
1819 eluted in 1X Laemmli buffer by heating the beads 5 min at 95°C. CLDN1 IP was validated by WB  
1820 analysis before analyzing the interactants by mass-spectrometry (IGBMC proteomic platform,  
1821 Illkirch-Graffenstaden).

1822  
1823 **Single-cell and single nucleus RNAseq analyses.** Single-cell (sc) RNAseq data: Based on  
1824 the clustering and data normalization of the whole human liver cell atlas (GSE124395)(15), we

1825 analyzed *CLDN1* expression in different cell types. Thereby, we used RaceID methods to draw  
1826 expression t-SNE maps and ggplot2(92) to draw corresponding boxplots of normalized expression  
1827 values. Based on the clustering and provided data of the fibrotic liver cell atlas (GSE136103), we  
1828 analyzed *CLDN1* expression in different cell types. We used Seurat(93) to generate expression  
1829 UMAPs and violin plots, and ggplot2(92) to generate correlation figures. Single nucleus (sn)  
1830 RNAseq data: Based on the clustering of the whole snRNA-seq data set as published in(21), we  
1831 analyzed *CLDN1* expression using Seurat(93). We extracted all epithelial cell clusters  
1832 (hepatocytes, cholangiocytes and bipotent progenitor cells) and performed a pseudotime analysis  
1833 applying slingshot(50). Cell types were annotated based on specific marker gene expression  
1834 including *ALB* (hepatocytes), *EPCAM* (bipotent progenitor cells), and *CK19* (cholangiocytes). An  
1835 expression plot overlayed with the resulting pseudotime trajectories was generated using  
1836 ggplot2(92).  
1837

1838 **SUPPLEMENTARY FIGURES**

1839



1840

1841

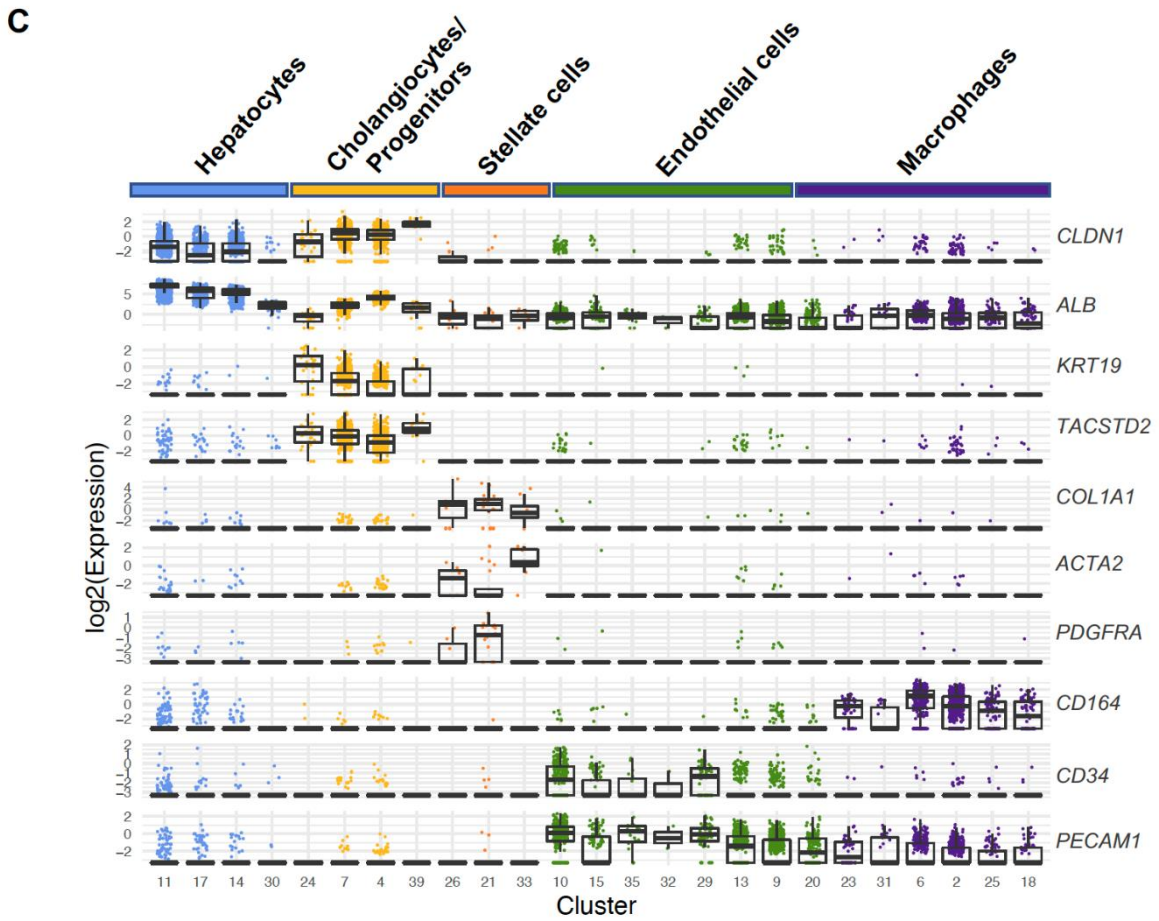
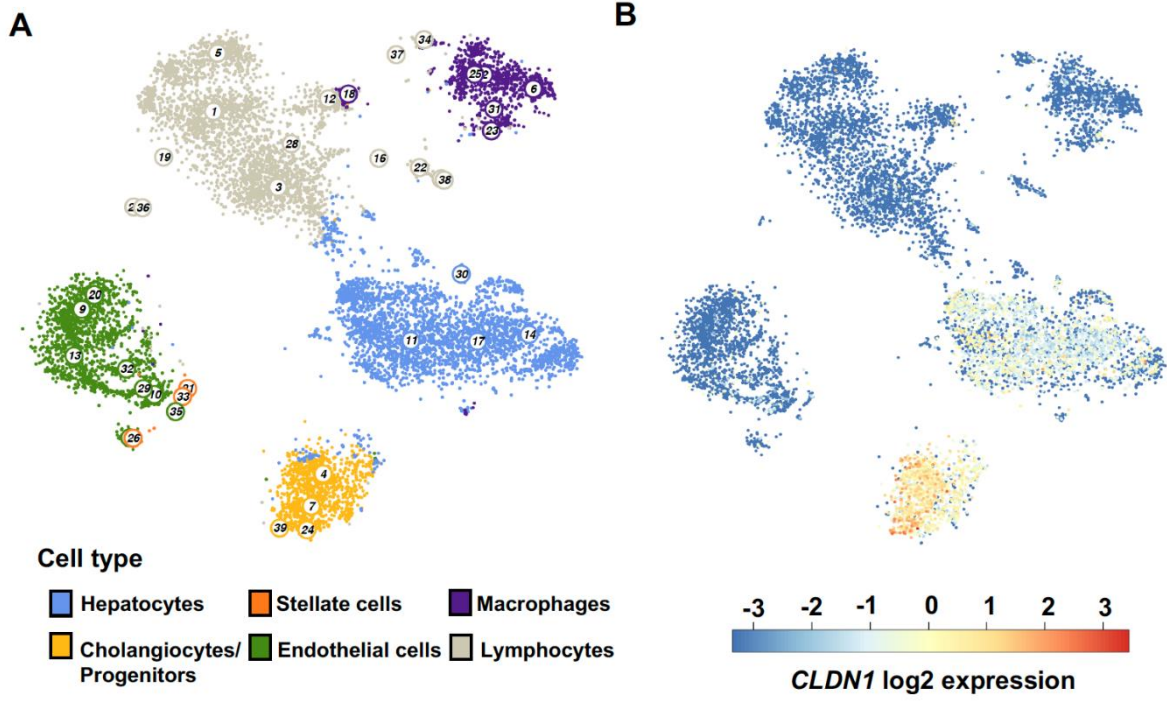
1842 **Figure S1, related to Fig. 1. Expression of different CLDN isoforms in the diseased liver. A.**

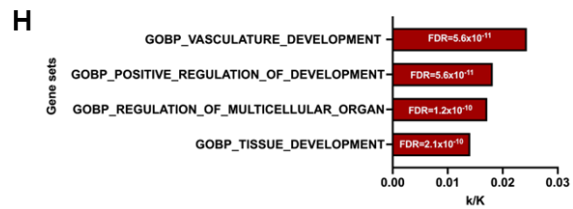
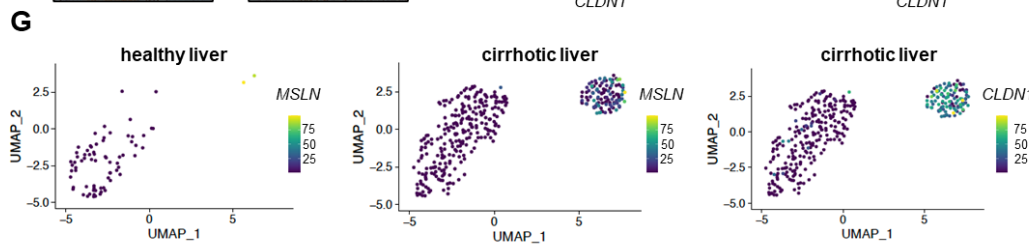
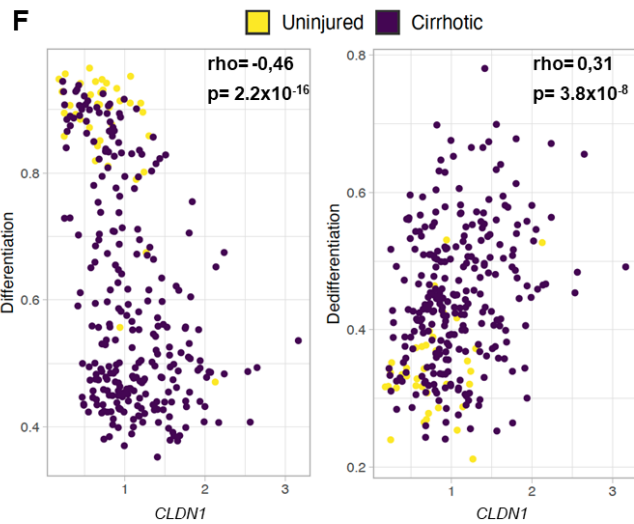
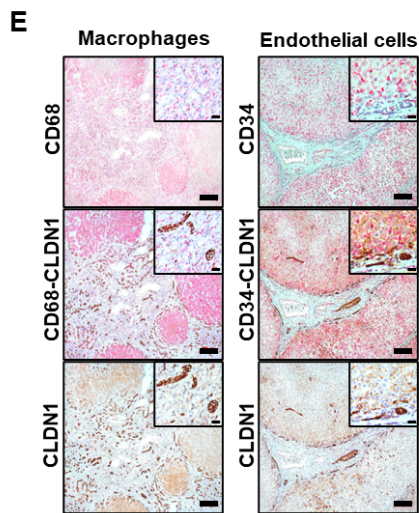
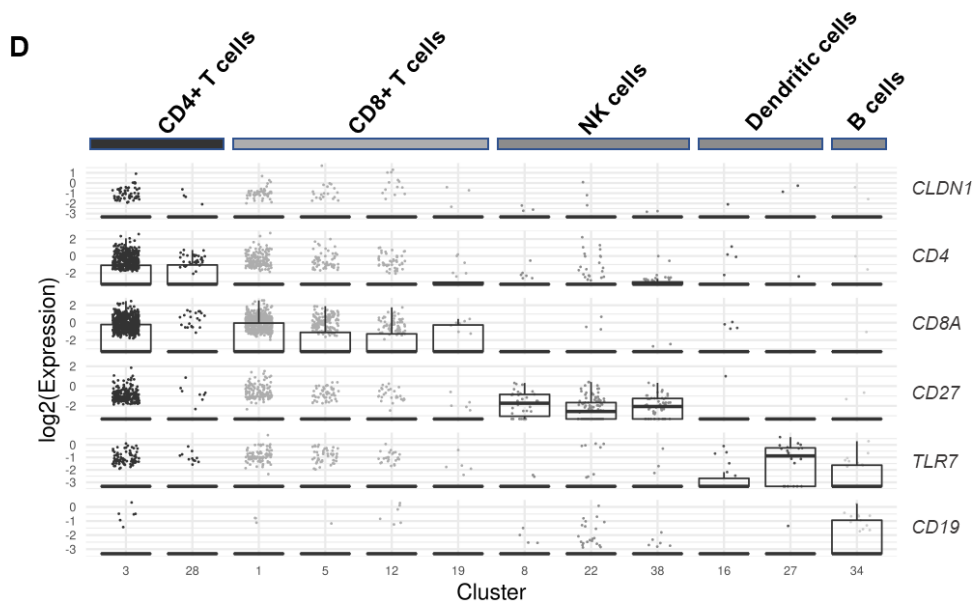
1843 **Expression in NASH fibrotic liver (GSE49541) is shown for all CLDN isoforms. B. Expression of**

1844 **Claudins in livers of patients with NASH with mild (F0-1) or advanced fibrosis (F3-4) (GSE49541,**

1845 **left panel) and liver tissues of HCV-infected patients after liver transplantation with stable or**

1846 progressive fibrotic disease (GSE34798, right panel). Heatmaps indicate significance of induction  
1847 (red) or suppression (blue) compared to control tissue samples of the indicated cohorts. Grey boxes  
1848 indicates that the gene is not covered in the data provided. \*\*\*\*p<0.0001, Kruskal-wallis test.  
1849 Abbreviations: *CLDN*= Claudin.  
1850

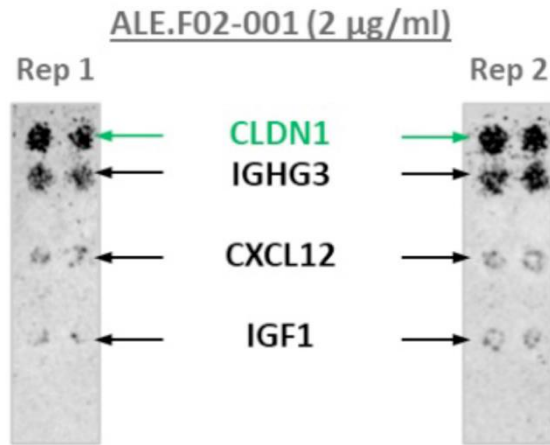






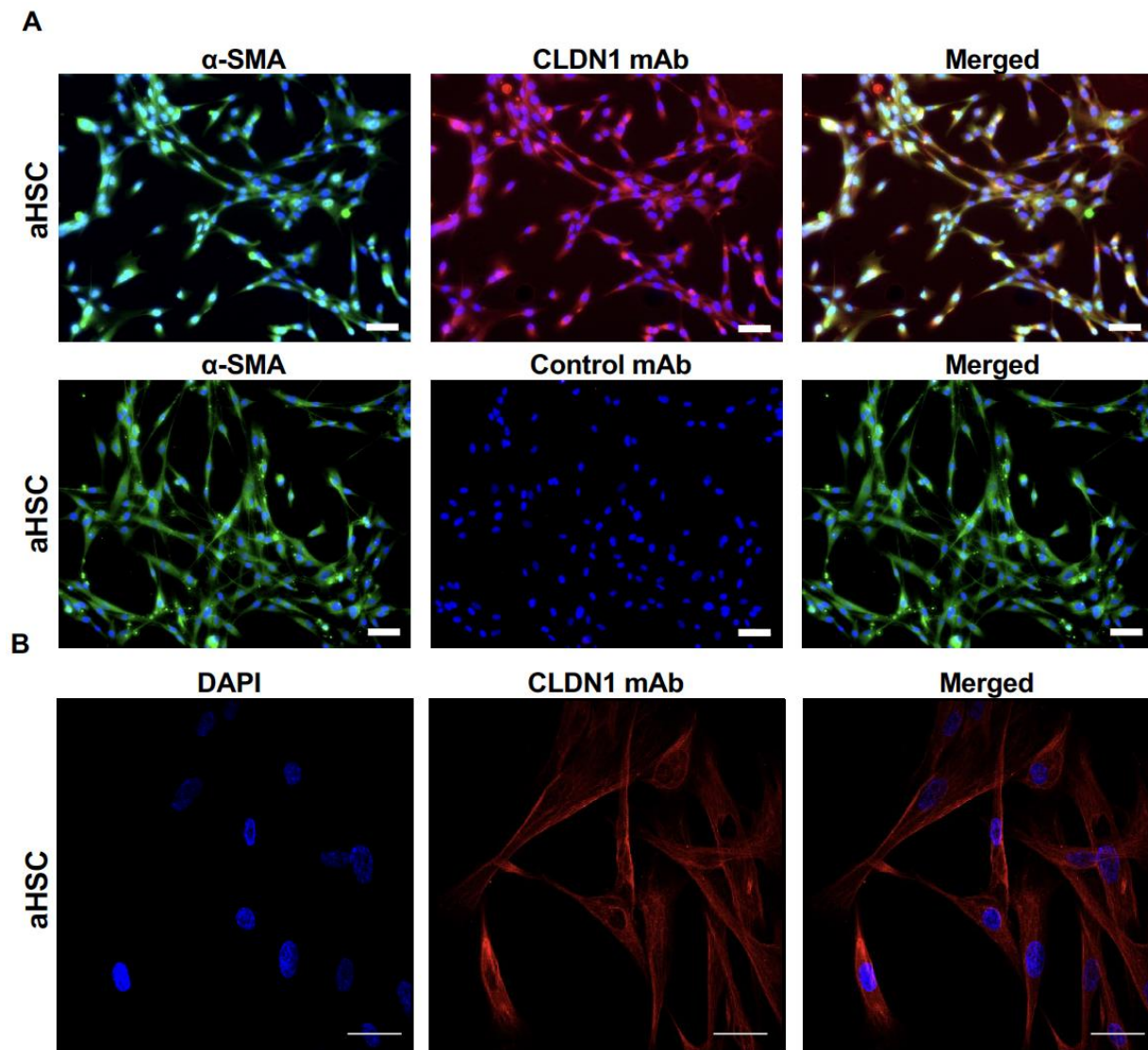
1853 **Figure S2, related to Fig. 1. *CLDN1* expression in different liver cell types analyzed**  
1854 **by scRNAseq. A.** t-SNE map of the human liver cell atlas (GSE124395). **B.** *CLDN1* expression  
1855 **in the human liver cell atlas (GSE124395).** **C.** *CLDN1* and marker gene expression in specific  
1856 **parenchymal and non-parenchymal cell types of the human liver (GSE124395).** **D.** *CLDN1* and  
1857 **marker gene expression in lymphoid cells of the human liver (GSE124395).** **E.** Double staining of  
1858 ***CLDN1* and CD68 (left panel) or CD34 (right panel) by immunohistochemistry indicates absent**  
1859 **expression of *CLDN1* in endothelial cells and macrophages. Scale bars indicate 200  $\mu$ m (large**  
1860 **image) and 100  $\mu$ m (small image), respectively.** **F.** Negative or positive correlation of *CLDN1*  
1861 **expression with grade of differentiation ( $r= -0.46$ ,  $p < 2.2 \times 10^{-16}$ , gene set**  
1862 **“AIZARANI\_LIVER\_C14\_HEPATOCYTES\_2”, left panel) or de-differentiation ( $r= 0.31$ ,**  
1863  **$p=3.75 \times 10^{-8}$ , gene set “AIZARANI\_LIVER\_C39\_EPCAM\_POS\_BILE\_DUCT\_CELLS\_4”,**  
1864 **right panel).** The grade of differentiation or de-differentiation corresponds to the extent of  
1865 **enrichment of gene sets related to mature hepatocytes or *EPCAM*<sup>+</sup> bile duct cells(15) as published**  
1866 **in MSigDB(49). Only cells with *CLDN1* expression covered were included.** **G.** UMAPs of  
1867 ***Mesothelin (MSLN)* and *CLDN1* expression in healthy or fibrotic liver (GSE136103(16)) is shown.**  
1868 **H.** Overlap of *CLDN1* co-expressed genes in human fibroblasts (E-MTAB-10324) with gene sets  
1869 **related to tissue development and differentiation is shown. Abbreviations: *ACTA2*= alpha smooth**  
1870 **muscle actin; *ALB*=Albumin; *CD*= cluster of differentiation; *COL1A1*= Collagen 1A1; *CLDN1*=**  
1871 **Claudin 1; *KRT19*= Keratin 19; *MSLN*= Mesothelin; NK cells= Natural Killer cells; *PDGFRA*=**  
1872 **platelet derived growth factor receptor alpha; *TLR7*= Toll-like receptor 7.**

1873

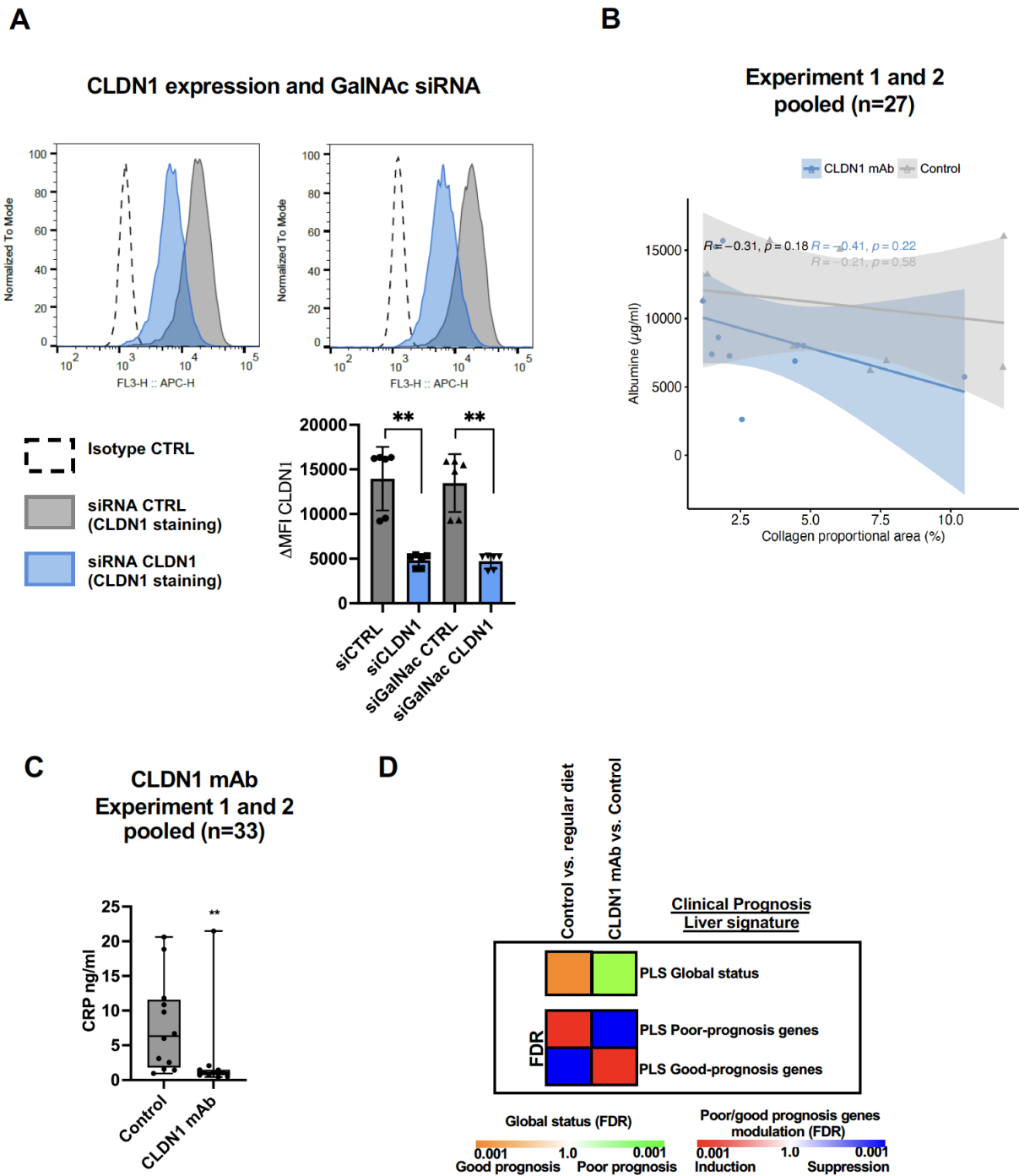


Gene Id	ALE.F02-001 interaction detected?
CLDN1	Yes
CLDN2	No
CLDN3	No
CLDN4	No
CLDN5	No
CLDN6	No
CLDN7	No
CLDN8	No
CLDN9	No
CLDN10	No
CLDN11	No
CLDN12	No
CLDN14	No
CLDN15	No
CLDN16	No
CLDN17	No
CLDN18	No
CLDN19	No
CLDN20	No
CLDN22	No
CLDN23	No
CLDN24	No
CLDN25	No
CLDN34	No

1874 **Figure S3, related to Fig. 1. CLDN1 mAbs are highly specific for human CLDN1.**  
1875 **Interaction of CLDN1 mAbs (representatively shown for ALE.F02) with human plasma membrane**  
1876 **and secreted proteins, as assessed by Retrogenix assay is shown. A strong positive signal was only**  
1877 **detected for hCLDN1 and the IgG heavy chain. No cross-reactivity was found for >5000 other**  
1878 **proteins tested. Minor non-specific interactions were found for CXCL12 and IGF1. Abbreviations:**  
1879 **CLDN=Claudin; CXCL12=C-X-C Motif Chemokine Ligand 12; IGHG3=Immunoglobulin Heavy**  
1880 **Constant Gamma 3; IGF=Insulin like growth factor 1; Rep=Replicate.**  
1881



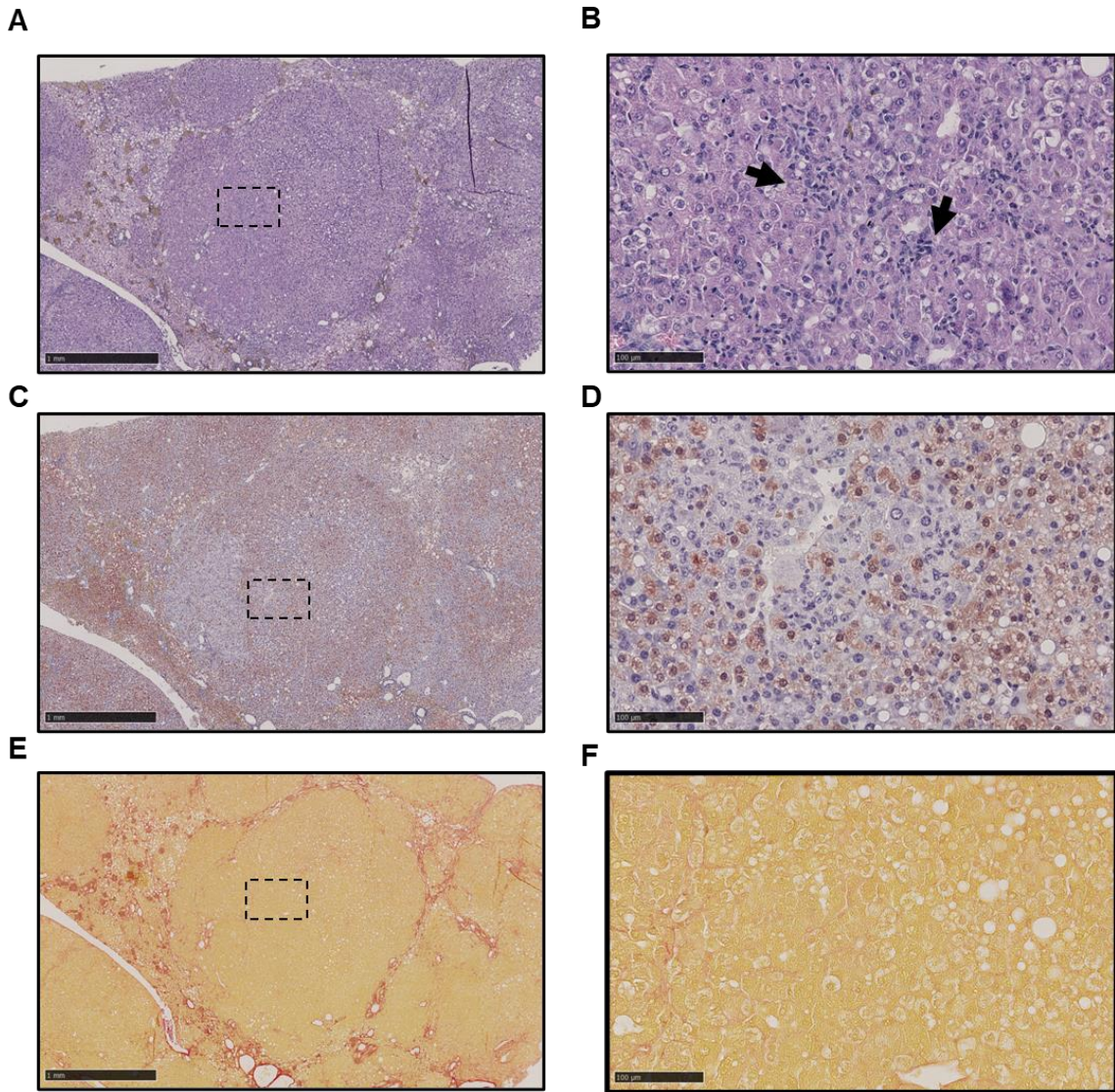
1883 **Figure S4, related to Fig. 1. Non-junctional CLDN1 expression in activated stellate**  
 1884 **cells. A. Representative images of CLDN1 mAb H3L3 binding to patient derived HLMFs, as**  
 1885 **assessed by immunofluorescence. Scale bars indicate 100  $\mu$ m. B. Representative confocal**  
 1886 **microscopic images CLDN1 mAb H3L3 binding to patient derived HLMFs. Scale bars indicate**  
 1887 **100  $\mu$ m. Abbreviations:  $\alpha$ -SMA= alpha smooth muscle actin; CLDN1= Claudin 1; aHSC=**  
 1888 **activated Hepatic stellate cells.**



1891 **Figure S5 related to Fig. 2. Validation of cell surface CLDN1 knockdown by GalNAc**  
 1892 **siRNA in Huh7 liver cells. A. Effect of GalNAc siRNA mediated suppression of CLDN1**  
 1893 **expression and validation in Huh7 cells. CLDN1 protein expression following siCLDN1 or**

1894 GalNAc-siCLDN1 mediated knockdown in Huh7 cells was assessed by flow cytometry (n=2  
1895 independent experiments with n=3 biological replicates per condition). Graphs shows  $\Delta$ MFI of  
1896 CLDN1 mAb compared to Control mAb binding to the respective cells. \*\* p<0.01, U-test. **B.**  
1897 Humanization and fibrosis in humanized liver fibrosis mice. Similar baseline levels of human  
1898 albumin in both treatment groups and absent correlation of humanization with observed  
1899 antifibrotic effects (total collagen proportional area) is shown. **C.** Effect of CLDN1 mAb treatment  
1900 on serum C-reactive protein. Significant reduction of plasma CRP levels in CLDN1 mAb treated  
1901 mice compared to control. Pooled data of experiments 1 and 2 are shown, control n=12, CLDN1  
1902 mAb n=11. \*\* p<0.01, KW test. **D.** Modulation of PLS to good (green) or poor (orange) prognosis  
1903 status(25)in liver tissues of humanized NASH fibrosis mice treated with CLDN1 mAb or control.  
1904 The significance (FDR, Kolmogorov-Smirnov test) of induction (red) or suppression (blue) of PLS  
1905 poor- or good-prognosis genes is illustrated below. Abbreviations: CLDN1= Claudin 1; CRP= C-  
1906 reactive protein; FDR= False discovery rate; PLS= prognostic liver signature.

1907



1908  
1909  
1910  
1911  
1912  
1913  
1914

**Figure S6, related to Fig. 2. Human liver chimeric mice fed with CDA-HFD diet show expansive regenerative nodules of hepatocytes with reactive ductules consisting of mouse and human hepatocytes. A-B. H&E staining at low (A) and high (B) magnification showing an expansive nodule consisting of nodular growing mouse hepatocytes (negative for FAH see C and D), reactive ductules (arrow) and human hepatocytes (positive for FAH see C and D). C-D. Human hepatocytes identified by FAH staining in the chimeric liver are shown at low (A) and high (B)**

1915 magnification. E-F. Sirius Red staining at low (A) and high (B) magnification showing less  
1916 fibrosis in the nodule suggesting a higher proliferation rate of cells in nodules compared to the  
1917 surrounding liver. Scale bar in A, C and E =1 mm. Scale bar in B, D and F=100 μm. Rectangles  
1918 in the left panels correspond to the area illustrated in the right panels. Abbreviations: CDA-HFD  
1919 = choline-deficient, L-amino acid-defined, high fat diet.

1920

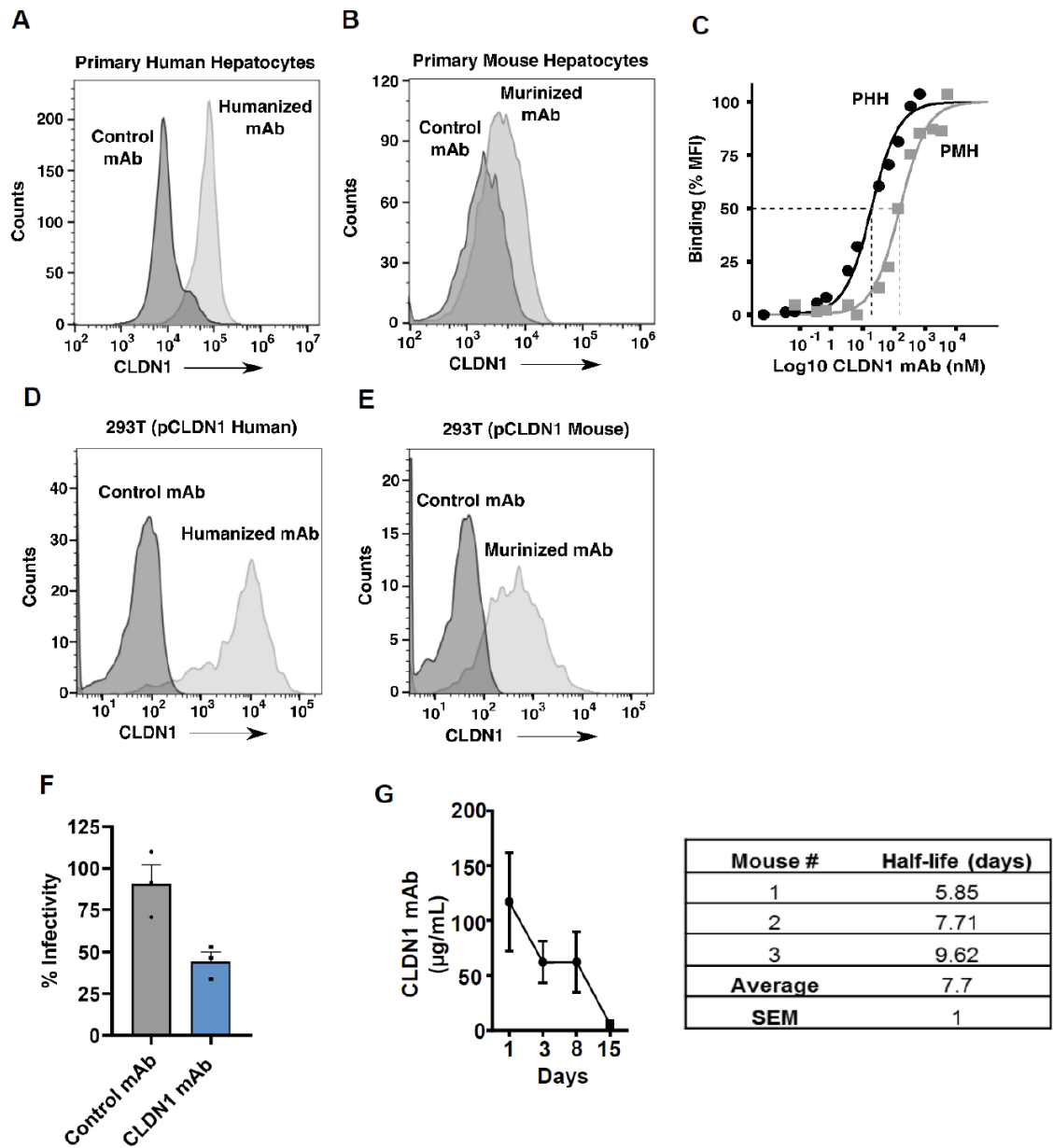
1921

1922

1923

1924

1925



1926

1927

1928

1929

1930

1931

**Figure S7, related to Fig. 3. Functional assessment and pharmacokinetics of the murinized and humanized anti-human CLDN1-specific mAb. A-B.** Binding of humanized anti-CLDN1 mAb H3L3 or murinized CLDN1 mAb to CLDN1 expressed on primary human (PHH) (A) or mouse hepatocytes (PMH) (B) as assessed by flow cytometry is shown **C**. The binding kinetics of the interaction between humanized or murinized mAb against human or mouse



1932 CLDN1 expressed on PHH and PMH were determined by applying the Michaelis-Menten  
1933 mathematical model (PHH: black, apparent Kd of  $\approx 19$  nM; PMH: grey, apparent Kd of  $\approx 154$  nM),  
1934 respectively. D-E. The humanized and murinized CLDN1 mAb show robust binding to 293T cells,  
1935 engineered to express human or murine CLDN1 (mCLDN1), respectively. F. mCLDN1 expressing  
1936 293T cells were incubated with a murinized CLDN1 mAb (100  $\mu$ g/mL) for 1 h at 37  $^{\circ}$ C prior to  
1937 incubation with HCV pseudoparticles bearing glycoproteins JHF1 genotype 2a of HCV. HCVpp  
1938 entry into 293T cells was assessed by measuring luciferase activity after 72 h and is shown as  
1939 percentage relative to entry into untreated cells. \*p<0.05, Student's t-test. G. Left panel: Serum  
1940 concentrations of the murinized CLDN1 mAb were determined at the indicated time points after a  
1941 single i.p. injection of 500  $\mu$ g (25 mg/kg) of murinized mAb into three C3H mice. Right panel:  
1942 The half-life of the murinized CLDN1-specific is shown, as determined using regression curve  
1943 analyses. Results in A-E are representative for at least 3 independent experiments with biological  
1944 duplicates per condition. Abbreviations: SEM=standard error of the mean; PHH=primary human  
1945 hepatocytes; PMH=primary mouse hepatocytes.

1946

1947

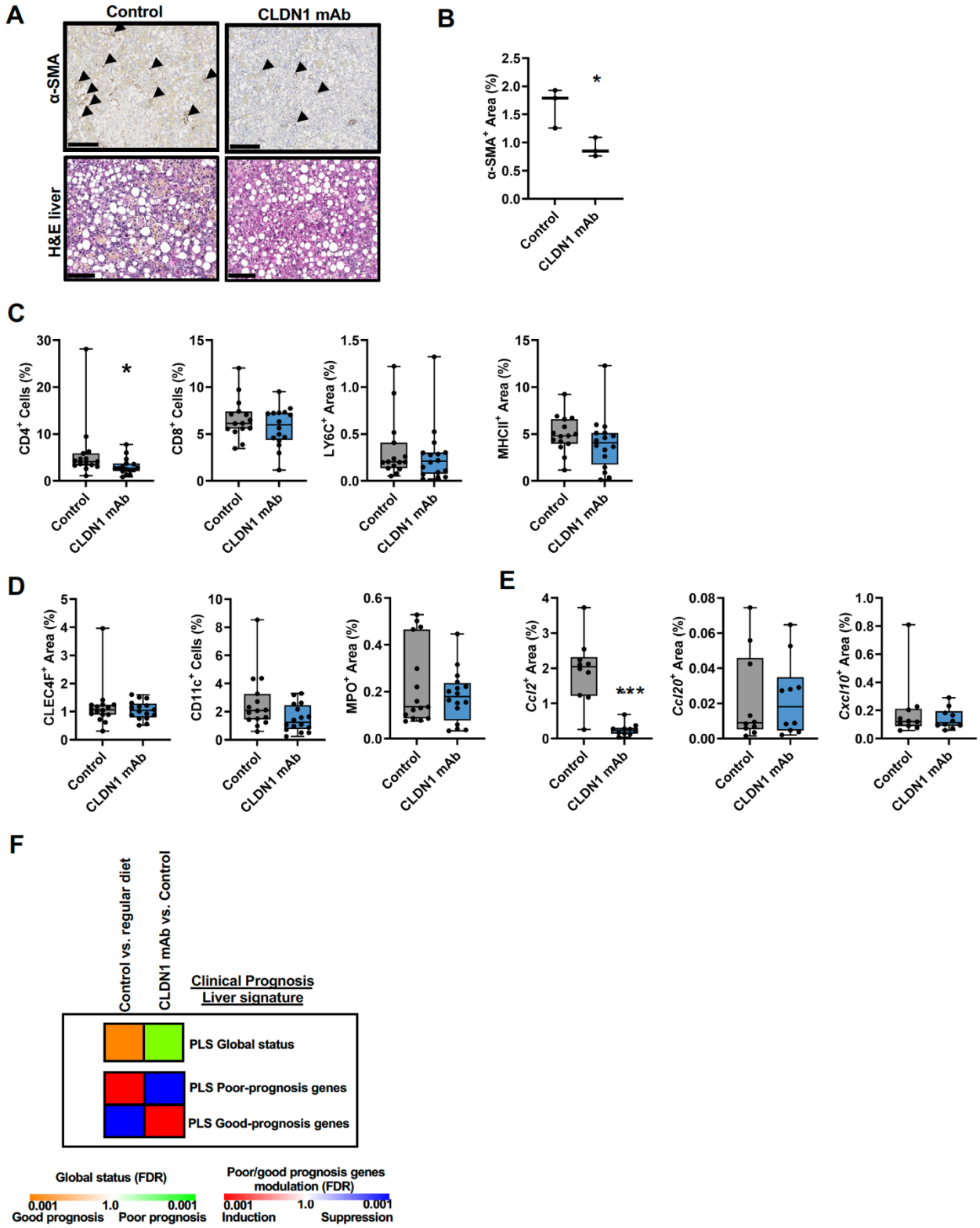
1948

1949

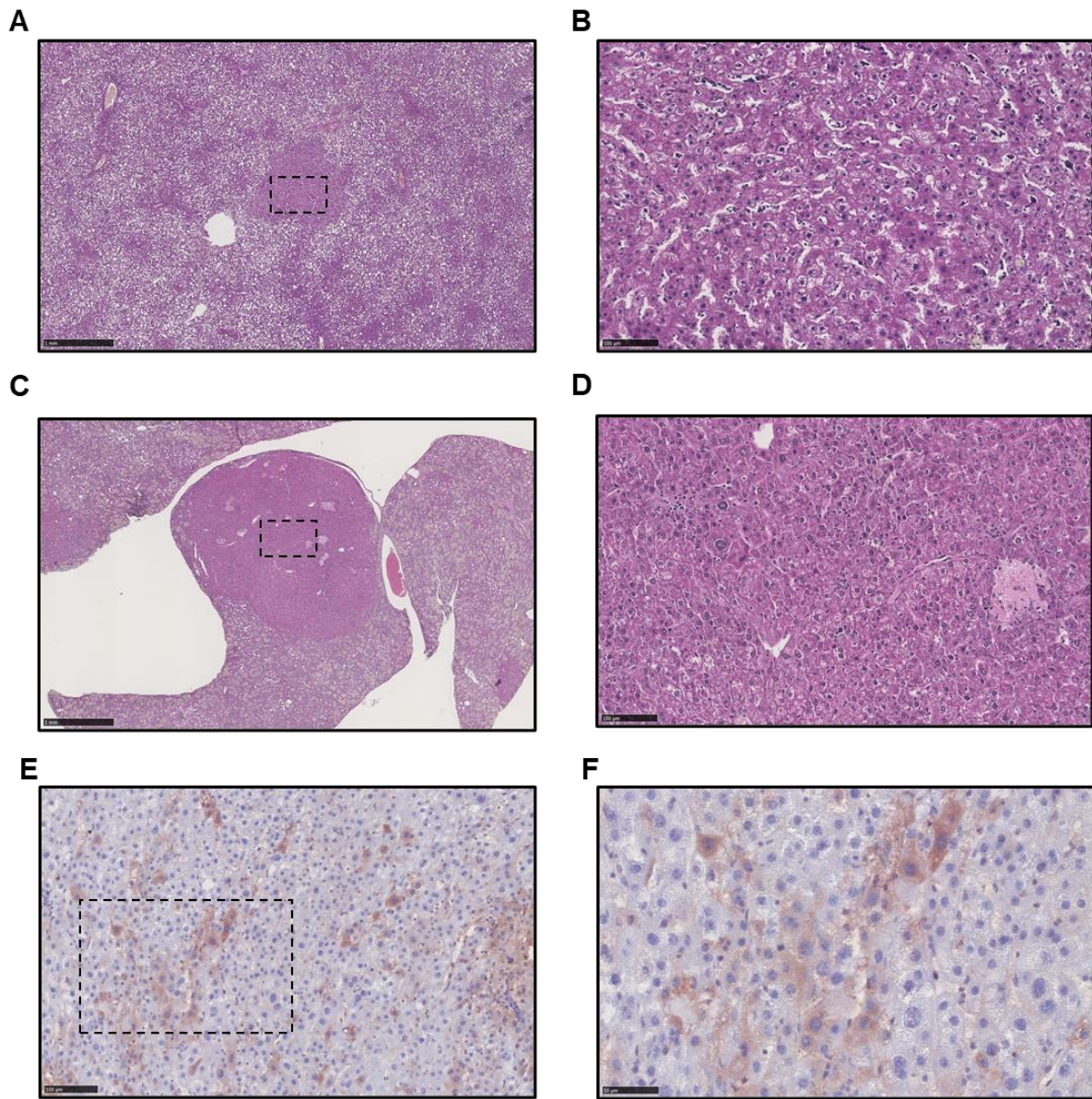
1950

1951

1952



1954 **Figure S8, related to Fig. 3. Analyses of liver inflammatory changes and effects on**  
1955 **the prognostic liver signature (PLS) following CLDN1 mAb treatment in DEN-CDAHFD**  
1956 **mice. A. Representative histological images of myofibroblast activation (upper panel) and**  
1957 **steatosis (bottom panel) in mouse livers. B. Quantitative assessment of  $\alpha$ -SMA proportional areas**  
1958 **in treatment groups. C. Immunostaining shows significant suppression of CD4<sup>+</sup> T cell infiltration**  
1959 **in murine livers of mice treated with CLDN1 mAb (p=0.02, U-test, left panel). No effect was**  
1960 **observed on presence of CD8<sup>+</sup> T cells, LY6C<sup>+</sup> macrophages and MHCII<sup>+</sup> antigen presenting cells.**  
1961 **D. Immunostaining did not reveal any significant changes in the quantity of CLEC4F<sup>+</sup> Kupffer**  
1962 **cells, CD11c<sup>+</sup> dendritic cells and MPO<sup>+</sup> neutrophils in CLDN1 mAb versus control treated mice.**  
1963 **E. Cytokine in situ hybridization reveals significant suppression of *Ccl2* expression in CLDN1**  
1964 **mAb treated DEN-CDAHFD mice (p=0.0003, U-test, left panel), but no effect of *Ccl20* and**  
1965 ***Cxcl10*. F. Modulation of PLS to good (green) or poor (orange) prognosis status(25) in liver tissues**  
1966 **of DEN-CDAHFD mice treated with CLDN1 mAb or control. The significance (FDR,**  
1967 **Kolmogorov-Smirnov test) of induction (red) or suppression (blue) of PLS poor- or good-**  
1968 **prognosis genes is illustrated below. Abbreviations:  $\alpha$ -SMA= alpha smooth muscle actin; *Ccl2*=**  
1969 **chemokine ligand 2; *Ccl20*= chemokine ligand 20; CD= Cluster of differentiation; CLDN1=**  
1970 **Claudin 1; *Cxcl10*= C-X-C motif chemokine 10; CLEC4F= C-Type Lectin Domain Family 4**  
1971 **Member F; FDR= False discovery rate; H&E= Hematoxylin and eosin; LY6C= lymphocyte**  
1972 **antigen 6 complex, locus C; MHCII= major histocompatibility complex II; PLS= Prognostic liver**  
1973 **signature.**



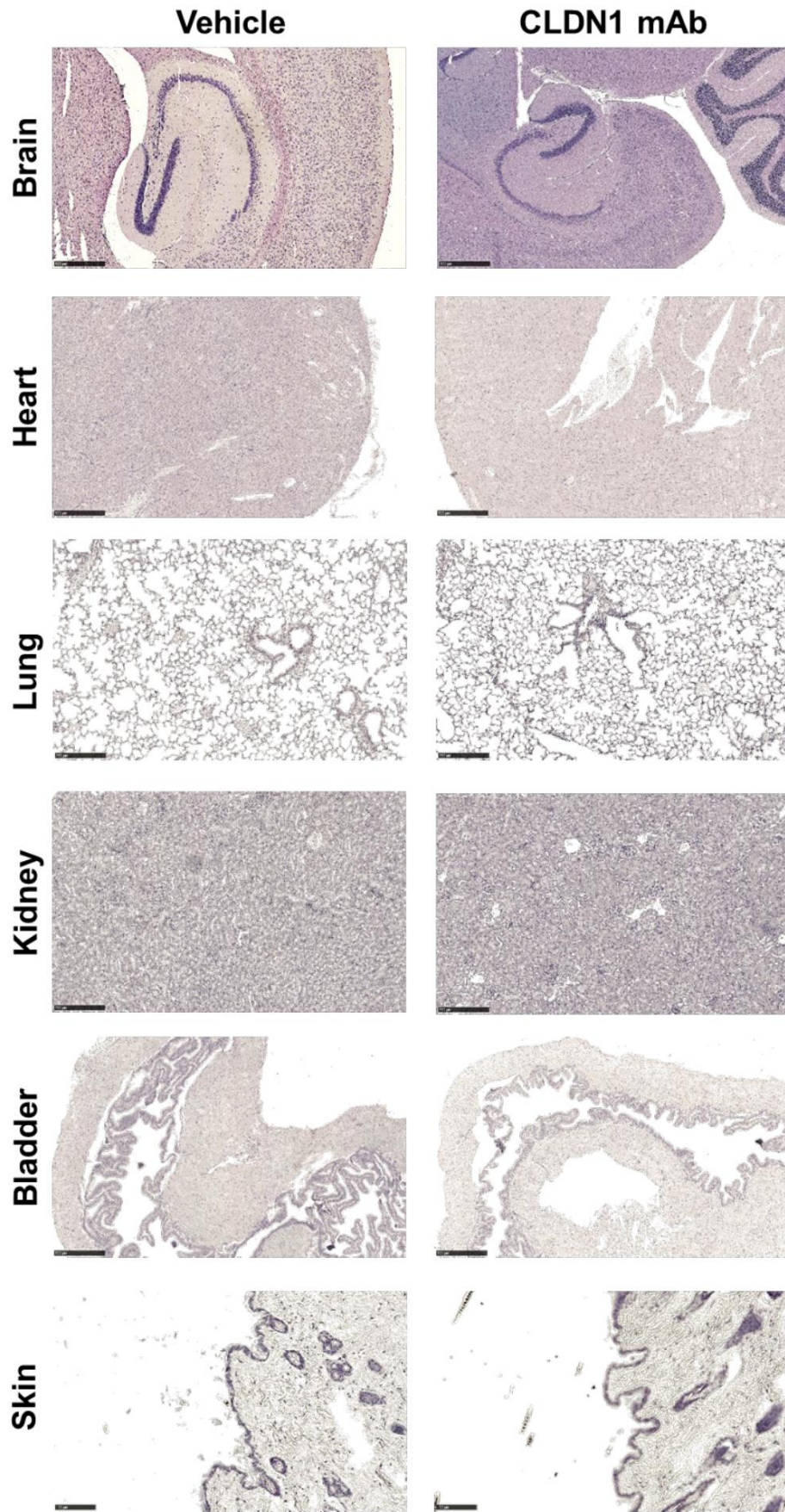
1977  
 1978  
 1979  
 1980  
 1981  
 1982

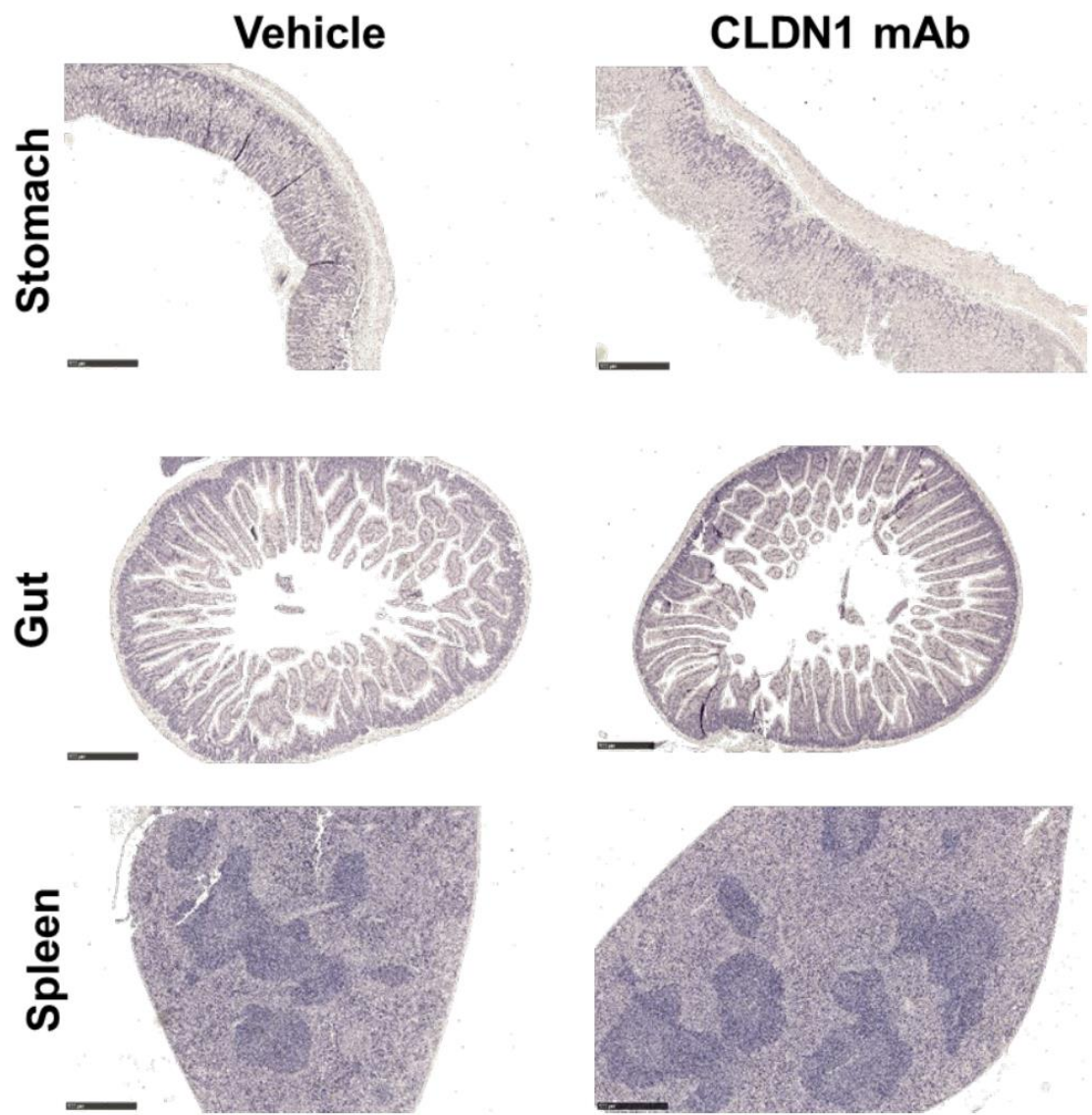
**Figure S9, related to Fig. 3. DEN-CDAHFD mice develop nodules consisting of HCC and preneoplastic lesions. A-B. Example of a preneoplastic lesion at low (A) and high (B) magnification. H&E staining shows an irregular nodule with more compact growth pattern and conserved 1-cell thick liver cell plates. Portal tracts are missing in the nodule. C-D. Example of HCC nodule at low (A) and high (B) magnification. H&E staining shows an expansive nodule**

1983 with compact growth pattern with thickened liver cell plates, anisokaryosis of hepatocytes and the  
1984 absence of portal tracts. E-F. Example of HCC nodule positive for HSP70 by  
1985 immunohistochemistry at low (E) and high magnification (F). Scale bar in A and C=1 mm. Scale  
1986 bar in B, D and E=100  $\mu$ m. Scale bar in F=50  $\mu$ m. Rectangles in the left panels correspond to the  
1987 area illustrated in the right panels.

1988

1989





1991

1992

1993

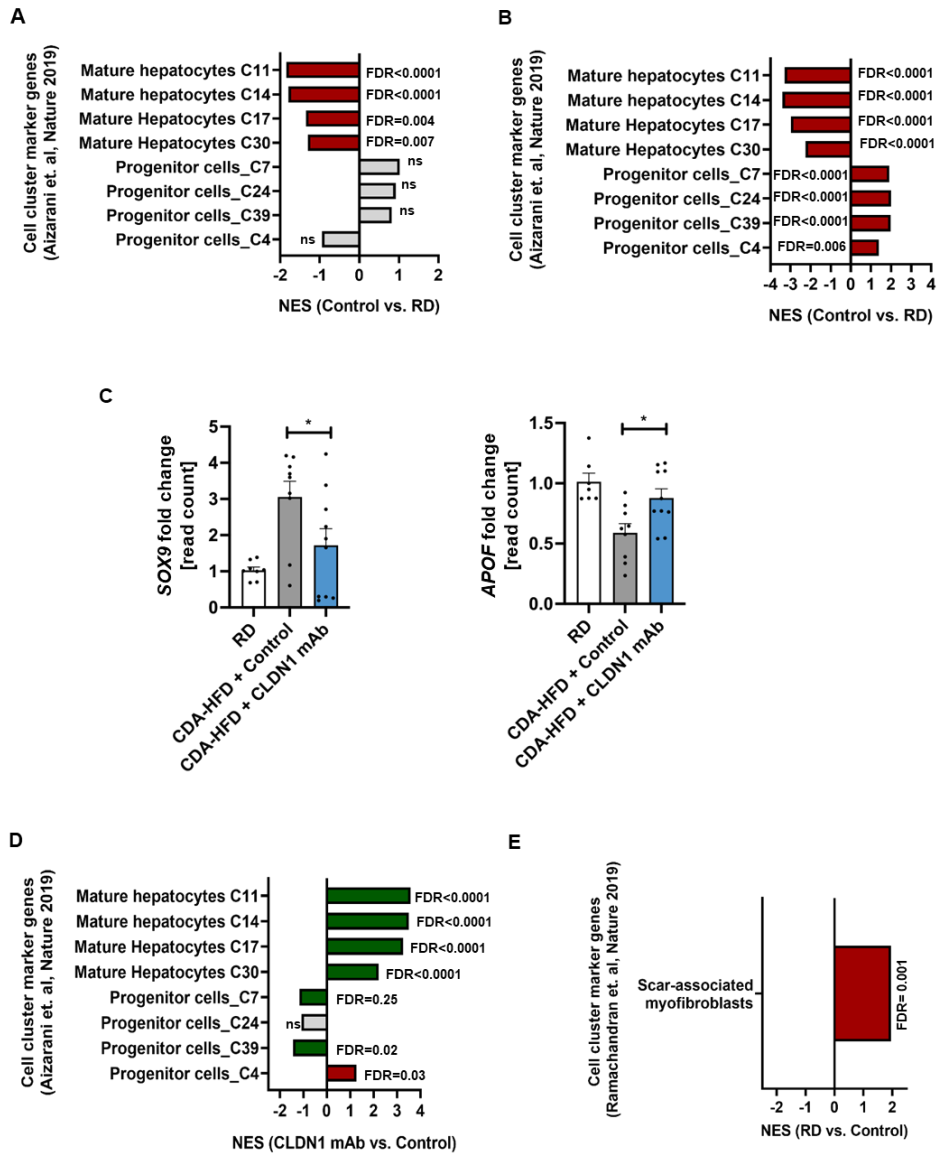
1994

1995

---

Figure S10, related to Fig 3. Histopathology of organs in DEN-CDA-HFD mouse model treated with CLDN1-specific mAb or vehicle control for 16 weeks. All the organs were fixed in formalin, embedded in paraffin, stained by hematoxylin and eosin and analyzed by an expert veterinary pathologist from Pheomonin-ICS, Illkirch, France. One-hundred-twenty-eight

1996 histological slides were analyzed. Eosin was weak on some sections (as shown in the brain image  
 1997 of the vehicle control group) without affecting the quality of the analysis.

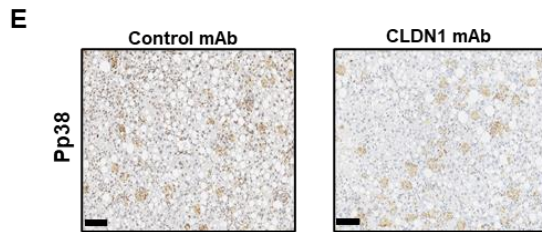
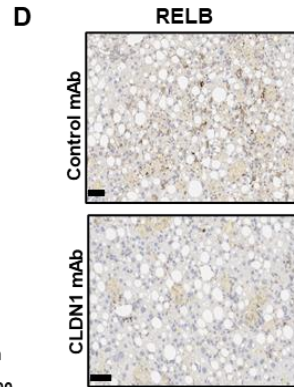
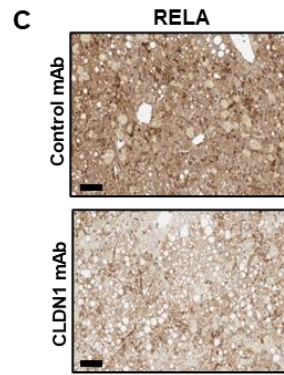
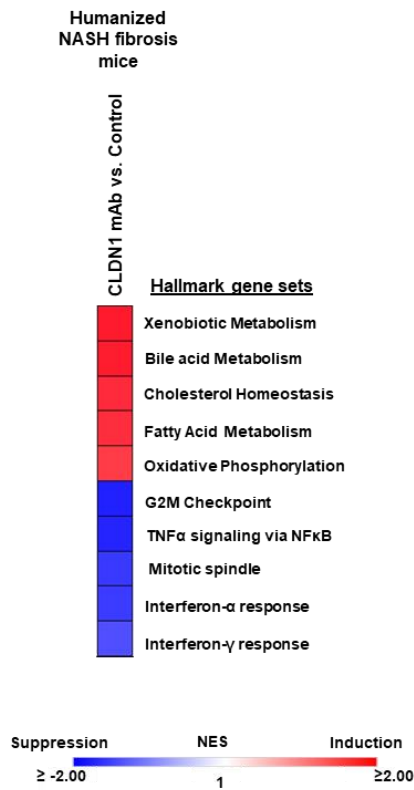
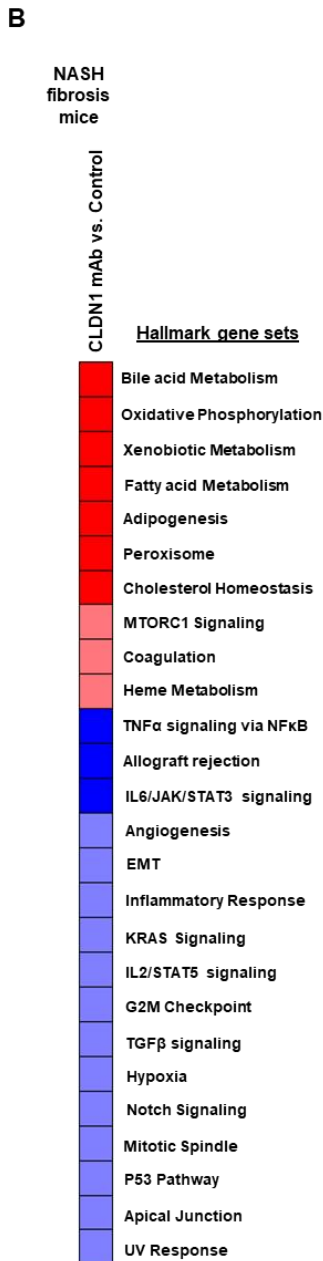
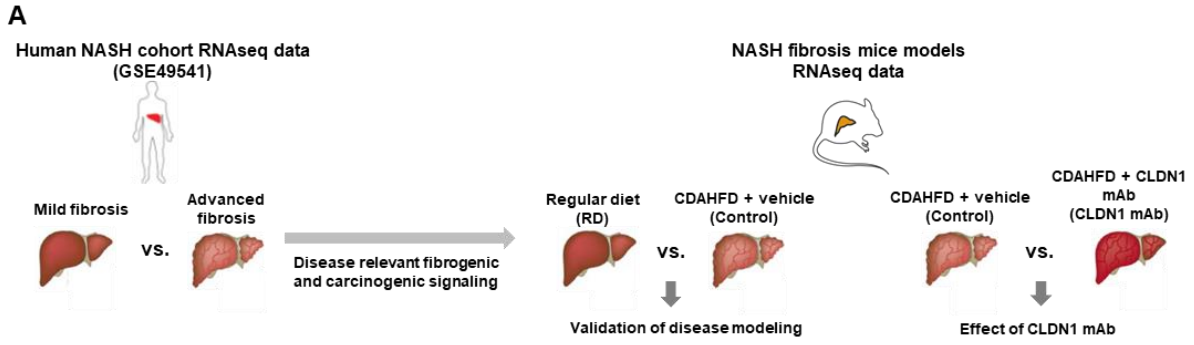


1998

1999 Figure S11, related to Fig. 5. CLDN1 mAb affects cell plasticity *in vivo* and in cell-  
 2000 based model systems. A-B. Differential expression of gene sets characterizing mature hepatocytes  
 2001 ((15) and MSigDB: AIZARANI LIVER C11/C14/C17C30 HEPATOCYTES) and immature  
 2002 progenitor cells ((15) and



2003 MSigDB:AIZARANI LIVER C4/C7/C24/C39 EPCAM POS BILE DUCT CELLS) in  
2004 healthy (RD) versus fibrotic livers in the humanized (A) and classical NASH fibrosis mouse model  
2005 (B) is shown. C. Effect of CLDN1 mAb on progenitor/stem cell marker *SOX9* or *Sox9* and mature  
2006 hepatocyte marker *APOF* or *Apof* in humanized and DEN-CDA-HFD mice respectively (pooled  
2007 data, humanized mice: RD, n=3; CDA-HFD+Control, n=3, CDA-HFD+ CLDN1 mAb, n=4; DEN-  
2008 CDA-HFD mice: RD, n=5, CDA-HFD+Control, n=6, CDA-HFD+ CLDN1 mAb, n=6, p=0.05 and  
2009 p=0.04, U-test, respectively). D. Effect of CLDN1 mAb on hepatocyte de-differentiation in NASH  
2010 fibrosis mice. E. Modulation of gene sets characterizing scar-associated myofibroblasts (table S9)  
2011 in healthy (RD) versus fibrotic livers in the classical NASH fibrosis mouse model. Colored  
2012 horizontal bars indicate NES of significantly (FDR<0.25, Kolmogorov-Smirnov test, respectively)  
2013 altered gene sets. Vertical bars show mean  $\pm$  SEM. \*p<0.05, t-test, respectively. Abbreviations:  
2014 CLDN1= Claudin 1; FDR= False discovery rate; NASH= Non-alcoholic steatohepatitis; RD=  
2015 Regular diet; NES= Normalized enrichment score.



2025 Figure S12, related to Fig. 5. CLDN1 mAb affects cell signaling *in vivo*. A. Graphical  
2026 illustration of methodological approach to assess fibrosis associated signaling in NASH mouse  
2027 models. B. Unbiased assessment of Hallmark gene sets by GSEA in two NASH fibrosis mouse  
2028 models. Heatmaps indicate NES of significantly (FDR <0.05) altered gene sets. C-E.  
2029 Representative immunohistochemistry of RELA, RELB and phospho-p38 in CLDN1 or Control  
2030 mAb treated NASH fibrosis mice.

2031

2032

2033

2034

2035

2036

2037

2038

2039

2040

2041

2042

2043

2044

2045

2046

2047

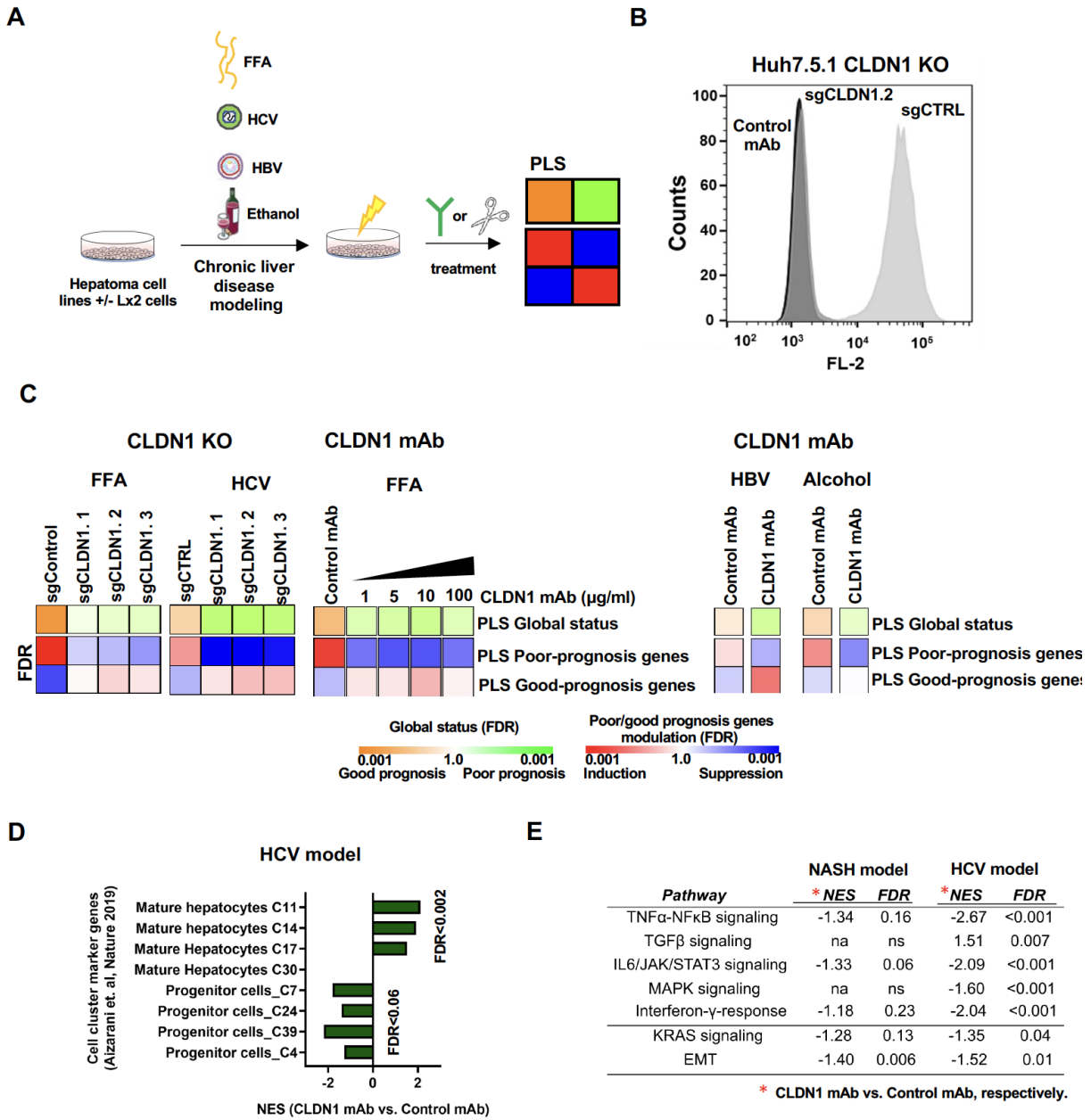


**Figure S13, related to Fig. 5. CLDN1 mAb affects cell circuits relevant for patient prognosis in cell-based model systems. A.** Graphical illustration of PLS assessment in *in vitro* models of all major etiologies of chronic liver disease. **B.** Absent binding of humanized CLDN1

2052 mAb to Huh7.5.1-Cas9 cells expressing single guide RNAs (sgRNAs), assessed by flow cytometry  
2053 is shown. C. Modulation of PLS to good (green) or poor (orange) prognosis status in sgCLDN1 or  
2054 sgCTRL transfected- as well as CLDN1 mAb or control mAb-treated *in vitro* models of NASH,  
2055 alcoholic liver disease, HBV and HCV infection compared to Mock cells. The significance (FDR,  
2056 Kolmogorov-Smirnov test) of induction (red) or suppression (blue) of PLS poor- or good-  
2057 prognosis genes is illustrated below. D. Modulation of liver progenitor and mature hepatocyte  
2058 related gene sets in Huh7.5.1<sup>dif</sup> infected with HCV and treated with CLDN1 mAb or control mAb.  
2059 E. Modulation of fibrosis- and carcinogenesis-associated signaling pathways by CLDN1 mAb in  
2060 the HCV and NASH *in vitro* model. Abbreviations: HBV= Hepatitis B Virus; HCV= Hepatitis C  
2061 virus; EMT= epithelial-mesenchymal transition; FDR= False discovery rate; FFA= Free fatty  
2062 acids; KO= Knockout; NES= Normalized enrichment score; PLS= Prognostic Liver Signature;  
2063 SEM= Standard error of the mean; sg= single guides.

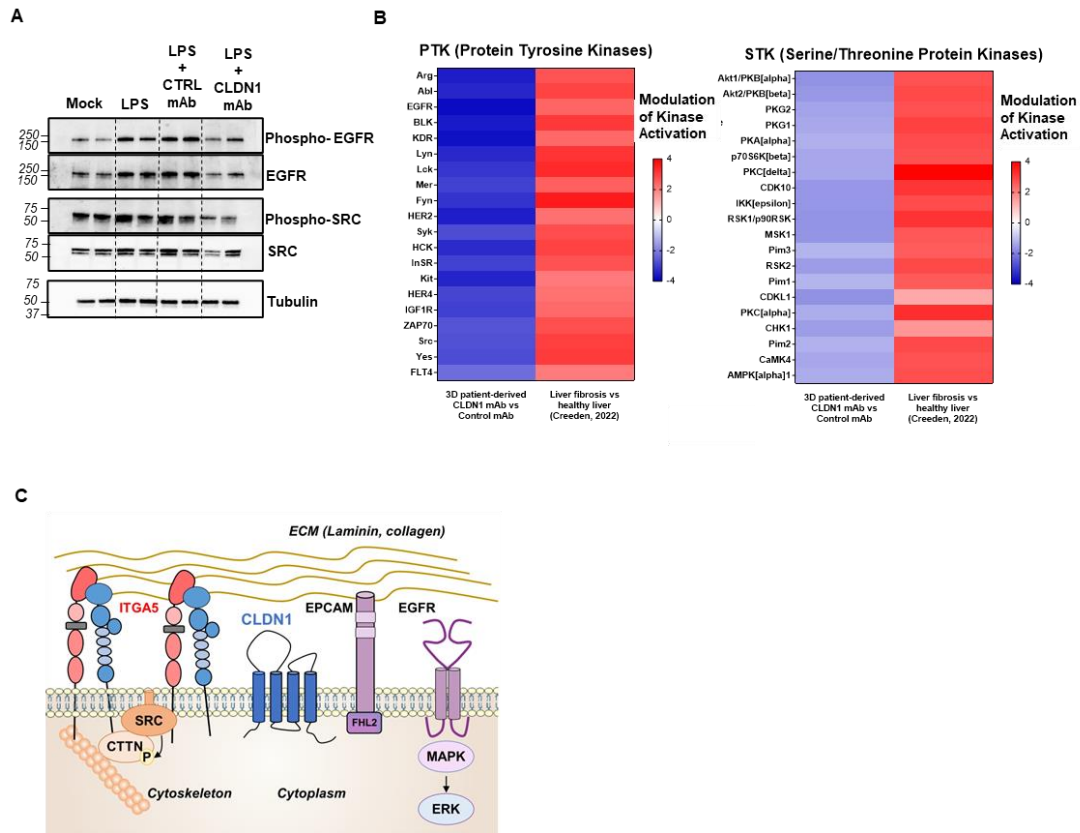
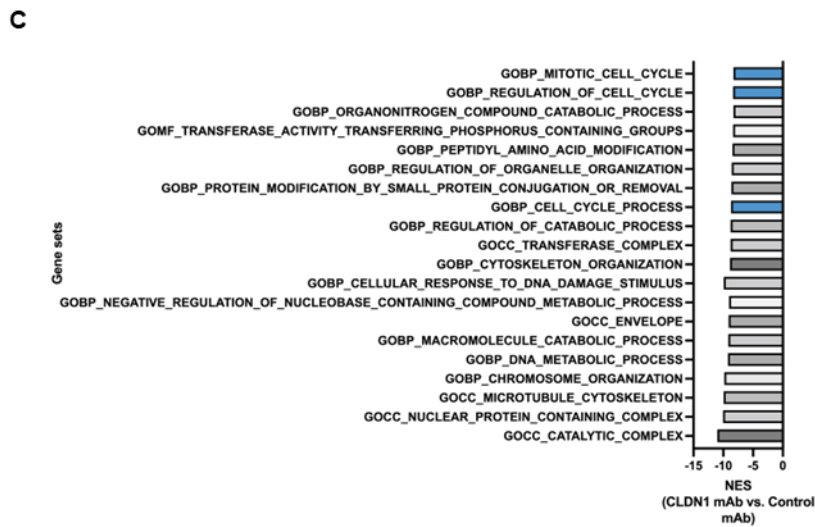
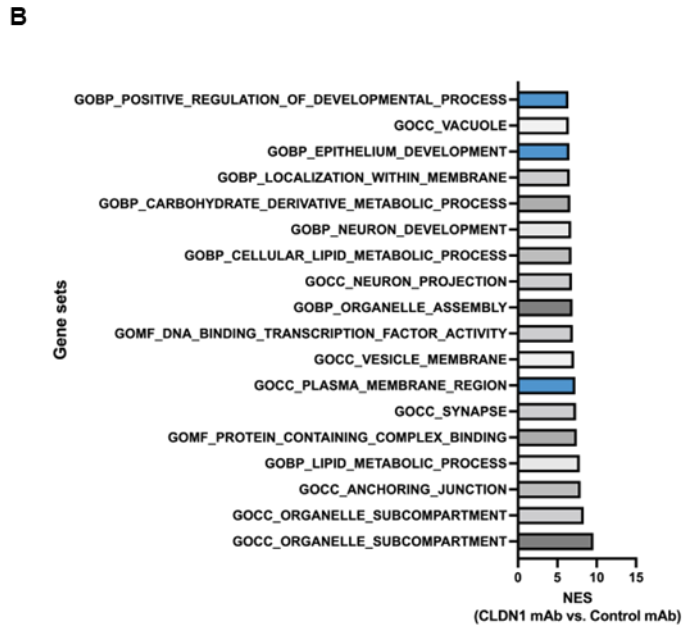
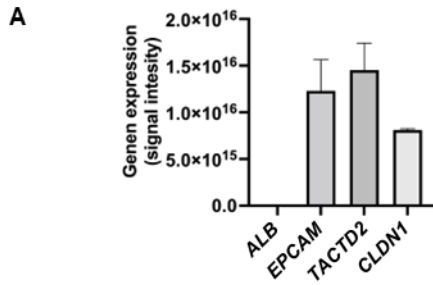


**Figure S14, related to Fig. 5-6. CLDN1 mAb modulates membrane receptor signaling**

**in precision cut liver slices and spheroids. A. CLDN1 mAb suppresses ERK and Src phosphorylation in precision cut liver slices. One representative experiment out of two is shown. B. Heatmap showing the 20 most strongly modulated Protein Tyrosine kinases (PTK) and Serin/Threonine Protein Kinases (STK) in CLDN1 mAb vs. Control mAb treated spheroids (left panels). The modulation of the activities of the same kinases in fibrotic vs. healthy liver as described in a recently published kinome atlas of the fibrotic liver(34) is shown in the right panels. C. Model of CLDN1 receptor membrane biology. CLDN1 interacts with EGFR, ITGA5 and EPCAM mediating SRC and EGFR/ERK signaling. Abbreviations: CLDN1 = Claudin 1; EGFR= Epithelial growth factor receptor; LPS= Lipopolysaccharide, PTK= Protein Tyrosine Kinase; STK= Serin/threonine Protein Kinase.**



2086

2087

2088 Figure S15, related to Fig. 5. CLDN1mAb modulates gene expression related to cell  
2089 proliferation and epithelial cell development in cirrhotic liver derived organoids. A. Gene  
2090 expression of *ALB*, *EPCAM*, *TACSTD2* and *CLDN1* by RNAseq in cirrhosis-derived liver  
2091 organoids. B-C. RNAseq data of CLDN1 mAb or control mAb-treated cirrhotic liver derived  
2092 organoids were assessed by GSEA. Bars indicate normalized enrichment score of all significantly  
2093 (FDR< 0.05, Kolmogorov-Smirnov test) enriched gene ontology pathways in CLDN1 mAb (A) or  
2094 control mAb-(B) treated organoids. Blue color highlight most relevant pathways in liver organoids  
2095 shown in Fig. 7D. Abbreviations: CLDN1= Claudin 1.

2096  
2097  
2098  
2099  
2100  
2101  
2102  
2103  
2104  
2105  
2106  
2107  
2108  
2109  
2110



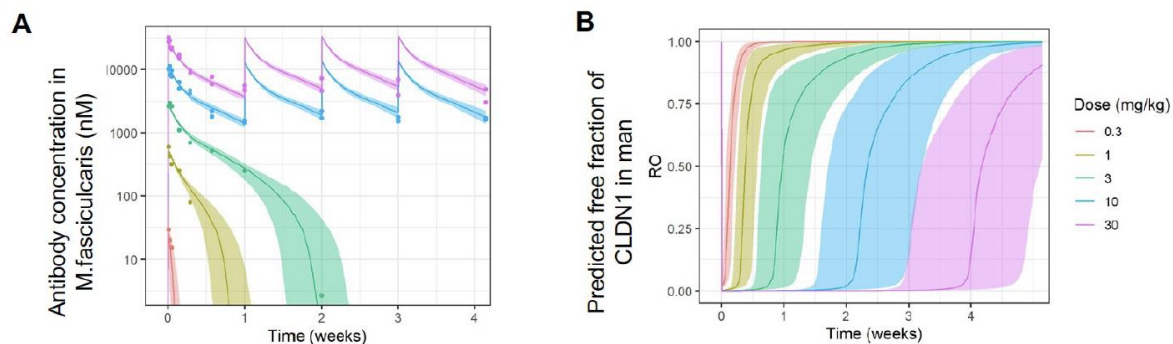


**Figure S16. Anti-CLDN1 mAb pharmacokinetics in non-human primates. A.**

Predicted exposure of the anti-CLDN1 antibody ALE.F02 in macaques (median, 5th and 95th percentiles from 200 simulated profiles). Dots are the observed serum concentrations. All data in nmol/L, color correspond to the dose levels. B. Predicted receptor occupancy in human, indicating the total systemic free accessible CLDN1 not occupied by the administered antibody as a function of time. Shown are median, 5<sup>th</sup> and 95<sup>th</sup> percentiles from 100 simulated PK/PD profiles.

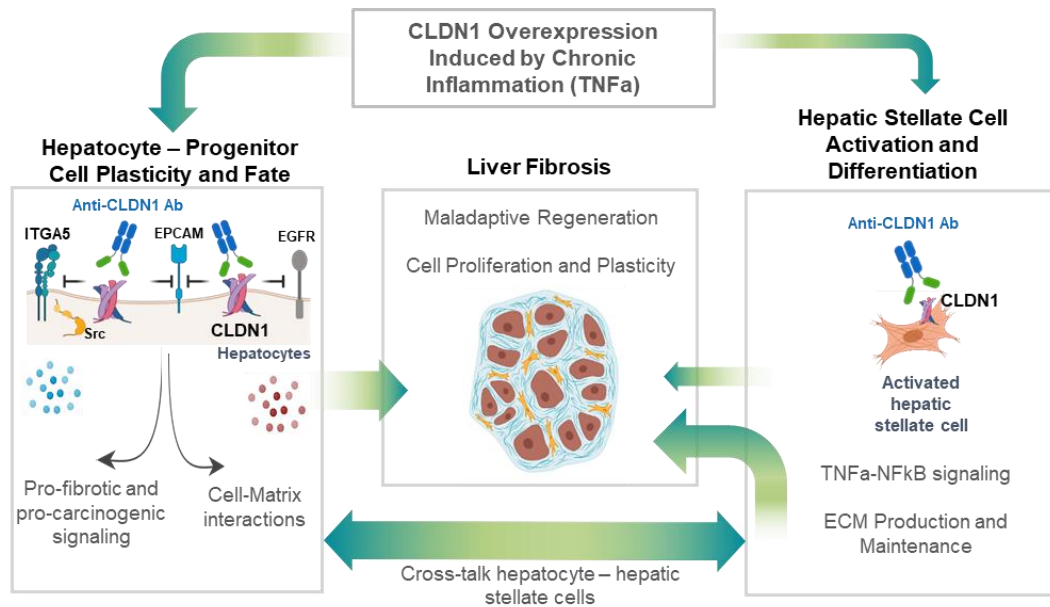


**Figure S17. Mechanistic model of the anti-fibrotic effect of CLDN1 mAb in the liver.**

CLDN1 expression is regulated by the TNF- $\alpha$ -NF $\kappa$ B pathway and upregulated upon chronic inflammation. Liver epithelial cells including hepatocytes and its progenitors are the primary target cells of CLDN1 mAb mediating its anti-fibrotic effect. CLDN1 binds to EPCAM, EGFR and ITGA5 in the epithelial cell membrane and perturbation of these interactions by CLDN1 mAb inhibits downstream SRC and MAPK pathway, playing a key role in cell plasticity, cell-matrix interactions as well as fibrogenesis and carcinogenesis. The second cell type mediating the anti-fibrotic properties of the mAb are hepatic stellate cells/myofibroblasts. CLDN1 mAb inhibits TNF- $\alpha$ -NF $\kappa$ B signaling resulting in robust inhibition of myofibroblast activation and differentiation. Cross-talk between hepatocyte epithelial cells and fibroblasts ultimately results in suppression of maladaptive regeneration, cell proliferation and plasticity leading to ECM accumulation and fibrosis.

2142  
2143  
2144  
2145  
2146  
2147  
2148  
2149  
2150  
2151  
2152  
2153  
2154  
2155  
2156  
2157  
2158  
2159  
2160  
2161  
2162

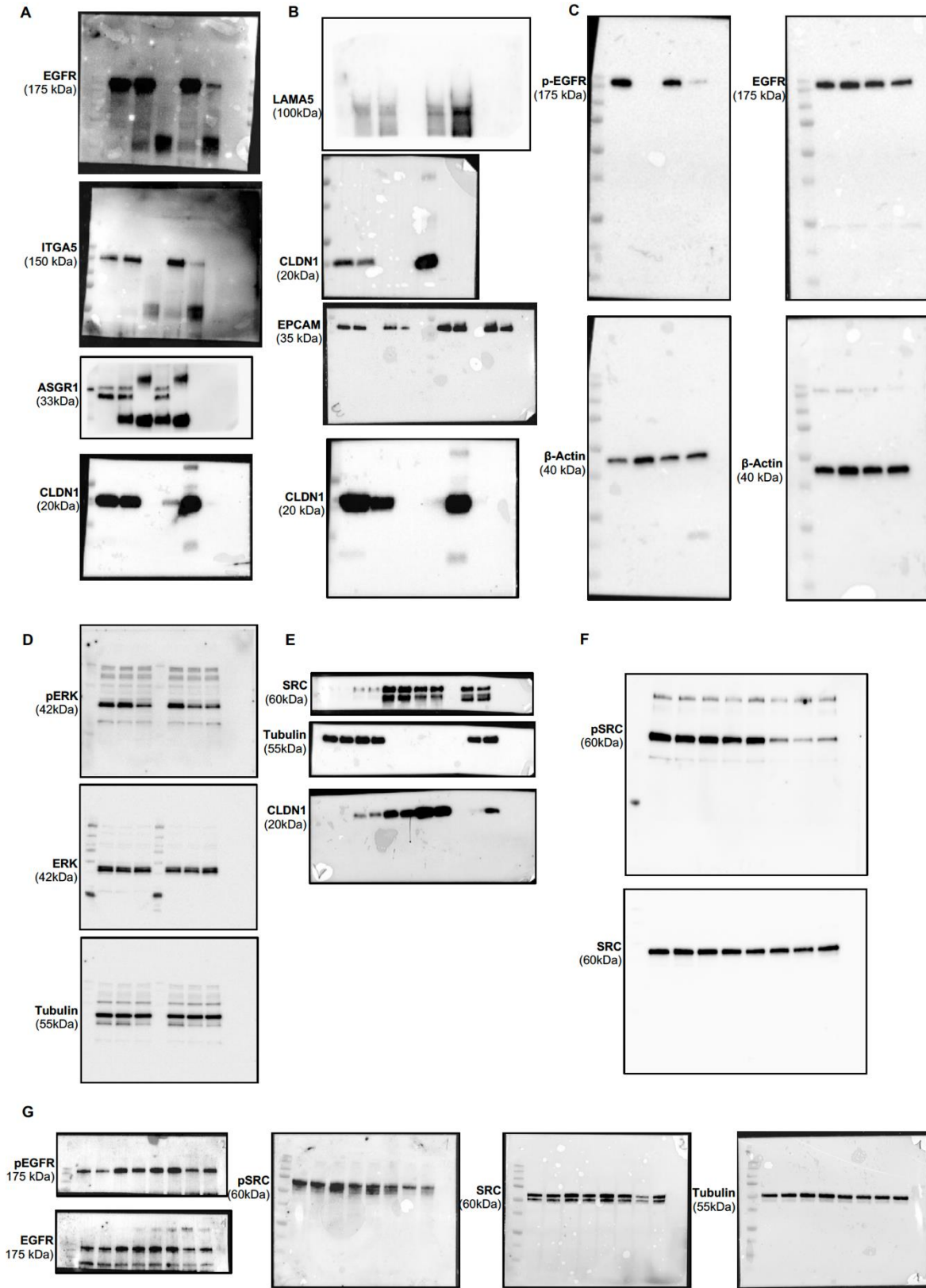


**Figure S18. Original blots shown in Figure 6 and figure S14.**

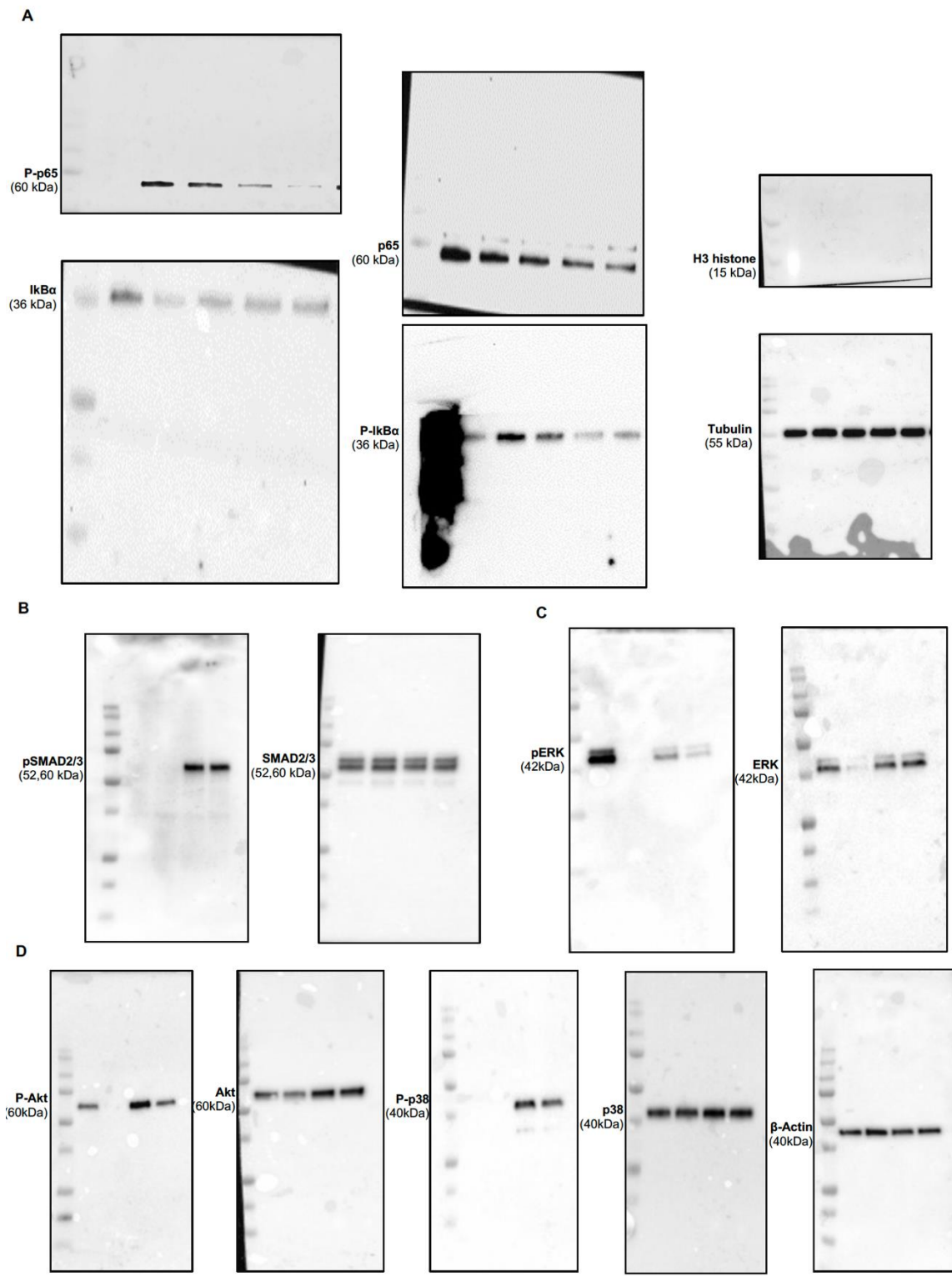


**Figure S19. Original blots shown in Figure 7.**

2166 **SUPPLEMENTARY TABLES**

2167 **Table S1, related to Fig. 1A. Demographic and clinical characteristics of the University of**  
 2168 **Strasbourg NASH cohort.**

	<b><u>Control</u></b> <b><u>(n=10)</u></b>	<b><u>NASH</u></b> <b><u>(n=10)</u></b>
<b><u>Age (years)</u></b>	<b><u>43 (23-73)</u></b>	<b><u>39 (25-54)</u></b>
<b><u>Female (%)</u></b>	<b><u>18 (90)</u></b>	<b><u>4 (40)</u></b>
<b><u>Waist circumference (cm)</u></b>	<b><u>98.5 (75-149)</u></b>	<b><u>136 (100-170)</u></b>
<b><u>BMI (kg/m<sup>2</sup>)</u></b>	<b><u>31.9 (22.4-50.0)</u></b>	<b><u>46.9 (40.5-60.5)</u></b>
<b><u>Blood fasting glucose (mg/dL)</u></b>	<b><u>84 (66-130)</u></b>	<b><u>114 (83-162)</u></b>
<b><u>Insulin (μUI/mL)</u></b>	<b><u>6.1 (1.7-29.5)</u></b>	<b><u>9.2 (4.8-83.5)</u></b>
<b><u>HOMA-IR index</u></b>	<b><u>1.14 (0.33-5.90)</u></b>	<b><u>3.31 (0.99-33.40)</u></b>
<b><u>Total cholesterol (mg/dL)</u></b>	<b><u>166 (113-288)</u></b>	<b><u>151 (93-181)</u></b>
<b><u>Triglycerides (mg/dL)</u></b>	<b><u>122 (60-209)</u></b>	<b><u>194 (93-273)</u></b>
<b><u>FFA (mg/dL)</u></b>	<b><u>26 (8-36)</u></b>	<b><u>24 (13-35)</u></b>
<b><u>LDL cholesterol (mg/dL)</u></b>	<b><u>106 (59-217)</u></b>	<b><u>81 (46-101)</u></b>
<b><u>HDL cholesterol (mg/dL)</u></b>	<b><u>41 (31-67)</u></b>	<b><u>31 (18-42)</u></b>
<b><u>AST (UI/L)</u></b>	<b><u>21.5 (12-85)</u></b>	<b><u>48.5 (20-176)</u></b>
<b><u>ALT (UI/L)</u></b>	<b><u>18 (5-122)</u></b>	<b><u>56.5 (27-229)</u></b>
<b><u>ALP (UI/L)</u></b>	<b><u>60 (36-122)</u></b>	<b><u>54.5 (35-97)</u></b>
<b><u>GGT (UI/L)</u></b>	<b><u>20.5 (5-221)</u></b>	<b><u>35.5 (19-114)</u></b>
<b><u>Total bilirubin (mg/dL)</u></b>	<b><u>0.6 (0.3-1.01)</u></b>	<b><u>0.6 (0.3-0.9)</u></b>
<b><u>Iron (μg/dL)</u></b>	<b><u>76 (30-197)</u></b>	<b><u>66 (30-146)</u></b>
<b><u>Ferritin (ng/mL)</u></b>	<b><u>70.5 (14-399)</u></b>	<b><u>155 (10-2380)</u></b>
<b><u>Transferrin saturation %</u></b>	<b><u>27.5 (9-81)</u></b>	<b><u>23.5 (10-49)</u></b>
<b><u>CRP (mg/L)</u></b>	<b><u>2.84 (0.18-9.59)</u></b>	<b><u>6.27 (1.39-19.40)</u></b>

2169  
 2170 **Continuous variables are indicated as median and range. Abbreviations: ALP=alkaline phosphate,**  
 2171 **ALT=alanine aminotransferase, AST=aspartate aminotransferase, BMI=Body Mass Index,**  
 2172 **CRP=C-reactive protein, FFA=free fatty acid, GGT=gamma-glutamyl transferase, HDL=high**  
 2173 **density lipoprotein, HOMA-IR=homeostatic model assessment of insulin resistance, LDL=low**  
 2174 **density lipoprotein, NAFL=non-alcoholic fatty liver, NASH=non-alcoholic steatohepatitis.**

2175  
2176  
2177  
2178  
2179  
2180  
2181  
2182  
2183  
2184  
2185  
2186  
2187  
2188  
2189  
2190  
2191  
2192  
2193  
2194  
2195  
2196  
2197  
2198  
2199  
2200  
2201  
2202  
2203  
2204  
2205  
2206  
2207  
2208  
2209

**Table S2, related to Fig. 2. Individual data of the main efficacy endpoints of the humanized NASH mice treated GalNac siCLDN1 and siCTRL.**

<b><u>Group</u></b>	<b><u>Mouse ID</u></b>	<b><u>Fibrosis in humanized area %</u></b>	<b><u>Tumor Number</u></b>
<b><u>siCTRL</u></b>	<u>1512</u>	<u>4.874</u>	<u>83</u>
	<u>1513</u>	<u>3.738</u>	<u>31</u>
	<u>1515</u>	<u>3.782</u>	<u>25</u>
	<u>1528</u>	<u>3.819</u>	<u>28</u>
	<u>1555</u>	<u>5.94</u>	<u>25</u>
	<u>1558</u>	<u>4.33</u>	<u>45</u>
	<b><u>Median</u></b>	<b><u>4.07</u></b>	<b><u>29.5</u></b>
<b><u>Mean</u></b>	<b><u>4.41</u></b>	<b><u>39.5</u></b>	
<b><u>s.e.m.</u></b>	<b><u>0.35</u></b>	<b><u>9.2</u></b>	
<b><u>siCLDN1</u></b>	<u>1505</u>	<u>2.743</u>	<u>23</u>
	<u>1506</u>	<u>0.596</u>	<u>6</u>
	<u>1509</u>	<u>3.295</u>	<u>17</u>
	<u>1511</u>	<u>4.79</u>	<u>4</u>
	<u>1722</u>	<u>2.633</u>	<u>34</u>
	<b><u>Median</u></b>	<b><u>2.74</u></b>	<b><u>17.0</u></b>
<b><u>Mean</u></b>	<b><u>2.81</u></b>	<b><u>16.8</u></b>	
<b><u>s.e.m.</u></b>	<b><u>0.67</u></b>	<b><u>5.5</u></b>	
<b><u>Test</u></b>	<b><u>KW</u></b>	<b><u>KW</u></b>	
<b><u>p-value</u></b>	<b><u>0.045</u></b>	<b><u>0.044</u></b>	

**Abbreviations: KW= Kruskal-Wallis test, s.e.m.= standard error of the mean.**

2210 Table S3, related to Fig. 2. Individual data of the main efficacy endpoints of the humanized  
 2211 NASH mice treated with vehicle control or humanized CLDN1 mAb.

2212

2213 Experiment #1

<u>Group</u>	<u>Mouse ID</u>	<u>Total fibrosis %</u>	<u>Fibrosis in humanized area %</u>	<u>Tumor Number</u>
<u>Vehicle</u>	<u>4409</u>	<u>10.495</u>	<u>6.30</u>	<u>24</u>
	<u>4411</u>	<u>6.589</u>	<u>4.66</u>	<u>30</u>
	<u>4412</u>	<u>6.261</u>	<u>3.35</u>	<u>17</u>
<u>Median</u>		<u>6.59</u>	<u>4.66</u>	<u>24.00</u>
<u>Mean</u>		<u>7.78</u>	<u>4.77</u>	<u>23.67</u>
<u>s.e.m.</u>		<u>1.36</u>	<u>0.86</u>	<u>3.76</u>
<u>CLDN1 mAb</u>	<u>4405</u>	<u>1.101</u>	<u>0.51</u>	<u>17</u>
	<u>4407</u>	<u>5.843</u>	<u>1.80</u>	<u>5</u>
	<u>4408</u>	<u>3.168</u>	<u>1.51</u>	<u>12</u>
	<u>4424</u>	<u>1.516</u>	<u>0.68</u>	<u>11</u>
<u>Median</u>		<u>2.34</u>	<u>1.09</u>	<u>11.50</u>
<u>Mean</u>		<u>2.91</u>	<u>1.12</u>	<u>11.25</u>
<u>s.e.m.</u>		<u>1.08</u>	<u>0.31</u>	<u>2.46</u>
<u>Test</u>		<u>MW</u>	<u>MW</u>	<u>MW</u>
<u>p-value</u>		<u>0.0339</u>	<u>0.0339</u>	<u>0.0498</u>

2214

2215 Abbreviations: MW= Mann Whitney U test, s.e.m.= standard error of the mean.

2216

2217

2218



2219

**Experiment #2**

<b><u>Group</u></b>	<b><u>Mouse ID</u></b>	<b><u>Total fibrosis %</u></b>	<b><u>Fibrosis in humanized area %</u></b>	<b><u>Tumor Number</u></b>
<b><u>Vehicle</u></b>	<u>1005</u>	<u>7.708</u>	<u>7.708</u>	<u>9</u>
	<u>1006</u>	<u>11.862</u>	<u>12.531</u>	<u>10</u>
	<u>4472</u>	<u>11.8925</u>	<u>11.8925</u>	<u>NA</u>
	<u>4477</u>	<u>6.048</u>	<u>4.438</u>	<u>22</u>
	<u>4478</u>	<u>1.167</u>	<u>0.886</u>	<u>13</u>
	<u>4479</u>	<u>10.4915</u>	<u>9.34</u>	<u>14</u>
	<u>4490</u>	<u>4.751</u>	<u>4.046</u>	<u>7</u>
	<u>4491</u>	<u>1.881</u>	<u>2.017</u>	<u>7</u>
	<u>4492</u>	<u>7.13</u>	<u>7.13</u>	<u>7</u>
	<u>4493</u>	<u>4.401</u>	<u>6.152</u>	<u>5</u>
<b><u>Median</u></b>	<b><u>6.59</u></b>	<b><u>6.64</u></b>	<b><u>9.00</u></b>	
<b><u>Mean</u></b>	<b><u>6.73</u></b>	<b><u>6.61</u></b>	<b><u>10.44</u></b>	
<b><u>s.e.m.</u></b>	<b><u>1.21</u></b>	<b><u>0.84</u></b>	<b><u>1.75</u></b>	

<b><u>CLDN1 mAb</u></b>	<u>1001</u>	<u>2.11</u>	<u>2.667</u>	<u>5</u>
	<u>1002</u>	<u>4.55</u>	<u>5.352</u>	<u>5</u>
	<u>1008</u>	<u>1.48</u>	<u>1.48</u>	<u>4</u>
	<u>1009</u>	<u>4.446</u>	<u>4.5225</u>	<u>4</u>
	<u>1010</u>	<u>1.716</u>	<u>1.716</u>	<u>4</u>
	<u>4470</u>	<u>1.618</u>	<u>1.864</u>	<u>2</u>
	<u>4471</u>	<u>1.1705</u>	<u>1.5995</u>	<u>4</u>
	<u>4483</u>	<u>2.556</u>	<u>2.308</u>	<u>5</u>
	<u>4484</u>	<u>3.552</u>	<u>0.96</u>	<u>13</u>
	<u>4485</u>	<u>1.322</u>	<u>0.583</u>	<u>10</u>
<b><u>Median</u></b>	<b><u>1.91</u></b>	<b><u>1.79</u></b>	<b><u>4.50</u></b>	
<b><u>Mean</u></b>	<b><u>2.45</u></b>	<b><u>2.31</u></b>	<b><u>5.60</u></b>	
<b><u>s.e.m.</u></b>	<b><u>0.41</u></b>	<b><u>0.48</u></b>	<b><u>1.05</u></b>	
<b><u>Test</u></b>	<b><u>MW</u></b>	<b><u>MW</u></b>	<b><u>MW</u></b>	
<b><u>p-value</u></b>	<b><u>0.013</u></b>	<b><u>0.013</u></b>	<b><u>0.0093</u></b>	

2220

2221

Abbreviations: MW= Mann Whitney U test, s.e.m.= standard error of the mean.

2222

2223

2224

2225

**Table S4, related to Fig. 3.** Individual data of the main efficacy endpoints of DEN-CDA-HFD

2226

mice treated with vehicle control or CLDN1 mAb.

<u>Group</u>	<u>Mouse ID</u>	<u>Fibrosis %</u>	<u>Tumor macroscopy (Y=1/N=0)</u>	<u>Tumor N at histology</u>	<u>Max tumor size (mm)</u>	<u>Tumor HSP70+ (Y=1/N=0)</u>
<u>Vehicle</u>	621	11.25	1	9	5.8	1
	622	8.59	1	7	2.2	1
	623	14.19	1	8	7.0	1
	624	9.95	1	3	1.5	0
	625	11.07	1	1	1.2	0
	631	9.53	0	0	NA	0
	632	18.69	1	3	1.5	0
	633	6.83	1	2	0.9	0
	634	7.69	1	1	2.1	0
	635	11.46	1	2	1.6	0
	641	8.28	1	11	1.2	1
	642	11.89	1	4	0.6	0
	643	8.24	1	3	1.0	0
	644	8.01	1	13	1.6	0
	645	8.79	1	10	8.1	1
	652	9.52	1	11	9.3	1
	653	6.67	1	17	13.0	1
654	9.26	1	4	1.6	1	
<u>Median</u>		<u>9.39</u>	<u>NA</u>	<u>4.00</u>	<u>1.62</u>	<u>NA</u>
<u>Mean</u>		<u>10.00</u>	<u>0.94</u>	<u>6.06</u>	<u>3.55</u>	<u>0.44</u>
<u>s.e.m.</u>		<u>0.68</u>	<u>0.06</u>	<u>1.15</u>	<u>0.89</u>	<u>0.12</u>
<u>CLDN1 mAb</u>	626	9.92	0	1	1.4	0
	627	11.76	1	7	6.0	1
	628	8.29	0	0	NA	0
	629	8.93	0	0	NA	0
	630	8.81	0	1	0.9	0
	636	5.16	0	2	0.5	0
	637	4.64	0	3	0.8	0
	638	6.57	1	2	1.3	0
	639	4.76	1	2	1.3	0
	640	6.87	0	1	1.1	0
	646	6.05	0	0	NA	0
	647	6.29	0	1	0.7	0
	648	13.55	1	2	1.1	0
	649	4.33	0	1	0.6	0

	<u>650</u>	<u>6.06</u>	<u>0</u>	<u>1</u>	<u>0.6</u>	<u>0</u>
	<u>656</u>	<u>4.39</u>	<u>1</u>	<u>6</u>	<u>1.5</u>	<u>0</u>
	<u>657</u>	<u>7.91</u>	<u>0</u>	<u>0</u>	<u>NA</u>	<u>0</u>
	<u>658</u>	<u>8.60</u>	<u>0</u>	<u>2</u>	<u>0.4</u>	<u>0</u>
	<u>659</u>	<u>4.94</u>	<u>0</u>	<u>2</u>	<u>0.8</u>	<u>0</u>
	<u>660</u>	<u>7.97</u>	<u>1</u>	<u>3</u>	<u>1.1</u>	<u>0</u>
<b><u>Median</u></b>	<b><u>6.72</u></b>	<b><u>N/A</u></b>	<b><u>1.50</u></b>	<b><u>1.00</u></b>	<b><u>N/A</u></b>	<b><u>N/A</u></b>
<b><u>Mean</u></b>	<b><u>7.29</u></b>	<b><u>0.30</u></b>	<b><u>1.85</u></b>	<b><u>1.25</u></b>	<b><u>0.05</u></b>	<b><u>0.05</u></b>
<b><u>s.e.m.</u></b>	<b><u>0.56</u></b>	<b><u>0.11</u></b>	<b><u>0.41</u></b>	<b><u>0.33</u></b>	<b><u>0.05</u></b>	<b><u>0.05</u></b>
<b><u>Test</u></b>	<b><u>MW</u></b>	<b><u>FT</u></b>	<b><u>MW</u></b>	<b><u>MW</u></b>	<b><u>FT</u></b>	<b><u>FT</u></b>

	<b><u>Per mouse</u></b>				
<b><u>p-value</u></b>	<b><u>0.003</u></b>	<b><u>&lt;0.001</u></b>	<b><u>0.001</u></b>	<b><u>0.001</u></b>	<b><u>0.007</u></b>
	<b><u>Per image</u></b>				
	<b><u>&lt;0.001</u></b>				

2227

2228 Abbreviations: FT= Fisher test, HSP70= heat shock protein 70, MW= Mann Whitney U test, N/A=2229 not applicable.. s.e.m.= Standard error of the mean.

2230

2231

2232

2233

2234

2235

2236

2237

2238

2239

2240

2241

2242 **Table S5, related to Fig. 3. Metabolic parameters and CLDN1 mAb concentrations in DEN-CDA-**  
 2243 **HFD mice treated with vehicle control or murinized CLDN1 mAb.**

	<b><u>Vehicle</u></b> <b><u>(mean ± s.e.m.)</u></b>	<b><u>CLDN1 mAb</u></b> <b><u>(mean ± s.e.m.)</u></b>	<b><u>p-value</u></b> <b><u>(MW test)</u></b>
<b><u>ALT (UI/L)</u></b>	<b><u>244 ± 12</u></b>	<b><u>217 ± 14</u></b>	<b><u>0.033</u></b>
<b><u>AST (UI/L)</u></b>	<b><u>276 ± 16</u></b>	<b><u>271 ± 20</u></b>	<b><u>0.664</u></b>
<b><u>ALP (UI/L)</u></b>	<b><u>129 ± 30.2</u></b>	<b><u>103.1 ± 3.3</u></b>	<b><u>0.584</u></b>
<b><u>Total bilirubin (µmol/L)</u></b>	<b><u>3.89 ± 0.40</u></b>	<b><u>4.57 ± 0.62</u></b>	<b><u>0.511</u></b>
<b><u>Total proteins (g/L)</u></b>	<b><u>46.2 ± 0.8</u></b>	<b><u>49.1 ± 0.4</u></b>	<b><u>0.013</u></b>
<b><u>Albumin (g/L)</u></b>	<b><u>22.4 ± 0.7</u></b>	<b><u>23.8 ± 0.5</u></b>	<b><u>0.275</u></b>
<b><u>Creatinine (µmol/L)</u></b>	<b><u>8.79 ± 0.50</u></b>	<b><u>7.98 ± 0.39</u></b>	<b><u>0.316</u></b>
<b><u>Urea (mmol/L)</u></b>	<b><u>9.01 ± 0.18</u></b>	<b><u>8.75 ± 0.39</u></b>	<b><u>0.371</u></b>
<b><u>Sodium (mmol/L)</u></b>	<b><u>145.0 ± 1.7</u></b>	<b><u>147.7 ± 0.7</u></b>	<b><u>0.059</u></b>
<b><u>Potassium (mmol/L)</u></b>	<b><u>5.33 ± 0.14</u></b>	<b><u>5.04 ± 0.13</u></b>	<b><u>0.152</u></b>
<b><u>Calcium (mmol/L)</u></b>	<b><u>2.05 ± 0.04</u></b>	<b><u>2.09 ± 0.02</u></b>	<b><u>0.602</u></b>
<b><u>Glucose (mmol/L)*</u></b>	<b><u>8.25 ± 0.51</u></b>	<b><u>9.12 ± 0.31</u></b>	<b><u>0.179</u></b>
<b><u>Total cholesterol (mmol/L)*</u></b>	<b><u>1.08 ± 0.06</u></b>	<b><u>1.12 ± 0.05</u></b>	<b><u>0.784</u></b>
<b><u>CLDN1 mAb (µg/mL)</u></b>	<b><u>--</u></b>	<b><u>125.8 ± 8.5</u></b>	<b><u>--</u></b>

2244  
 2245 **\*Mice not fasted.**

2246 **Abbreviations: ALT= alanine aminotransferase, AST= aspartate aminotransferase, ALP= alkaline**  
 2247 **phosphatases, MW= Mann Whitney U test, s.e.m.= standard error of the mean.**

2248  
 2249  
 2250  
 2251

2252 **Table S6, related to Fig. 3. Individual data of the main efficacy endpoints of DDC mice treated**  
 2253 **with vehicle control or anti-CLDN1 mAb.**

<u>Group</u>	<u>Mouse ID</u>	<u>CPA %</u>	<u>Ishak score</u>
<u>Vehicle</u>	<u>1746</u>	<u>9.505</u>	<u>3</u>
	<u>1747</u>	<u>8.77</u>	<u>3</u>
	<u>1748</u>	<u>10.46</u>	<u>2</u>
	<u>1749</u>	<u>11.456</u>	<u>4</u>
	<u>1750</u>	<u>12.03</u>	<u>2</u>
	<u>1756</u>	<u>8.542</u>	<u>2</u>
	<u>1757</u>	<u>12.4</u>	<u>4</u>
	<u>1758</u>	<u>8.902</u>	<u>3</u>
	<u>1759</u>	<u>12.488</u>	<u>3</u>
	<u>1760</u>	<u>8.505</u>	<u>3</u>
	<u>1766</u>	<u>10.725</u>	<u>3</u>
	<u>1767</u>	<u>11.172</u>	<u>4</u>
	<u>1768</u>	<u>10.103</u>	<u>3</u>
	<u>1769</u>	<u>10.774</u>	<u>3</u>
	<u>1770</u>	<u>12.057</u>	<u>3</u>
	<u>1776</u>	<u>11.539</u>	<u>4</u>
	<u>1777</u>	<u>10.485</u>	<u>3</u>
	<u>1778</u>	<u>11.498</u>	<u>3</u>
<u>1779</u>	<u>9.644</u>	<u>4</u>	
<u>1780</u>	<u>12.207</u>	<u>4</u>	
<u>Median</u>		<u>10.749</u>	
<u>IQR</u>		<u>2.053</u>	
<u>Mean</u>		<u>10.663</u>	
<u>sd</u>		<u>1.328203</u>	
<u>CLDN1 mAb</u>	<u>1741</u>	<u>6.917</u>	<u>2</u>
	<u>1742</u>	<u>10.031</u>	<u>3</u>
	<u>1743</u>	<u>6.557</u>	<u>2</u>
	<u>1744</u>	<u>8.872</u>	<u>3</u>
	<u>1745</u>	<u>8.099</u>	<u>2</u>
	<u>1751</u>	<u>7.08</u>	<u>2</u>
	<u>1752</u>	<u>7.487</u>	<u>3</u>
	<u>1753</u>	<u>8.559</u>	<u>3</u>
	<u>1754</u>	<u>8.314</u>	<u>4</u>
	<u>1755</u>	<u>7.207</u>	<u>2</u>
	<u>1761</u>	<u>8.167</u>	<u>2</u>
	<u>1762</u>	<u>8.723</u>	<u>2</u>

	<u>1763</u>	<u>8.792</u>	<u>3</u>
	<u>1764</u>	<u>8.366</u>	<u>3</u>
	<u>1765</u>	<u>8.925</u>	<u>3</u>
	<u>1771</u>	<u>7.227</u>	<u>3</u>
	<u>1772</u>	<u>7.07</u>	<u>3</u>
	<u>1773</u>	<u>7.327</u>	<u>2</u>
	<u>1774</u>	<u>6.595</u>	<u>3</u>
	<u>1775</u>	<u>5.54</u>	<u>2</u>

**Median** 7.793  
**IQR** 1.523  
**Mean** 7.793  
**sd** 1.064973

<b><u>Test</u></b>	<b><u>T</u></b>
<b><u>95% C.I.</u></b>	<u>-3.64 to -2.09</u>
<b><u>p-value</u></b>	<u>&lt;0.0001</u>

2254  
2255  
2256  
2257  
2258  
2259  
2260  
2261  
2262  
2263  
2264  
2265  
2266  
2267  
2268

Abbreviations: IQR = Interquartile range; sd = standard deviation; T = Student's T-test; 95% C.I.  
= 95% Confidence Interval.

2269 **Table S7, related to Fig. 4.** Demographic and clinical characteristics of patients shown in **Fig.**

2270 **4C-G.**

	<u>Age(y)</u>	<u>Sex</u>	<u>Chronic liver disease</u>	<u>Indication for liver resection</u>	<u>Fibrosis stage</u>	<u>Applied type of tissue</u>
<u>353</u>	<u>83</u>	<u>M</u>	<u>NAFLD</u>	<u>HCC</u>	<u>F2</u>	<u>diseased, non-tumorous</u>
<u>351</u>	<u>78</u>	<u>M</u>	<u>NAFLD</u>	<u>CCM</u>	<u>F0</u>	<u>diseased, non-tumorous</u>
<u>410</u>	<u>70</u>	<u>M</u>	<u>-</u>	<u>CCM</u>	<u>F0</u>	<u>healthy, non-tumorous</u>
<u>471</u>	<u>70</u>	<u>M</u>	<u>-</u>	<u>GBC</u>	<u>F0</u>	<u>healthy, non-tumorous</u>
<u>525</u>	<u>50</u>	<u>F</u>	<u>-</u>	<u>BCM</u>	<u>F0</u>	<u>healthy, non-tumorous</u>
<u>452</u>	<u>75</u>	<u>M</u>	<u>-</u>	<u>NETM</u>	<u>F0</u>	<u>healthy, non-tumorous</u>
<u>506</u>	<u>48</u>	<u>F</u>	<u>-</u>	<u>CCM</u>	<u>F0</u>	<u>healthy, non-tumorous</u>
<u>514</u>	<u>31</u>	<u>F</u>	<u>-</u>	<u>CCM</u>	<u>F0</u>	<u>healthy, non-tumorous</u>
<u>515</u>	<u>44</u>	<u>M</u>	<u>-</u>	<u>CCM</u>	<u>F0</u>	<u>healthy, non-tumorous</u>
<u>480</u>	<u>-</u>	<u>-</u>	<u>-</u>	<u>CCM</u>	<u>F0</u>	<u>healthy, non-tumorous</u>
<u>481</u>	<u>-</u>	<u>-</u>	<u>-</u>	<u>CCM</u>	<u>F0</u>	<u>healthy, non-tumorous</u>
<u>484</u>	<u>-</u>	<u>-</u>	<u>-</u>	<u>CCM</u>	<u>F0</u>	<u>healthy, non-tumorous</u>
<u>488</u>	<u>-</u>	<u>-</u>	<u>-</u>	<u>CCM</u>	<u>F0</u>	<u>healthy, non-tumorous</u>
<u>489</u>	<u>-</u>	<u>-</u>	<u>-</u>	<u>HCC</u>	<u>F4</u>	<u>diseased, non-tumorous</u>

2271  
 2272 Abbreviations: BCM= breast cancer metastasis, CCM= colon cancer liver metastasis, F= female,

2273 GBC= Gallbladder adenocarcinoma, HCC= Hepatocellular carcinoma, M= male, NAFLD= Non-  
 2274 alcoholic fatty liver disease, NASH=Non-alcoholic steatohepatitis, NETM: pancreatic  
 2275 neuroendocrine tumor metastasis; y= years.

2276

2277

**Table S8, related to Fig. 4. Demographic and clinical characteristics of patients shown in Fig.4H.**

	<u>NASH #1</u>	<u>NASH #2</u>	<u>NASH #3</u>	<u>NASH #4</u>	<u>NASH #5</u>
<u>Age (years)</u>	<u>74</u>	<u>60</u>	<u>74</u>	<u>81</u>	<u>75</u>
<u>Sex (Male/Female)</u>	<u>Male</u>	<u>Male</u>	<u>Male</u>	<u>Male</u>	<u>Male</u>
<u>Fibrosis stage(26)</u>	<u>4</u>	<u>3</u>	<u>3</u>	<u>4</u>	<u>2</u>
<u>Obesity (Yes/No)</u>	<u>Yes</u>	<u>No</u>	<u>No</u>	<u>No</u>	<u>No</u>
<u>Diabetes (Yes/No)</u>	<u>Yes</u>	<u>Yes</u>	<u>No</u>	<u>No</u>	<u>Yes</u>
<u>Hypertension (Yes/No)</u>	<u>Yes</u>	<u>Yes</u>	<u>No</u>	<u>No</u>	<u>No</u>

2278

2288

2289

Abbreviations: NASH= Non-alcoholic steatohepatitis.

2290



2291

**Table S9, related to Fig. 5. Genes used to define the scar-associated myofibroblast\*.**

<u>DCN</u>	<u>TMSB10</u>	<u>FBLN1</u>	<u>RPL36</u>	<u>CYR61</u>	<u>MARCKSL1</u>
<u>C1R</u>	<u>EFEMP1</u>	<u>CD81</u>	<u>PRSS23</u>	<u>CCL2</u>	<u>THBS2</u>
<u>LUM</u>	<u>BGN</u>	<u>MMP2</u>	<u>IL32</u>	<u>RPS12</u>	<u>CTSC</u>
<u>COL3A1</u>	<u>MMP23B</u>	<u>PDGFRA</u>	<u>ANXA1</u>	<u>ADAMTSL2</u>	<u>TCEAL4</u>
<u>C1S</u>	<u>IFITM3</u>	<u>FBLN5</u>	<u>NR2F1</u>	<u>IGFBP7</u>	<u>EMP3</u>
<u>C7</u>	<u>PPIB</u>	<u>COLEC11</u>	<u>TSPAN4</u>	<u>CTSD</u>	<u>WBP5</u>
<u>COL1A2</u>	<u>NNMT</u>	<u>CD74</u>	<u>COL5A1</u>	<u>ITGBL1</u>	<u>RPLP1</u>
<u>COL1A1</u>	<u>NPC2</u>	<u>SPON2</u>	<u>ENG</u>	<u>IGFBP3</u>	<u>RPS17</u>
<u>CFH</u>	<u>COL6A1</u>	<u>COL6A3</u>	<u>RPL37</u>	<u>FSTL1</u>	<u>RPS23</u>
<u>TIMP1</u>	<u>MARCKS</u>	<u>COL14A1</u>	<u>ISLR</u>	<u>PPIC</u>	<u>RPS15</u>
<u>PCOLCE</u>	<u>AEBP1</u>	<u>G0S2</u>	<u>RPS15A</u>	<u>FCGRT</u>	<u>HLA-DPA1</u>
<u>CST3</u>	<u>THY1</u>	<u>LTBP4</u>	<u>PTGDS</u>	<u>PLTP</u>	<u>COL4A2</u>
<u>OLFML3</u>	<u>HLA-DRB1</u>	<u>RCN3</u>	<u>RRBP1</u>	<u>SSR2</u>	<u>TFPI</u>
<u>CXCL12</u>	<u>SRPX</u>	<u>IGFBP4</u>	<u>EFEMP2</u>	<u>RPS18</u>	<u>HLA-DRA</u>
<u>CLEC11A</u>	<u>COL6A2</u>	<u>LY6E</u>	<u>INMT</u>	<u>CLEC2B</u>	<u>IGF2</u>
<u>GGT5</u>	<u>S100A10</u>	<u>MGP</u>	<u>SPARC</u>	<u>IGFBP6</u>	<u>LAMB1</u>
<u>CD63</u>	<u>MEG3</u>	<u>RPL13</u>	<u>ECM1</u>	<u>TIMP2</u>	<u>CCL21</u>
<u>FTL</u>	<u>EMILIN1</u>	<u>LGALS3BP</u>	<u>CCDC80</u>	<u>VCAN</u>	<u>CEBPD</u>
<u>RARRES2</u>	<u>RPL12</u>	<u>TMEM176A</u>	<u>SERPING1</u>	<u>ALDH1A1</u>	<u>RARRES1</u>
<u>ASPN</u>	<u>S100A11</u>	<u>PRELP</u>	<u>FN1</u>	<u>TPT1</u>	<u>DAAMI</u>
<u>S100A13</u>	<u>LRP1</u>	<u>TYROBP</u>	<u>LXN</u>	<u>OSOX1</u>	
<u>RBP1</u>	<u>ADH1B</u>	<u>TMEM176B</u>	<u>MFAP4</u>	<u>RPS24</u>	
<u>SERPINF1</u>	<u>CYBA</u>	<u>IFITM1</u>	<u>RPL39</u>	<u>RAMP1</u>	
<u>DPT</u>	<u>RPL28</u>	<u>RPS28</u>	<u>VKORC1</u>	<u>F2R</u>	

2292

2293 \*derived from(16).

2294

2295

2296

2297

2298

2299

2300

**Table S10, related to Fig. 7. Genes used to define the scar-associated myofibroblast type A\*.**

<u><i>COLEC11</i></u>	<u><i>HLA-A</i></u>	<u><i>EDNRB</i></u>	<u><i>CALM2</i></u>	<u><i>MASP1</i></u>	<u><i>PTGIR</i></u>
<u><i>IGFBP7</i></u>	<u><i>HLA-DRB1</i></u>	<u><i>HGF</i></u>	<u><i>CITED2</i></u>	<u><i>ALDH1A1</i></u>	<u><i>HLA-DRB5</i></u>
<u><i>PPP1R14A</i></u>	<u><i>HLA-B</i></u>	<u><i>HLA-C</i></u>	<u><i>TMEM204</i></u>	<u><i>TMSB4X</i></u>	<u><i>ITM2C</i></u>
<u><i>GGT5</i></u>	<u><i>C11orf96</i></u>	<u><i>TPM1</i></u>	<u><i>COX7A1</i></u>	<u><i>CTSD</i></u>	<u><i>SGCA</i></u>
<u><i>CALD1</i></u>	<u><i>LTBP4</i></u>	<u><i>ENG</i></u>	<u><i>BST2</i></u>	<u><i>HLA-DPA1</i></u>	<u><i>ARHGAP15</i></u>
<u><i>TYROBP</i></u>	<u><i>4-Sep</i></u>	<u><i>COL4A2</i></u>	<u><i>CCL21</i></u>	<u><i>MARCKS</i></u>	<u><i>RGS16</i></u>
<u><i>B2M</i></u>	<u><i>MYL9</i></u>	<u><i>RAMP1</i></u>	<u><i>RBPM5</i></u>	<u><i>ASPN</i></u>	<u><i>COL4A1</i></u>
<u><i>ADAMTSL2</i></u>	<u><i>C8orf4</i></u>	<u><i>IGFBP3</i></u>	<u><i>RBP1</i></u>	<u><i>GPX3</i></u>	

2301

2302

2303

2304

2305

2306

2307

2308

\*derived from(16).

2309

2310

2311 **Table S11, related to Fig. 7. Genes used to define the scar-associated myofibroblast type B\*.**

<u>COL1A2</u>	<u>IGF1</u>	<u>NNMT</u>	<u>RPLP0</u>	<u>YBX3</u>	<u>LXN</u>
<u>S100A6</u>	<u>RARRES1</u>	<u>TSHZ2</u>	<u>VIM</u>	<u>MMP2</u>	<u>CCND2</u>
<u>C3</u>	<u>SERPINF1</u>	<u>ADIRF</u>	<u>ANXA1</u>	<u>RPSA</u>	<u>SFRP2</u>
<u>FBLN1</u>	<u>MDK</u>	<u>STEAP1</u>	<u>RPS3</u>	<u>PTGIS</u>	<u>IGFBP4</u>
<u>CCDC80</u>	<u>CLU</u>	<u>CTHRC1</u>	<u>S100A16</u>	<u>IGFBP2</u>	<u>DNAJB1</u>
<u>COL1A1</u>	<u>FSTL1</u>	<u>COL6A3</u>	<u>DHRS3</u>	<u>NR4A2</u>	<u>PLP2</u>
<u>OGN</u>	<u>SLIT3</u>	<u>LGALS1</u>	<u>VCAN</u>	<u>SVIL</u>	<u>CAV1</u>
<u>SPARCL1</u>	<u>ANXA2</u>	<u>OSR1</u>	<u>COL6A1</u>	<u>BOC</u>	<u>MGP</u>
<u>S100A4</u>	<u>IGFBP6</u>	<u>OAF</u>	<u>MMP23B</u>	<u>GPRC5A</u>	<u>CAPZB</u>
<u>NBL1</u>	<u>COL3A1</u>	<u>S100A10</u>	<u>CRABP2</u>	<u>PCOLCE</u>	

2312  
2313 \*derived from(16).

2314  
2315 **Table S12, related to Fig. 7. Demographic and clinical characteristics of patients recruited for**  
2316 **isolation of HSCs.**

<u>ID</u>	<u>Age(y)</u>	<u>Sex</u>	<u>Chronic liver disease</u>	<u>Indication for liver resection</u>	<u>Isolated cell type</u>
<u>352</u>	<u>48</u>	<u>M</u>	<u>No</u>	<u>CCM</u>	<u>HSCs</u>
<u>372</u>	<u>51</u>	<u>M</u>	<u>No</u>	<u>CCM</u>	<u>HSCs</u>
<u>374</u>	<u>59</u>	<u>F</u>	<u>No</u>	<u>CCM</u>	<u>HSCs</u>
<u>383</u>	<u>71</u>	<u>F</u>	<u>No</u>	<u>CCM</u>	<u>HSCs</u>
<u>389</u>	<u>82</u>	<u>F</u>	<u>NAFLD (F2)*</u>	<u>CCA</u>	<u>HSCs</u>
<u>397</u>	<u>23</u>	<u>F</u>	<u>No</u>	<u>PHL</u>	<u>HSCs</u>
<u>401</u>	<u>36</u>	<u>F</u>	<u>No</u>	<u>CCM</u>	<u>HSCs</u>

2317  
2318 \*Fibrosis stage(26)

2319 Abbreviations: CCA= Cholangiocellular Carcinoma, CCM= Colon cancer liver metastasis;  
2320 HSC=Hepatic stellate cells, NAFLD= Non-alcoholic fatty liver disease, PHL= Primary hepatic  
2321 leiomyosarcoma, y= years.

2323 **Table S13, related to Fig. 8. Individual Sirius-red positive areas in renal fibrosis UO mice**  
 2324 **treated with vehicle control or CLDN1 mAb.**

Control						CLDN1-specific mAb					
Mouse ID	Photo No.	Total area (pixel)	Positive area (pixel)	Positive area (%)	Positive area (%)	Mouse ID	Photo No.	Total area (pixel)	Positive area (pixel)	Positive area (%)	Positive area (%)
101	1	3145728	344415	10.95	8.88	201	1	2942661	91823	3.12	3.14
	2	3145728	277600	8.82			2	3145728	9667	0.31	
	3	3145728	616310	19.59			3	3145728	178982	5.69	
	4	3145728	106844	3.40			4	3145728	105012	3.34	
	5	2525427	41941	1.66			5	3145728	102614	3.26	
102	1	3145728	54042	1.72	6.88	202	1	2955677	149707	5.07	4.26
	2	1852892	282606	15.25			2	3145728	157964	5.02	
	3	2901737	105846	3.65			3	3145728	158958	5.05	
	4	2680358	270561	10.09			4	3145728	137962	4.39	
	5	1677944	61894	3.69			5	3145728	55942	1.78	
103	1	2613185	45756	1.75	12.74	203	1	3145728	106839	3.40	3.01
	2	3145728	79596	2.53			2	3145728	96460	3.07	
	3	3145728	105531	3.35			3	3145728	104407	3.32	
	4	2128925	256408	12.04			4	3145728	108886	3.46	
	5	1805725	795103	44.03			5	3145728	56876	1.81	
104	1	1907636	96743	5.07	5.62	204	1	2053687	221370	10.78	7.07
	2	3145728	116189	3.69			2	2922969	175727	6.01	
	3	2498956	300009	12.01			3	3145728	280234	8.91	
	4	3145728	197408	6.28			4	3145728	95235	3.03	
	5	3145728	32587	1.04			5	3145728	208497	6.63	
105	1	3145728	107920	3.43	5.12	205	1	3145728	26479	0.84	1.70
	2	3145728	228570	7.27			2	3145728	113376	3.60	
	3	3145728	57914	1.84			3	3145728	31501	1.00	
	4	3145728	163861	5.21			4	3145728	24949	0.79	
	5	3145728	247323	7.86			5	3145728	71784	2.28	
106	1	2391160	25941	1.08	5.31	206	1	3145728	56743	1.80	1.77
	2	2481193	192484	7.76			2	3145728	84916	2.70	
	3	2409692	128920	5.35			3	3145728	52829	1.68	
	4	3145728	46287	1.47			4	3145728	61369	1.95	
	5	3145728	343353	10.91			5	3145728	22164	0.70	
107	1	2952140	36770	1.25	9.96	207	1	3145728	44821	1.42	0.79
	2	1283270	262341	20.44			2	3145728	33427	1.06	
	3	1882451	145227	7.71			3	3145728	33393	1.06	
	4	3145728	140876	4.48			4	3145728	5123	0.16	
	5	2652902	421933	15.90			5	3145728	7575	0.24	
108	1	3145728	225836	7.18	5.42	208	1	3054515	39178	1.28	1.41
	2	3145728	302298	9.61			2	3016949	51887	1.72	
	3	3145728	207383	6.59			3	2771583	44394	1.60	
	4	3145728	88954	2.83			4	2615483	39127	1.50	
	5	3145728	28495	0.91			5	2568128	23833	0.93	

2326  
2327  
2328

**Table S14, related to Fig. 8. Individual Ashcroft scores in bleomycin pulmonary fibrosis mice treated with vehicle control or anti-CLDN1 mAb.**

Group	Mouse ID	Photo No.																			Mean	
		1	2	3	4	5	6	7	8	9	10	11	12	13	14	15	16	17	18	19		20
Control	101																					
	102	5	3	3	3	3	3	1	2	2	2	1	2	1	2	1	2	2	2	2	1	2.2
	103	4	6	7	7	3	6	7	7	6	6	7	5	4	3	5	3	2	1	3	1	4.7
	104	5	3	3	3	3	3	2	3	3	4	3	3	3	3	3	3	2	3	1	1	2.9
	105	5	6	6	6	6	3	4	8	7	3	3	4	6	5	6	7	5	3	2	1	4.8
	106	4	5	3	4	5	5	3	3	5	6	6	3	3	2	2	4	3	4	3	3	3.8
	107	3	3	3	3	5	2	3	5	6	8	8	7	6	7	6	3	4	3	8	8	5.1
	108																					
	109	3	6	8	8	5	2	5	3	4	3	7	8	8	8	5	4	5	8	6	6	5.6
	110	2	1	2	1	1	1	1	1	2	1	1	1	1	1	1	1	1	1	2	1	1.2
	111	2	2	2	2	1	2	2	2	1	3	3	2	1	1	1	2	2	2	2	2	1.9
	112																					
	113																					
	114	4	5	4	4	2	2	2	3	3	4	3	2	1	2	2	2	3	3	3	3	2.9
	115	4	4	6	3	5	3	3	3	3	3	3	3	3	4	4	3	2	3	2	3	3.4
	116	7	7	7	7	7	7	7	7	7	7	7	8	7	7	6	6	5	4	3	3	6.3
	117	5	5	3	5	7	7	3	8	5	7	7	7	7	5	4	5	3	3	3	5	5.2
	118	5	7	6	5	7	6	6	3	4	5	6	3	3	8	5	5	4	3	4	3	4.9
CLDN1-specific mAb	201	2	3	3	2	2	3	1	3	1	1	1	3	1	3	4	1	3	2	3	2	2.2
	202																					
	203	1	1	1	3	0	2	3	3	1	2	0	0	1	1	0	2	2	2	4	3	1.6
	204	1	1	2	3	2	1	0	0	1	1	0	0	2	1	2	5	4	3	2	3	1.7
	205	4	3	3	3	3	3	3	4	3	3	2	4	3	2	3	3	3	3	3	5	3.2
	206	3	4	2	3	4	4	2	3	3	3	3	2	1	2	3	3	3	3	3	2	2.8
	207	3	4	3	3	3	3	3	3	2	2	2	2	3	3	3	4	3	3	2	3	2.9
	208	2	1	3	1	2	2	2	2	3	3	1	1	1	4	3	4	2	3	3	2	2.3
	209	3	1	3	3	3	3	1	3	3	3	3	1	2	4	2	3	3	3	3	2	2.6
	210																					
	211																					
	212	1	1	3	4	3	3	3	4	3	4	2	3	3	2	3	5	2	4	3	2	2.9
	213	2	3	3	3	3	3	3	3	3	4	5	7	8	8	8	8	7	3	7	5	4.8
	214	3	3	3	3	3	2	3	2	3	3	2	3	4	3	4	2	3	3	3	2	2.9
	215	3	5	3	6	4	5	3	3	4	2	3	3	4	6	6	8	2	4	3	3	4.0
	216	2	3	3	2	3	3	3	3	3	2	3	3	3	3	2	3	3	3	3	3	2.8
	217																					
	218																					

2329  
2330  
2331  
2332

**Table S15, related to Fig. 8. *HAS*<sup>high</sup> fibroblast marker genes\*.**

<u>AC09049</u> <u>8.1</u>	<u>ETF1</u>	<u>GNPTAB</u>	<u>CSTB</u>	<u>MESDC1</u>	<u>ANKRD37</u>	<u>ATPIF1</u>	<u>HLA-C</u>
<u>MT-CYB</u>	<u>KIAA132</u> <u>4L</u>	<u>LITAF</u>	<u>RCAN1</u>	<u>RAB3A</u>	<u>TLE1</u>	<u>ZFAND3</u>	<u>METAP2</u>
<u>A2M</u>	<u>PGM3</u>	<u>MYL9</u>	<u>MID1</u>	<u>SLC25A3</u> <u>3</u>	<u>RCN3</u>	<u>CD70</u>	<u>PPP4R2</u>
<u>CDKN2A</u>	<u>PTGES3</u>	<u>ISG20L2</u>	<u>PKM</u>	<u>CEBPZ</u>	<u>OSER1</u>	<u>PFKFB3</u>	<u>NR2F2</u>
<u>GALNT13</u>	<u>FAT1</u>	<u>CDKN1A</u>	<u>MAP1LC3</u> <u>B</u>	<u>CACNA2</u> <u>D1</u>	<u>IGF2</u>	<u>VCAN</u>	<u>ADD3</u>
<u>HSP90AA</u> <u>1</u>	<u>CXorf40</u> <u>B</u>	<u>SLC16A1</u>	<u>MTRNR2L</u> <u>12</u>	<u>SMARCA</u> <u>1</u>	<u>CD276</u>	<u>EDNRA</u>	<u>WTAP</u>
<u>HSPE1</u>	<u>PTP4A1</u>	<u>GPRC5A</u>	<u>COL6A2</u>	<u>SEMA3C</u>	<u>YPEL2</u>	<u>EMP1</u>	<u>EFEMP1</u>
<u>LINC016</u> <u>05</u>	<u>CD9</u>	<u>PRRC2C</u>	<u>GXYLT2</u>	<u>SKIL</u>	<u>GOLM1</u>	<u>CDC42E</u> <u>P2</u>	<u>MT1M</u>
<u>HSPD1</u>	<u>CERCAM</u>	<u>MGP</u>	<u>ATXN7</u>	<u>UCK2</u>	<u>HINT1</u>	<u>SPCS1</u>	<u>ARPC5L</u>
<u>FHL2</u>	<u>ARF4</u>	<u>PNPLA8</u>	<u>CTSL</u>	<u>HBEGF</u>	<u>CREM</u>	<u>QSOX1</u>	<u>PDLIM4</u>
<u>KIAA121</u> <u>7</u>	<u>COL1A1</u>	<u>HAS1</u>	<u>RALGPS2</u>	<u>S1PR3</u>	<u>PPIC</u>	<u>ARMCX3</u>	<u>WT1</u>
<u>PDLIM3</u>	<u>EIF5A</u>	<u>PLK2</u>	<u>THBS3</u>	<u>FGF2</u>	<u>OAF</u>	<u>JARID2</u>	<u>FRZB</u>
<u>NAF1</u>	<u>FAM180</u> <u>A</u>	<u>FKBP4</u>	<u>MT-ND5</u>	<u>TOB1</u>	<u>BAG2</u>	<u>TFG</u>	<u>KDELR2</u>
<u>TNFSF9</u>	<u>MORF4L</u> <u>2</u>	<u>BTAFL1</u>	<u>ARC</u>	<u>SFTPC</u>	<u>CCDC71L</u>	<u>SOCS3</u>	<u>IFITM3</u>
<u>LINC001</u> <u>52</u>	<u>ISLR</u>	<u>RPL17</u>	<u>GAS7</u>	<u>FLNA</u>	<u>THBS2</u>	<u>CXCL14</u>	<u>XBPI</u>
<u>MT-ATP8</u>	<u>INSIG1</u>	<u>ARHGAP5</u>	<u>CYB5A</u>	<u>RHOC</u>	<u>PCDH7</u>	<u>MAP2K3</u>	<u>CYP11B1</u>
<u>SELK</u>	<u>MEDAG</u>	<u>VEGFA</u>	<u>PITPNB</u>	<u>ATP5G2</u>	<u>ERVK3-1</u>	<u>ARSI</u>	<u>ADGRD1</u>
<u>SLC12A8</u>	<u>ZBTB21</u>	<u>IFITM2</u>	<u>CMTM3</u>	<u>PPRC1</u>	<u>NAV1</u>	<u>MYH9</u>	<u>LIMCH1</u>
<u>MT-CO2</u>	<u>MAP4K5</u>	<u>SLC4A7</u>	<u>TAF13</u>	<u>MT-ND4</u>	<u>CPNE8</u>	<u>WWTR1</u>	<u>H3F3A</u>
<u>TLL1</u>	<u>BLOC1S</u> <u>6</u>	<u>C16orf45</u>	<u>TCF21</u>	<u>SCGB1A1</u>	<u>ARHGDIB</u>	<u>MINOS1</u>	<u>SFPQ</u>
<u>AC11340</u> <u>4.1</u>	<u>STIP1</u>	<u>KLHL21</u>	<u>IPMK</u>	<u>PTRH2</u>	<u>MAP3K4</u>	<u>SCG2</u>	<u>PSAP</u>
<u>MT-CO3</u>	<u>TPM2</u>	<u>FERMT2</u>	<u>BAZ1A</u>	<u>ECM1</u>	<u>ALDH2</u>	<u>HLA-</u> <u>DPB1</u>	<u>CHSY1</u>
<u>HSP90AB</u> <u>1</u>	<u>RP11-</u> <u>210L7.3</u>	<u>ROR1</u>	<u>HSPB8</u>	<u>ADAMTS</u> <u>16</u>	<u>YWHAQ</u>	<u>GLA</u>	<u>KDM5B</u>
<u>CDKN2B</u>	<u>AHSA1</u>	<u>PAMR1</u>	<u>VAT1</u>	<u>TEX10</u>	<u>COX4I2</u>	<u>PGAP1</u>	<u>PTGES</u>

<u>HSPA4L</u>	<u>GEM</u>	<u>TXN</u>	<u>JOSD1</u>	<u>CLDN11</u>	<u>EBF1</u>	<u>MAGED1</u>	<u>LAMC1</u>
<u>FEM1C</u>	<u>ITGB1</u>	<u>UBE2B</u>	<u>CTC-444N24.11</u>	<u>MICAL2</u>	<u>CALM1</u>	<u>LY96</u>	<u>USP2</u>
<u>ABL2</u>	<u>OSMR-ASI</u>	<u>ZNF460</u>	<u>VIM</u>	<u>TFB2M</u>	<u>IGF1</u>	<u>SRGN</u>	<u>ATP5L</u>
<u>HSPA8</u>	<u>MEG3</u>	<u>BAIAP2</u>	<u>NDEL1</u>	<u>CTSD</u>	<u>EIF3J</u>	<u>GOPC</u>	<u>PCBP2</u>
<u>MXRA5</u>	<u>KDM6B</u>	<u>ASB1</u>	<u>MCC</u>	<u>TUBB2A</u>	<u>EIF2S1</u>	<u>CHIC2</u>	<u>PDGFRL</u>
<u>MT-CO1</u>	<u>PTHLH</u>	<u>IQCJ-SCHIP1</u>	<u>UBAP1</u>	<u>NGF</u>	<u>SEPW1</u>	<u>RSL1D1</u>	<u>ZFC3H1</u>
<u>GPX3</u>	<u>SULF1</u>	<u>MYC</u>	<u>MIR22HG</u>	<u>JAG1</u>	<u>SAMD9</u>	<u>CTSK</u>	<u>BNC2</u>
<u>RP11-474O21.5</u>	<u>ACLY</u>	<u>COL3A1</u>	<u>TUBB3</u>	<u>HTRA3</u>	<u>COX4I1</u>	<u>PNO1</u>	<u>HNRNPA B</u>
<u>RABGEF1</u>	<u>MIR4435-2HG</u>	<u>HSD3B7</u>	<u>HMG2</u>	<u>MAPRE1</u>	<u>GART</u>	<u>ANGPT1</u>	<u>SPG20</u>
<u>LINC01060</u>	<u>CCT2</u>	<u>HSPA1A</u>	<u>RUNX2</u>	<u>HMG3</u>	<u>RCN1</u>	<u>CSNK1A1</u>	<u>MAPK11L</u>
<u>UGDH</u>	<u>PDK4</u>	<u>GNG12</u>	<u>LRRC59</u>	<u>MLF1</u>	<u>STAG1</u>	<u>ANXA5</u>	<u>KRT18</u>
<u>GCLM</u>	<u>TES</u>	<u>ARL5B</u>	<u>BMP1</u>	<u>GTPBP4</u>	<u>LSM12</u>	<u>NNMT</u>	<u>SRP14</u>
<u>USP12</u>	<u>FAM3C</u>	<u>CEBPD</u>	<u>SDC2</u>	<u>DOT1L</u>	<u>DENND4A</u>	<u>LOX</u>	<u>LRRC17</u>
<u>TAGLN</u>	<u>CHMP1B</u>	<u>PLIN3</u>	<u>OSMR</u>	<u>CCNK</u>	<u>PXDN</u>	<u>TGIF1</u>	<u>PHGDH</u>
<u>NR1P1</u>	<u>NR4A3</u>	<u>PRKCI</u>	<u>MSC</u>	<u>3-Mar</u>	<u>CD248</u>	<u>EPHX1</u>	<u>CLIP1</u>
<u>DNAJA1</u>	<u>EIF1</u>	<u>ANKRD28</u>	<u>TSR1</u>	<u>TMEM263</u>	<u>SMS</u>	<u>ANK2</u>	<u>HNRNPF</u>
<u>DCBLD2</u>	<u>NR4A2</u>	<u>PRRX1</u>	<u>HBP1</u>	<u>RRM1</u>	<u>ANGPTL4</u>	<u>C1QTNF3</u>	<u>IGFBP7</u>
<u>CRABP2</u>	<u>ELOVL5</u>	<u>FBN1</u>	<u>NOTCH2</u>	<u>ADAMTS1L</u>	<u>SESN3</u>	<u>CDC42SE1</u>	<u>AMD1</u>
<u>ZBTB38</u>	<u>STX4</u>	<u>RARG</u>	<u>KIAA1462</u>	<u>CRIP2</u>	<u>RGS2</u>	<u>FKBP14</u>	<u>TMEM59</u>
<u>RLF</u>	<u>FNIP2</u>	<u>VAPB</u>	<u>TGM2</u>	<u>NDFIP2</u>	<u>SSR4</u>	<u>SH3D19</u>	<u>LOXL1</u>
<u>BAG3</u>	<u>SCGB3A1</u>	<u>CDK17</u>	<u>KPNA4</u>	<u>AC05879.1.1</u>	<u>TPBG</u>	<u>FLNB</u>	<u>TOR1AIP2</u>
<u>CHORDC1</u>	<u>SERTAD1</u>	<u>SLC19A2</u>	<u>SERTAD2</u>	<u>KTNI</u>	<u>UBQLN1</u>	<u>ARPC3</u>	<u>ANKLE2</u>
<u>SPARC</u>	<u>SGK1</u>	<u>RND3</u>	<u>ADAMTS2</u>	<u>NOP58</u>	<u>MYL6</u>	<u>FKBP5</u>	<u>CTTN</u>
<u>DYRK3</u>	<u>SLC30A1</u>	<u>BZW2</u>	<u>EGR3</u>	<u>KLF4</u>	<u>BDNF</u>	<u>NUP58</u>	<u>PER3</u>
<u>ZSWIM6</u>	<u>HERC4</u>	<u>TXNRD1</u>	<u>FOSB</u>	<u>ZMAT3</u>	<u>GALNT2</u>	<u>UOCR10</u>	<u>GLUD1</u>
<u>PLA2G4A</u>	<u>HAS2</u>	<u>HIVEP2</u>	<u>TUBA1C</u>	<u>FSCN1</u>	<u>RBPI</u>	<u>CXCL6</u>	<u>CCDC80</u>
<u>CPXM1</u>	<u>ZDBF2</u>	<u>RAB7A</u>	<u>NFE2L2</u>	<u>CCNT1</u>	<u>ZC3HAV1</u>	<u>CMSS1</u>	<u>SMDT1</u>

<u>SERPINH1</u>	<u>DPYSL3</u>	<u>PANX1</u>	<u>SMIM3</u>	<u>SLFN11</u>	<u>PSME1</u>	<u>ITPRIP</u>	<u>KPNA2</u>
<u>DOK5</u>	<u>PRRG3</u>	<u>SELM</u>	<u>RNF149</u>	<u>UBE2D3</u>	<u>RNASEK</u>	<u>HSPB1</u>	<u>PEG10</u>
<u>MT-ND4L</u>	<u>HDLBP</u>	<u>ALDH1A3</u>	<u>AKAP12</u>	<u>FNDC1</u>	<u>AGO2</u>	<u>OTUD4</u>	<u>COX6A1</u>
<u>HSPA4</u>	<u>COQ10B</u>	<u>CPZ</u>	<u>EGFL6</u>	<u>SEPP1</u>	<u>CLMP</u>	<u>TUBB2B</u>	<u>CHCHD10</u>
<u>ANXA1</u>	<u>ASCC3</u>	<u>CADPS2</u>	<u>CTNNA1</u>	<u>TIMP2</u>	<u>H3F3B</u>	<u>RC3H1</u>	<u>GPC1</u>
<u>ARL4C</u>	<u>DNAJB6</u>	<u>ATP13A3</u>	<u>HMOX1</u>	<u>TCEB1</u>	<u>S100A4</u>	<u>NUPR1</u>	<u>MYL12A</u>
<u>COL1A2</u>	<u>MT-ND2</u>	<u>FBXO34</u>	<u>C10orf10</u>	<u>RPS6KA3</u>	<u>TAF1D</u>	<u>RARRES1</u>	<u>ARHGAP21</u>
<u>SQSTM1</u>	<u>TIPARP</u>	<u>IPO7</u>	<u>ITGAV</u>	<u>CIRBP</u>	<u>AFG3L2</u>	<u>SERINC5</u>	<u>EPB41L2</u>
<u>TCP1</u>	<u>MTRNR2L8</u>	<u>HRH1</u>	<u>MAPK6</u>	<u>DDX21</u>	<u>SH3PXD2B</u>	<u>EDIL3</u>	<u>LY6E</u>
<u>PHLDA1</u>	<u>TSC22D2</u>	<u>INPP1</u>	<u>RGMB</u>	<u>ID1</u>	<u>NIFK</u>	<u>ADH1C</u>	<u>ADAMTS15</u>
<u>NT5E</u>	<u>P4HA1</u>	<u>TNFRSF10B</u>	<u>MMP2</u>	<u>CCDC109B</u>	<u>CD44</u>	<u>PTPN1</u>	<u>CXCL12</u>
<u>ARID5B</u>	<u>MT-ND3</u>	<u>TNFAIP6</u>	<u>METRNL</u>	<u>MYOF</u>	<u>FAM110B</u>	<u>TRAF4</u>	<u>ETNK1</u>
<u>ROR1-ASI</u>	<u>JAM3</u>	<u>UAP1</u>	<u>SPON2</u>	<u>BZW1</u>	<u>DDX3X</u>	<u>ABHD2</u>	<u>PLA2G5</u>
<u>SNAI2</u>	<u>TWIST1</u>	<u>PLAUR</u>	<u>TIMP3</u>	<u>NTM</u>	<u>SEMA4A</u>	<u>DSTN</u>	<u>GRPEL1</u>
<u>GJA1</u>	<u>PPP1R14A</u>	<u>UCHL3</u>	<u>MAP4K4</u>	<u>GPSM2</u>	<u>UHRF1BP1L</u>	<u>DSEL</u>	<u>CILP2</u>
<u>LIMA1</u>	<u>PTGIS</u>	<u>JUN</u>	<u>CNTN4</u>	<u>EMILIN2</u>	<u>TRIO</u>	<u>NFATC1</u>	<u>FBLN2</u>
<u>LRRC8C</u>	<u>LMCD1</u>	<u>CD74</u>	<u>UTP4</u>	<u>AFF4</u>	<u>KCNE4</u>	<u>FKBP10</u>	<u>SUMO2</u>
<u>ZFAND2A</u>	<u>TPM4</u>	<u>FGFR1</u>	<u>CLEC11A</u>	<u>NOP16</u>	<u>USP15</u>	<u>SPSB1</u>	<u>HMGB1</u>
<u>SPAG9</u>	<u>IL1R1</u>	<u>ERRF1</u>	<u>AFAP1</u>	<u>TSPO</u>	<u>MIR222HG</u>	<u>UBE3A</u>	<u>NOV</u>
<u>HSPH1</u>	<u>ANGPTL2</u>	<u>PLOD2</u>	<u>NOLC1</u>	<u>CADM3</u>	<u>GABPB1</u>	<u>TMEM2</u>	<u>ALDH1A1</u>
<u>RPS26</u>	<u>RPL41</u>	<u>GABARAPL1</u>	<u>TNFRSF12A</u>	<u>CTNNB1</u>	<u>AOC3</u>	<u>SOX4</u>	<u>CA12</u>
<u>CHD1</u>	<u>REL</u>	<u>GNAI3</u>	<u>LRIF1</u>	<u>TTC3</u>	<u>RGS5</u>	<u>SRGAP1</u>	<u>HIGD1B</u>
<u>EIF4E</u>	<u>KCTD9</u>	<u>YWHAZ</u>	<u>ZFP36L1</u>	<u>AKIRIN1</u>	<u>GNL2</u>	<u>IL33</u>	<u>PERP</u>
<u>YWHAG</u>	<u>ELL2</u>	<u>SACS</u>	<u>CLIC4</u>	<u>FRS2</u>	<u>MDM2</u>	<u>FABP5</u>	<u>KLF2</u>
<u>CBLB</u>	<u>DDX3Y</u>	<u>FRMD6</u>	<u>IFI16</u>	<u>GSTP1</u>	<u>EMP2</u>	<u>SEC23A</u>	<u>PABPC1</u>
<u>DNAJB4</u>	<u>FAM198B</u>	<u>PPTC7</u>	<u>NXT1</u>	<u>GNL3</u>	<u>UFM1</u>	<u>COX8A</u>	<u>NFAT5</u>



<u>MSX2</u>	<u>C1QTNF6</u>	<u>COL4A1</u>	<u>MRPL18</u>	<u>HIST3H2A</u>	<u>SLC40A1</u>	<u>CCT3</u>	<u>C14orf2</u>
<u>RAB23</u>	<u>PPDPF</u>	<u>COL4A2</u>	<u>DNTTIP2</u>	<u>ITGA11</u>	<u>IL6R</u>	<u>PEBP1</u>	<u>BCAP31</u>
<u>PEA15</u>	<u>TICAM1</u>	<u>MAFF</u>	<u>DNAJB9</u>	<u>SLC20A1</u>	<u>SEMA3B</u>	<u>NUFIP2</u>	<u>HOTAIRM1</u>
<u>DRAM1</u>	<u>TOP1</u>	<u>NBPF14</u>	<u>ALG13</u>	<u>PRMT9</u>	<u>ELN</u>	<u>RGCC</u>	<u>SEMA6A</u>
<u>EIF4A3</u>	<u>COL6A1</u>	<u>WDR43</u>	<u>FKBP9</u>	<u>NDUFA4</u>	<u>HLA-DPA1</u>	<u>DES</u>	<u>NDUFA3</u>
<u>LHFPL2</u>	<u>ETV3</u>	<u>MLLT11</u>	<u>MED13</u>	<u>CREB3L1</u>	<u>COL5A1</u>	<u>PIM1</u>	<u>ACSL3</u>
<u>DNAJB1</u>	<u>WBP5</u>	<u>HNRNPA2B1</u>	<u>LATS2</u>	<u>CCT4</u>	<u>PFDN2</u>	<u>DDX5</u>	<u>OLFML3</u>
<u>IL6ST</u>	<u>SOD3</u>	<u>DNMBP</u>	<u>NUP153</u>	<u>ESYT2</u>	<u>HIVEP1</u>	<u>AHNAK</u>	<u>EIF5</u>
<u>ACTA2</u>	<u>SLPI</u>	<u>SDCBP</u>	<u>SERBP1</u>	<u>TPT1</u>	<u>HIPK3</u>	<u>FLRT2</u>	<u>PHLDB2</u>
<u>YES1</u>	<u>ABI3BP</u>	<u>CD55</u>	<u>C3orf58</u>	<u>CRY1</u>	<u>APP</u>	<u>IGFBP6</u>	<u>CD68</u>
<u>ADH1B</u>	<u>CREB5</u>	<u>NAA50</u>	<u>FOSL1</u>	<u>TRIM69</u>	<u>EIF1AX</u>	<u>PAICS</u>	<u>MAP3K8</u>
<u>GLIS3</u>	<u>MMP14</u>	<u>MAT2A</u>	<u>KLF3</u>	<u>HEG1</u>	<u>FLNC</u>	<u>SSC5D</u>	<u>PCDHGC3</u>
<u>MT-ND1</u>	<u>DPT</u>	<u>CAMSAP2</u>	<u>FAM114A1</u>	<u>CYP51A1</u>	<u>ANKH</u>	<u>KDEL3</u>	<u>ANXA2</u>
<u>HSPA9</u>	<u>PTGFRN</u>	<u>RCOR1</u>	<u>PCBP1</u>	<u>HNRNPH3</u>	<u>ARL4D</u>	<u>IER3</u>	<u>KRTCAP2</u>
<u>C1orf21</u>	<u>SYAP1</u>	<u>HSPA1B</u>	<u>USP36</u>	<u>MRC2</u>	<u>UBL3</u>	<u>CKAP4</u>	<u>COL5A2</u>
<u>SNX9</u>	<u>APOD</u>	<u>GPC6</u>	<u>ACSL4</u>	<u>TSC22D1</u>	<u>PHLDB1</u>	<u>RAB1A</u>	<u>INHBA</u>
<u>RYBP</u>	<u>GFPT2</u>	<u>HNRNPA0</u>	<u>TSPAN5</u>	<u>NDUFA4L2</u>	<u>EDF1</u>	<u>ASAHI</u>	<u>NPM1</u>
<u>TXNIP</u>	<u>PRSS23</u>	<u>CYCS</u>	<u>SAMD8</u>	<u>PXDC1</u>	<u>CD200</u>	<u>SNRPB</u>	<u>CD81</u>
<u>CACYBP</u>	<u>RUNX1</u>	<u>HECTD2</u>	<u>COX5B</u>	<u>FAP</u>	<u>DCLK1</u>	<u>NIP7</u>	<u>FILIP1</u>
<u>FSTL1</u>	<u>BIN1</u>	<u>WDR45B</u>	<u>SARIA</u>	<u>AHNAK2</u>	<u>PPP1R15B</u>	<u>ATP1B3</u>	<u>HLA-A</u>
<u>GNPNAT1</u>	<u>MT-ND6</u>	<u>THBS1</u>	<u>HLA-DRB1</u>	<u>CSRNP1</u>	<u>EIF4G2</u>	<u>HSPA5</u>	<u>EEA1</u>
<u>RANBP2</u>	<u>FAM46A</u>	<u>STK17A</u>	<u>MEST</u>	<u>MEIS2</u>	<u>PPP2R2A</u>	<u>POLR1C</u>	<u>RP11-14N7.2</u>
<u>KLF6</u>	<u>PTGS2</u>	<u>SPRY2</u>	<u>SLC38A2</u>	<u>TSPAN3</u>	<u>KRAS</u>	<u>NR4A1</u>	<u>SLC39A14</u>
<u>ZFAND5</u>	<u>CALM2</u>	<u>IPO5</u>	<u>NRBF2</u>	<u>THAP2</u>	<u>NUP98</u>	<u>LHFP</u>	<u>FOSL2</u>
<u>U2AF1L5</u>	<u>DDX27</u>	<u>CMBL</u>	<u>TUBB6</u>	<u>SLC39A6</u>	<u>IFI27</u>	<u>HMGAI</u>	<u>LAMA4</u>
<u>ITIH5</u>	<u>NSUN2</u>	<u>DUSP5</u>	<u>SPHK1</u>	<u>CLIC2</u>	<u>ANTXR2</u>	<u>SEC31A</u>	<u>OPTN</u>
<u>JMJD1C</u>	<u>HNRNPU</u>	<u>H2AFJ</u>	<u>HLA-DRA</u>	<u>TOB2</u>	<u>COPS2</u>	<u>NR1D2</u>	<u>PAFAH1B1</u>

<u>HOMER1</u>	<u>COL14A1</u>	<u>APBB3</u>	<u>MMP23B</u>	<u>KLF9</u>	<u>MRPS6</u>	<u>PDGFD</u>	<u>NOTCH3</u>
<u>EPHB2</u>	<u>RASAL2</u>	<u>BACH1</u>	<u>S100A16</u>	<u>TMED5</u>	<u>B4GALT1</u>	<u>MYLK</u>	<u>DAZAP2</u>
<u>DCUN1D3</u>	<u>ZNF703</u>	<u>RAP1B</u>	<u>TSHZ2</u>	<u>PFKP</u>	<u>C2</u>	<u>ATF4</u>	<u>ATF3</u>
<u>PLXDC1</u>	<u>KLHL4</u>	<u>CLCF1</u>	<u>APOE</u>	<u>MCL1</u>	<u>MYO1E</u>	<u>PLAU</u>	<u>RASL11A</u>
<u>AES</u>	<u>GPM6B</u>	<u>KCTD20</u>	<u>LDHB</u>	<u>ZBTB16</u>	<u>SCGB3A2</u>	<u>LMOD1</u>	<u>PDPN</u>
<u>RBBP6</u>	<u>UGCG</u>	<u>HMCN1</u>	<u>C8orf4</u>	<u>ATP5D</u>	<u>PNP</u>	<u>SNHG12</u>	<u>TPI1</u>
<u>RELB</u>	<u>FTH1</u>	<u>MFAP5</u>	<u>ABCA1</u>	<u>ABCA9</u>	<u>TINAGL1</u>	<u>TRIB1</u>	<u>ARL6IP4</u>
<u>TNXB</u>	<u>PTP4A3</u>	<u>KITLG</u>	<u>F10</u>	<u>DBN1</u>	<u>GOLGA4</u>	<u>CAST</u>	<u>MIR155HG</u>
<u>HLA-DRB5</u>	<u>TALDO1</u>	<u>DCXR</u>	<u>PFDN5</u>	<u>LRRN4CL</u>	<u>CALU</u>	<u>OLFML2B</u>	<u>CFD</u>
<u>SLC3A2</u>	<u>PTRF</u>	<u>NDUFS5</u>	<u>SPATS2L</u>	<u>NUDT4</u>	<u>SAMHD1</u>	<u>LYZ</u>	<u>RORA</u>
<u>PLAGL1</u>	<u>PPP1R10</u>	<u>NEU1</u>	<u>CFI</u>	<u>WDR83OS</u>	<u>SGCE</u>	<u>EIF4G1</u>	<u>DUSP4</u>
<u>FAM126A</u>	<u>PTN</u>	<u>GUK1</u>	<u>ANTXR1</u>	<u>ACKR3</u>	<u>DBNDD2</u>	<u>CNN1</u>	<u>HIF1A</u>
<u>SFRP1</u>	<u>PTGDS</u>	<u>COL15A1</u>	<u>UGP2</u>	<u>CD82</u>	<u>FGF7</u>	<u>MGST3</u>	<u>PRR13</u>
<u>RPS19</u>	<u>NDUFB10</u>	<u>G3BP1</u>	<u>CAPN2</u>	<u>ARFGAP3</u>	<u>CD4</u>	<u>FNDC3B</u>	<u>UQCRI1</u>
<u>RPL22L1</u>	<u>ATP6V0E1</u>	<u>BRD2</u>	<u>FKBP1A</u>	<u>EIF3A</u>	<u>NFIL3</u>	<u>LGALS3BP</u>	<u>CIB1</u>
<u>NDUFV2</u>	<u>CLEC2B</u>	<u>CHN1</u>	<u>NDUFA13</u>	<u>VPS28</u>	<u>S100A6</u>	<u>ZEB2</u>	<u>CD34</u>
<u>MBNL2</u>	<u>GPC3</u>	<u>RRBP1</u>	<u>USMG5</u>	<u>DNAJA4</u>	<u>ANAPC16</u>	<u>LDHA</u>	<u>S100A11</u>
<u>SCPEP1</u>	<u>GGT5</u>	<u>COX5A</u>	<u>EIF3K</u>	<u>NGFRAP1</u>	<u>TCEB2</u>	<u>LINC00657</u>	<u>GDF15</u>
<u>KRT8</u>	<u>MARCKS</u>	<u>SELENBP1</u>	<u>GPCPD1</u>	<u>EDNRB</u>	<u>LXN</u>	<u>ABLIM1</u>	<u>NCL</u>
<u>UQCRB</u>	<u>MFAP2</u>	<u>IL1RL1</u>	<u>CHPF</u>	<u>RDH10</u>	<u>ADIRF</u>	<u>SPTAN1</u>	<u>ADAM12</u>
<u>EGFR</u>	<u>TNS1</u>	<u>TACC1</u>	<u>GPNMB</u>	<u>RGN</u>	<u>GRINA</u>	<u>SYNCRIP</u>	<u>MACF1</u>
<u>SLC7A5</u>	<u>C2orf40</u>	<u>LPL</u>	<u>CLEC3B</u>	<u>NDUFB7</u>	<u>TGFB1I1</u>	<u>COX6B1</u>	<u>VASN</u>
<u>PCOLCE</u>	<u>STAT3</u>	<u>CTSS</u>	<u>LEPR</u>	<u>DKK3</u>	<u>SFRP4</u>	<u>ITGA1</u>	<u>CXCL8</u>
<u>ATP5J</u>	<u>ADGRF5</u>	<u>COMP</u>	<u>MT1A</u>	<u>ROBO2</u>	<u>NME3</u>	<u>MEF2C</u>	<u>LSP1</u>
<u>CCL26</u>	<u>SCN7A</u>	<u>DKK1</u>	<u>RNASE1</u>	<u>SGCA</u>	<u>S100A10</u>	<u>OSR1</u>	<u>AURKAIP1</u>
<u>MXRA8</u>	<u>RSRP1</u>	<u>NPNT</u>	<u>ARL6IP5</u>	<u>PIEZO2</u>	<u>CHRD1</u>	<u>SLC16A7</u>	<u>SLC2A3</u>
<u>SYPL1</u>	<u>MT1X</u>	<u>HILPDA</u>	<u>TGFBR3</u>	<u>PSME2</u>	<u>CD302</u>	<u>MARCKSL1</u>	<u>TUBA1A</u>

<u>COMT</u>	<u>KCNMA1</u>	<u>CXCL2</u>	<u>TBX2</u>	<u>PODN</u>	<u>BCL3</u>	<u>NBL1</u>
<u>HGF</u>	<u>DDIT4</u>	<u>HOPX</u>	<u>NDFIP1</u>	<u>04-sept</u>	<u>THY1</u>	<u>CES1</u>
<u>CYBA</u>	<u>SFTPBP</u>	<u>ABHD5</u>	<u>TNFRSF1</u> <u>A</u>	<u>CSRPI</u>	<u>C7</u>	<u>ITGA8</u>
<u>RBM39</u>	<u>TYROBP</u>	<u>AKRIC1</u>	<u>SCARA5</u>	<u>IGFBP4</u>	<u>ATP6V1F</u>	<u>SH3BGR</u> <u>L</u>

2334

2335

\* Derived from(41).

2336

**Table S16, related to Fig.8. ACTA2<sup>+</sup> myofibroblast marker genes\*.**

<u><a href="#">FN1</a></u>	<u><a href="#">TFPI2</a></u>	<u><a href="#">FAP</a></u>	<u><a href="#">CD34</a></u>	<u><a href="#">MGST1</a></u>	<u><a href="#">SMPDL3A</a></u>	<u><a href="#">TNFRSF1A</a></u>	<u><a href="#">LPP</a></u>
<u><a href="#">LTBP2</a></u>	<u><a href="#">FGFR4</a></u>	<u><a href="#">CD302</a></u>	<u><a href="#">LGALS3</a></u>	<u><a href="#">SOD3</a></u>	<u><a href="#">CFH</a></u>	<u><a href="#">ATP13A3</a></u>	<u><a href="#">ID3</a></u>
<u><a href="#">LIMCH1</a></u>	<u><a href="#">SLC40A1</a></u>	<u><a href="#">CD248</a></u>	<u><a href="#">EFEMP1</a></u>	<u><a href="#">PMP22</a></u>	<u><a href="#">CPXM1</a></u>	<u><a href="#">PLN</a></u>	<u><a href="#">FHL1</a></u>
<u><a href="#">CDH11</a></u>	<u><a href="#">ASPN</a></u>	<u><a href="#">ARC</a></u>	<u><a href="#">CTGF</a></u>	<u><a href="#">ANTXR1</a></u>	<u><a href="#">SELENBP1</a></u>	<u><a href="#">MAFF</a></u>	<u><a href="#">SERPINA3</a></u>
<u><a href="#">ADIRF</a></u>	<u><a href="#">DNAJB1</a></u>	<u><a href="#">CD55</a></u>	<u><a href="#">SLC25A4</a></u>	<u><a href="#">NOLC1</a></u>	<u><a href="#">HNRNPF</a></u>	<u><a href="#">EIF4A1</a></u>	<u><a href="#">CILP</a></u>
<u><a href="#">PLA2G2A</a></u>	<u><a href="#">COL5A2</a></u>	<u><a href="#">CHD1</a></u>	<u><a href="#">NCL</a></u>	<u><a href="#">TCF12</a></u>	<u><a href="#">FAM162B</a></u>	<u><a href="#">ARL4D</a></u>	<u><a href="#">FIBIN</a></u>
<u><a href="#">A2M</a></u>	<u><a href="#">PALLD</a></u>	<u><a href="#">MDK</a></u>	<u><a href="#">MYH11</a></u>	<u><a href="#">ADGRD1</a></u>	<u><a href="#">IGFBP7</a></u>	<u><a href="#">MYOC</a></u>	<u><a href="#">FABP4</a></u>
<u><a href="#">MACF1</a></u>	<u><a href="#">EIF4A3</a></u>	<u><a href="#">GJA4</a></u>	<u><a href="#">NR4A2</a></u>	<u><a href="#">WDR43</a></u>	<u><a href="#">EZR</a></u>	<u><a href="#">EGR3</a></u>	<u><a href="#">C1R</a></u>
<u><a href="#">ITGBL1</a></u>	<u><a href="#">TCF21</a></u>	<u><a href="#">CALM1</a></u>	<u><a href="#">COL1A1</a></u>	<u><a href="#">NAMPT</a></u>	<u><a href="#">CLCF1</a></u>	<u><a href="#">RARRES1</a></u>	<u><a href="#">MAP1B</a></u>
<u><a href="#">CES1</a></u>	<u><a href="#">PLIN2</a></u>	<u><a href="#">EFHD1</a></u>	<u><a href="#">ESAM</a></u>	<u><a href="#">KCTD12</a></u>	<u><a href="#">MYL6</a></u>	<u><a href="#">PDK4</a></u>	<u><a href="#">C2orf40</a></u>
<u><a href="#">HAS1</a></u>	<u><a href="#">MT1M</a></u>	<u><a href="#">HMGNI</a></u>	<u><a href="#">NDNF</a></u>	<u><a href="#">PCBP1</a></u>	<u><a href="#">PDLIM5</a></u>	<u><a href="#">SFPQ</a></u>	<u><a href="#">KIAA1217</a></u>
<u><a href="#">MYC</a></u>	<u><a href="#">G0S2</a></u>	<u><a href="#">PTP4A1</a></u>	<u><a href="#">MMP19</a></u>	<u><a href="#">PRSS23</a></u>	<u><a href="#">SLC4A7</a></u>	<u><a href="#">PIK3R1</a></u>	<u><a href="#">HTRA1</a></u>
<u><a href="#">TM4SF1</a></u>	<u><a href="#">NPNT</a></u>	<u><a href="#">ITM2A</a></u>	<u><a href="#">RPL41</a></u>	<u><a href="#">ABLIM1</a></u>	<u><a href="#">MIR22HG</a></u>	<u><a href="#">SPTBN1</a></u>	<u><a href="#">SRGN</a></u>
<u><a href="#">MOXD1</a></u>	<u><a href="#">HSP90AB1</a></u>	<u><a href="#">FOSL1</a></u>	<u><a href="#">HNRNPAB</a></u>	<u><a href="#">FKBP4</a></u>	<u><a href="#">WISP2</a></u>	<u><a href="#">SEMA3C</a></u>	<u><a href="#">THBS1</a></u>
<u><a href="#">COL6A3</a></u>	<u><a href="#">TMEM119</a></u>	<u><a href="#">DNAJA1</a></u>	<u><a href="#">NT5E</a></u>	<u><a href="#">CXCL12</a></u>	<u><a href="#">CHMP1B</a></u>	<u><a href="#">AEBP1</a></u>	<u><a href="#">TGM2</a></u>
<u><a href="#">MAMDC2</a></u>	<u><a href="#">NR4A3</a></u>	<u><a href="#">BCAM</a></u>	<u><a href="#">WT1</a></u>	<u><a href="#">INPP4B</a></u>	<u><a href="#">CFB</a></u>	<u><a href="#">SRSF3</a></u>	<u><a href="#">SLC2A3</a></u>
<u><a href="#">ROBO2</a></u>	<u><a href="#">ANGPT1</a></u>	<u><a href="#">ENC1</a></u>	<u><a href="#">LMO4</a></u>	<u><a href="#">CLEC3B</a></u>	<u><a href="#">ACTG2</a></u>	<u><a href="#">UBC</a></u>	<u><a href="#">CEBPB</a></u>
<u><a href="#">ERRFI1</a></u>	<u><a href="#">SPINT2</a></u>	<u><a href="#">TPM2</a></u>	<u><a href="#">TNC</a></u>	<u><a href="#">PII6</a></u>	<u><a href="#">ADAMTS9</a></u>	<u><a href="#">UGP2</a></u>	<u><a href="#">SERPINA3.1</a></u>
<u><a href="#">COL8A1</a></u>	<u><a href="#">SLC38A5</a></u>	<u><a href="#">LSP1</a></u>	<u><a href="#">MTRNR2L12</a></u>	<u><a href="#">KRT8</a></u>	<u><a href="#">ZNF331</a></u>	<u><a href="#">PHLDA2</a></u>	<u><a href="#">MGP</a></u>
<u><a href="#">UGDH</a></u>	<u><a href="#">CTHRC1</a></u>	<u><a href="#">HMOX1</a></u>	<u><a href="#">ATF3</a></u>	<u><a href="#">MXRA8</a></u>	<u><a href="#">LGALS1</a></u>	<u><a href="#">LMOD1</a></u>	<u><a href="#">IFI6</a></u>
<u><a href="#">MFAP2</a></u>	<u><a href="#">SELK</a></u>	<u><a href="#">ISYNA1</a></u>	<u><a href="#">KLF9</a></u>	<u><a href="#">PFDN2</a></u>	<u><a href="#">CREB5</a></u>	<u><a href="#">CRISPLD2</a></u>	<u><a href="#">SERPINE1</a></u>
<u><a href="#">CCDC80</a></u>	<u><a href="#">PTGIS</a></u>	<u><a href="#">OSR1</a></u>	<u><a href="#">NOTCH3</a></u>	<u><a href="#">FLNC</a></u>	<u><a href="#">GABARAPL1</a></u>	<u><a href="#">LGALS3BP</a></u>	<u><a href="#">TXNIP</a></u>
<u><a href="#">MEDAG</a></u>	<u><a href="#">ADAMTS1</a></u>	<u><a href="#">NDRG1</a></u>	<u><a href="#">PLAU</a></u>	<u><a href="#">11-sept</a></u>	<u><a href="#">MEF2C</a></u>	<u><a href="#">PIM3</a></u>	<u><a href="#">CXCL1</a></u>
<u><a href="#">CDKN1A</a></u>	<u><a href="#">RGS5</a></u>	<u><a href="#">3-Mar</a></u>	<u><a href="#">PCOLCE2</a></u>	<u><a href="#">ZYX</a></u>	<u><a href="#">FAM46A</a></u>	<u><a href="#">IL32</a></u>	<u><a href="#">FHL2</a></u>
<u><a href="#">EMILIN1</a></u>	<u><a href="#">SFRP1</a></u>	<u><a href="#">NRP2</a></u>	<u><a href="#">SRSF2</a></u>	<u><a href="#">RABGEF1</a></u>	<u><a href="#">RANBP2</a></u>	<u><a href="#">ITGA5</a></u>	<u><a href="#">HIF1A</a></u>

<u>GPRC5A</u>	<u>SMOC2</u>	<u>ITGA2</u>	<u>MTHFD2</u>	<u>PPP1R12 A</u>	<u>ENO1</u>	<u>NUDT4</u>	<u>BGN</u>
<u>UAP1</u>	<u>DES</u>	<u>EPS8</u>	<u>ELL2</u>	<u>FIGF</u>	<u>YBX3</u>	<u>MT-CYB</u>	<u>FBN1</u>
<u>PLXDC2</u>	<u>LDHA</u>	<u>FKBP1A</u>	<u>FBLN5</u>	<u>OSTC</u>	<u>RP11- 14N7.2</u>	<u>NRIP1</u>	<u>PDPN</u>
<u>MT1A</u>	<u>DIO2</u>	<u>SEPP1</u>	<u>MMP2</u>	<u>JUNB</u>	<u>GNL3</u>	<u>ARID5B</u>	<u>THBD</u>
<u>PLEKH H2</u>	<u>NOP16</u>	<u>NDUFA4 L2</u>	<u>COL10A1</u>	<u>ITM2C</u>	<u>CCL11</u>	<u>S100A13</u>	<u>RGS16</u>
<u>QSOX1</u>	<u>CRIP1</u>	<u>HSD11B1</u>	<u>EGFL6</u>	<u>ENAH</u>	<u>HNRNPU</u>	<u>MMP14</u>	<u>BTG2</u>
<u>IGF2</u>	<u>TDO2</u>	<u>ETV1</u>	<u>GNG11</u>	<u>WDR1</u>	<u>UACA</u>	<u>HEYL</u>	<u>INHBA</u>
<u>C3</u>	<u>HIGD1B</u>	<u>PTP4A3</u>	<u>CTSB</u>	<u>YWHAG</u>	<u>INSIG1</u>	<u>EDNRA</u>	<u>RASD1</u>
<u>RHOB</u>	<u>LUM</u>	<u>RSPO3</u>	<u>LSAMP</u>	<u>ATP1A1</u>	<u>TUBB3</u>	<u>AKR1C1</u>	<u>CHRD1</u>
<u>RARRES 2</u>	<u>HSPH1</u>	<u>ELN</u>	<u>COL1A2</u>	<u>ACTA2</u>	<u>PLK2</u>	<u>TCF4</u>	<u>KLF2</u>
<u>GPC3</u>	<u>COL16A1</u>	<u>CIQTNF1</u>	<u>SPARC</u>	<u>TPT1</u>	<u>STMN1</u>	<u>TIMP3</u>	<u>C10orf10</u>
<u>SCN7A</u>	<u>DDX21</u>	<u>CNN2</u>	<u>LBH</u>	<u>TUBB2A</u>	<u>RSL1D1</u>	<u>CBLB</u>	<u>TSC22D3</u>
<u>DKK3</u>	<u>TUBB4B</u>	<u>SCARB2</u>	<u>LHFP</u>	<u>PA2G4</u>	<u>HSPB6</u>	<u>MINOS1</u>	<u>FGF7</u>
<u>ITGA8</u>	<u>SGK1</u>	<u>MFGE8</u>	<u>ZNF106</u>	<u>BTG3</u>	<u>ANGPTL4</u>	<u>FMO2</u>	<u>HSPB8</u>
<u>HSPD1</u>	<u>CDC42E P2</u>	<u>TAGLN2</u>	<u>ADGRF5</u>	<u>NPC2</u>	<u>XBP1</u>	<u>HSPA1A</u>	<u>TNFRSF1 2A</u>
<u>MT2A</u>	<u>CPE</u>	<u>PIIB</u>	<u>NAP1L1</u>	<u>LINC011 33</u>	<u>PTMA</u>	<u>DDX3X</u>	<u>MEG3</u>
<u>POSTN</u>	<u>KRT18</u>	<u>HSPA8</u>	<u>SCARA5</u>	<u>CADM3</u>	<u>SNRPB</u>	<u>TXN</u>	<u>EGR1</u>
<u>CD82</u>	<u>TSPAN13</u>	<u>COL5A1</u>	<u>VEGFA</u>	<u>DSTN</u>	<u>F2R</u>	<u>SOCS3</u>	<u>COL12A1</u>
<u>COMP</u>	<u>GDF10</u>	<u>F3</u>	<u>TSPAN8</u>	<u>DNTTIP2</u>	<u>ARL6IP5</u>	<u>FAT1</u>	<u>AC090498 .1</u>
<u>IGFBP6</u>	<u>HSP90AA 1</u>	<u>C16orf45</u>	<u>ZFAND5</u>	<u>ABL2</u>	<u>MLLT11</u>	<u>SPSB1</u>	<u>PTGDS</u>
<u>EIF1</u>	<u>NKD2</u>	<u>EIF5A</u>	<u>HES4</u>	<u>RPS27</u>	<u>TUBA1B</u>	<u>MT1G</u>	<u>LINC0015 2</u>
<u>NBL1</u>	<u>IFITM1</u>	<u>ID4</u>	<u>NXT1</u>	<u>FOSL2</u>	<u>HSPB1</u>	<u>VASN</u>	<u>FOSB</u>
<u>MAT2A</u>	<u>DST</u>	<u>CIQTNF7</u>	<u>TIPARP</u>	<u>BAZ1A</u>	<u>HSPA1B</u>	<u>CST3</u>	<u>ZFP36</u>
<u>FST</u>	<u>SLPI</u>	<u>PLPP1</u>	<u>LRRN4CL</u>	<u>SLC16A1</u>	<u>EMP2</u>	<u>IGF1</u>	<u>CFD</u>
<u>COX4I2</u>	<u>ACKR3</u>	<u>FAT4</u>	<u>FHL5</u>	<u>CIQTNF 3</u>	<u>RAB31</u>	<u>CYSTM1</u>	<u>CXCL2</u>
<u>HSPE1</u>	<u>ALDH1A 3</u>	<u>TUBA1C</u>	<u>GNPNAT1</u>	<u>NR2F1</u>	<u>SH3BP5</u>	<u>PIM1</u>	<u>IGFBP3</u>
<u>ENPP2</u>	<u>SNHG15</u>	<u>PTK7</u>	<u>ALDH2</u>	<u>MMP23B</u>	<u>PDLIM4</u>	<u>EPAS1</u>	<u>SOD2</u>
<u>BAG3</u>	<u>ROBO1</u>	<u>COL15A1</u>	<u>MFAP4</u>	<u>FMO3</u>	<u>HSPA9</u>	<u>HMGAI</u>	<u>PTGS2</u>

<u>LTBP1</u>	<u>BDKRB1</u>	<u>CYP7B1</u>	<u>DBNDD2</u>	<u>ADAMTS</u> <u>4</u>	<u>KLF3</u>	<u>CYR61</u>	<u>SFRP4</u>
<u>ATP1B3</u>	<u>AKAP12</u>	<u>STEAP4</u>	<u>PDGFRL</u>	<u>CEBPZ</u>	<u>EIF4E</u>	<u>MYO1B</u>	<u>CXCL3</u>
<u>CYCS</u>	<u>TNFRSF1</u> <u>9</u>	<u>SRSF7</u>	<u>ALDH1A1</u>	<u>KLF4</u>	<u>CSRNP1</u>	<u>IFI16</u>	<u>DPT</u>
<u>BMP5</u>	<u>MCAM</u>	<u>SORBS2</u>	<u>SH3PXD2</u> <u>A</u>	<u>EDNRB</u>	<u>ACTN4</u>	<u>MT1X</u>	<u>DCN</u>
<u>CTSL</u>	<u>CREM</u>	<u>NR4A1</u>	<u>TOB1</u>	<u>NPM1</u>	<u>LAMB1</u>	<u>RRBP1</u>	<u>CRABP2</u>
<u>GFPT2</u>	<u>COL3A1</u>	<u>EIF1B</u>	<u>ETF1</u>	<u>KDM6B</u>	<u>ISG15</u>	<u>MARCKS</u>	<u>GPX3</u>
<u>HMCN1</u>	<u>SNCG</u>	<u>SLC20A1</u>	<u>PHLDA1</u>	<u>SNU13</u>	<u>CSRP2</u>	<u>SRPX</u>	<u>SFRP2</u>
<u>MYL9</u>	<u>PNRC1</u>	<u>AMD1</u>	<u>RGS3</u>	<u>SLIT2</u>	<u>PDGFRB</u>	<u>TPM1</u>	<u>ADH1B</u>
<u>MFAP5</u>	<u>LAMA2</u>	<u>LITAF</u>	<u>APOLD1</u>	<u>TCP1</u>	<u>NREP</u>	<u>TAGLN</u>	<u>ADM</u>
<u>TINAGL</u> <u>1</u>	<u>GSN</u>	<u>TCEB1</u>	<u>UBA2</u>	<u>CRYAB</u>	<u>ZFP36L1</u>	<u>COL6A1</u>	<u>ICAM1</u>
<u>RGCC</u>	<u>EBF1</u>	<u>RAN</u>	<u>DKK1</u>	<u>NOP58</u>	<u>PLAUR</u>	<u>GPNMB</u>	<u>CH25H</u>
<u>SPON1</u>	<u>COL13A1</u>	<u>H3F3B</u>	<u>SH3D19</u>	<u>ACTB</u>	<u>TXNRD1</u>	<u>PPP1R15</u> <u>A</u>	<u>PPP1R14</u> <u>A</u>
<u>ACSL4</u>	<u>PIEZO2</u>	<u>MAOB</u>	<u>CNN1</u>	<u>CYP1B1</u>	<u>TMSB10</u>	<u>HILPDA</u>	<u>-</u>
<u>VCAN</u>	<u>PROCR</u>	<u>PMEPA1</u>	<u>NRP1</u>	<u>WNT2</u>	<u>SERTAD1</u>	<u>COL18A1</u>	<u>-</u>
<u>IFI27</u>	<u>MYH10</u>	<u>STOM</u>	<u>SFTA1P</u>	<u>MT1E</u>	<u>IGFBP2</u>	<u>CXCL8</u>	<u>-</u>

2338

2339 \* Derived from(41).

2340

**Table S17, related to Fig. 8. *PLIN2*<sup>+</sup> lipomyofibroblast marker genes\*.**

<u><i>CTSL</i></u>	<u><i>AOC3</i></u>	<u><i>ANGPT1</i></u>	<u><i>LARP4</i></u>	<u><i>METAP2</i></u>	<u><i>SARAF</i></u>	<u><i>ARF5</i></u>	<u><i>PLN</i></u>
<u><i>MT-CYB</i></u>	<u><i>EIF4A3</i></u>	<u><i>RABGEF1</i></u>	<u><i>KCTD20</i></u>	<u><i>NABP1</i></u>	<u><i>EMP3</i></u>	<u><i>MIR222HG</i></u>	<u><i>MINOS1</i></u>
<u><i>BGN</i></u>	<u><i>MGST1</i></u>	<u><i>PA2G4</i></u>	<u><i>ITGA8</i></u>	<u><i>NFIL3</i></u>	<u><i>ANAPC16</i></u>	<u><i>FAM180A</i></u>	<u><i>HIST1H4C</i></u>
<u><i>MYL9</i></u>	<u><i>DNAJC2</i></u>	<u><i>STK40</i></u>	<u><i>COX5B</i></u>	<u><i>C1S</i></u>	<u><i>PRRC2C</i></u>	<u><i>EIF3M</i></u>	<u><i>INPP4B</i></u>
<u><i>TAGLN</i></u>	<u><i>LIMA1</i></u>	<u><i>ZNF800</i></u>	<u><i>SLC43A3</i></u>	<u><i>OLFML3</i></u>	<u><i>ANXA6</i></u>	<u><i>MT1A</i></u>	<u><i>GJA4</i></u>
<u><i>ACTA2</i></u>	<u><i>MEG3</i></u>	<u><i>LINC00473</i></u>	<u><i>NRIP1</i></u>	<u><i>PHLDB1</i></u>	<u><i>RGN</i></u>	<u><i>NME3</i></u>	<u><i>ADAMTS9</i></u>
<u><i>UAP1</i></u>	<u><i>FBN1</i></u>	<u><i>IL1R1</i></u>	<u><i>THBS1</i></u>	<u><i>SRM</i></u>	<u><i>ARPC5</i></u>	<u><i>FGFR4</i></u>	<u><i>CNN3</i></u>
<u><i>ACSL4</i></u>	<u><i>NR4A3</i></u>	<u><i>CCND2</i></u>	<u><i>CD151</i></u>	<u><i>PRKCDBP</i></u>	<u><i>H3F3A</i></u>	<u><i>CSNK1A1</i></u>	<u><i>SI00A4</i></u>
<u><i>PLIN2</i></u>	<u><i>RNF149</i></u>	<u><i>DDX27</i></u>	<u><i>ESYT2</i></u>	<u><i>NNMT</i></u>	<u><i>PLSCR1</i></u>	<u><i>LGALS3BP</i></u>	<u><i>ADIRF</i></u>
<u><i>TMSB4X</i></u>	<u><i>TSC22D1</i></u>	<u><i>RSPO3</i></u>	<u><i>COLEC12</i></u>	<u><i>PTP4A3</i></u>	<u><i>ILF2</i></u>	<u><i>NEAT1</i></u>	<u><i>LGALS1</i></u>
<u><i>GFPT2</i></u>	<u><i>NDUFA4L2</i></u>	<u><i>FBL</i></u>	<u><i>BAG3</i></u>	<u><i>SRSF1</i></u>	<u><i>DAZAP2</i></u>	<u><i>ARL6IP4</i></u>	<u><i>CNN2</i></u>
<u><i>CRIP2</i></u>	<u><i>MT2A</i></u>	<u><i>SRGAP1</i></u>	<u><i>LMOD1</i></u>	<u><i>TCEB1</i></u>	<i>04-sept</i>	<u><i>CDKN1A</i></u>	<u><i>ALDH2</i></u>
<u><i>IGF2</i></u>	<u><i>CAV2</i></u>	<u><i>TMED5</i></u>	<u><i>SNED1</i></u>	<u><i>IVNS1ABP</i></u>	<u><i>CHCHD10</i></u>	<u><i>APOLD1</i></u>	<u><i>RUNX1</i></u>
<u><i>PPP1R14A</i></u>	<u><i>ARL4D</i></u>	<u><i>KDM6B</i></u>	<u><i>FAM162B</i></u>	<u><i>AKIRIN1</i></u>	<u><i>EDNRB</i></u>	<u><i>NFIA</i></u>	<u><i>LITAF</i></u>
<u><i>DKK3</i></u>	<u><i>SLC4A7</i></u>	<u><i>CLDN11</i></u>	<u><i>FGF2</i></u>	<u><i>CRIP1</i></u>	<u><i>ELL2</i></u>	<u><i>CHURC1</i></u>	<u><i>OGN</i></u>
<u><i>TPM2</i></u>	<u><i>F3</i></u>	<u><i>SH3BGR</i></u>	<u><i>PIM1</i></u>	<u><i>BICC1</i></u>	<u><i>H3F3B</i></u>	<u><i>RTN4</i></u>	<u><i>UGCG</i></u>
<u><i>NOP16</i></u>	<u><i>MYH9</i></u>	<u><i>GPNMB</i></u>	<u><i>PRDM2</i></u>	<u><i>SEMA3B</i></u>	<u><i>TGIF1</i></u>	<u><i>TCF21</i></u>	<u><i>HMOX1</i></u>
<u><i>EIF1B</i></u>	<u><i>CSRP1</i></u>	<u><i>SAT1</i></u>	<u><i>COX6A1</i></u>	<u><i>MAMDC2</i></u>	<u><i>ASAHI</i></u>	<u><i>SOD3</i></u>	<u><i>LTBP1</i></u>
<u><i>GPRC5A</i></u>	<u><i>C1R</i></u>	<u><i>FN1</i></u>	<u><i>FRZB</i></u>	<u><i>ADM</i></u>	<u><i>CTHRC1</i></u>	<u><i>SH3PXD2B</i></u>	<u><i>MFGE8</i></u>
<u><i>CXCL12</i></u>	<u><i>PNO1</i></u>	<u><i>LRRC59</i></u>	<u><i>TIPARP</i></u>	<u><i>INTS6</i></u>	<u><i>CES1</i></u>	<u><i>NUPR1</i></u>	<u><i>SLPI</i></u>
<u><i>MT-ATP8</i></u>	<u><i>SRSF2</i></u>	<u><i>EIF5A</i></u>	<u><i>B2M</i></u>	<u><i>CREM</i></u>	<u><i>CTSF</i></u>	<u><i>FIS1</i></u>	<u><i>ETS2</i></u>
<u><i>FST</i></u>	<u><i>THBS2</i></u>	<u><i>PTP4A1</i></u>	<u><i>PXDC1</i></u>	<u><i>CFD</i></u>	<u><i>PALLD</i></u>	<u><i>COX7C</i></u>	<u><i>CLEC3B</i></u>
<u><i>DDX21</i></u>	<u><i>BDKRB2</i></u>	<u><i>ASPN</i></u>	<u><i>DBNDD2</i></u>	<u><i>LURAP1L</i></u>	<u><i>RNASEK</i></u>	<u><i>JMJD1C</i></u>	<u><i>SRGN</i></u>
<i>3-Mar</i>	<u><i>GNPNAT1</i></u>	<u><i>MCL1</i></u>	<u><i>MTIX</i></u>	<u><i>MYL12A</i></u>	<u><i>GCLM</i></u>	<u><i>TMEM47</i></u>	<u><i>PIK3R1</i></u>
<u><i>MT-CO2</i></u>	<u><i>FLNA</i></u>	<u><i>PLTP</i></u>	<u><i>EIF1AX</i></u>	<u><i>CYCS</i></u>	<u><i>PTMS</i></u>	<u><i>CHMP1B</i></u>	<u><i>HSPA5</i></u>
<u><i>ITM2A</i></u>	<u><i>ATP1B3</i></u>	<u><i>C1orf21</i></u>	<u><i>WTAP</i></u>	<u><i>TWISTNB</i></u>	<u><i>SLC16A7</i></u>	<u><i>FCGRT</i></u>	<u><i>JUND</i></u>
<u><i>SPSB1</i></u>	<u><i>PIM3</i></u>	<u><i>VASH2</i></u>	<u><i>TWIST2</i></u>	<u><i>GABARAPL1</i></u>	<u><i>RPS29</i></u>	<u><i>LPP</i></u>	<u><i>TFPI2</i></u>
<u><i>NCL</i></u>	<u><i>BRIX1</i></u>	<u><i>HLA-C</i></u>	<u><i>TSPAN8</i></u>	<u><i>EIF4E</i></u>	<u><i>SPAG9</i></u>	<u><i>SRSF3</i></u>	<u><i>HSPB8</i></u>
<u><i>DSTN</i></u>	<u><i>HSPD1</i></u>	<u><i>FAM126A</i></u>	<u><i>TXNIP</i></u>	<u><i>MEF2C</i></u>	<u><i>TFRC</i></u>	<u><i>GJA1</i></u>	<u><i>GPC3</i></u>

<u>HNRNPAB</u>	<u>SERPINF1</u>	<u>ALDH1A3</u>	<u>EIF3A</u>	<u>TCP1</u>	<u>RAN</u>	<u>HSPB6</u>	<u>S100A13</u>
<u>MYLK</u>	<u>UBC</u>	<u>NR2F2</u>	<u>TUBB2B</u>	<u>ABLIM1</u>	<u>TIMP3</u>	<u>HSPA2</u>	<u>IFITM1</u>
<u>ERRF1</u>	<u>SFPO</u>	<u>EDIL3</u>	<u>C2orf40</u>	<u>G3BP1</u>	<u>TGM2</u>	<u>TRIB1</u>	<u>CSRP2</u>
<u>IGFBP7</u>	<u>HNRNPF</u>	<u>DKC1</u>	<u>BZW2</u>	<u>CHN1</u>	<u>EPAS1</u>	<u>PEA15</u>	<u>TM4SF1</u>
<u>MEDAG</u>	<u>NDUFA4</u>	<u>SOD2</u>	<u>ABCA9</u>	<u>PPP1R12A</u>	<u>PDLIM7</u>	<u>PLAT</u>	<u>ARID5B</u>
<u>MT-CO1</u>	<u>ZFP36L2</u>	<u>FGFR1</u>	<u>EFEMP1</u>	<u>TUBA4A</u>	<u>EHD2</u>	<u>RPS26</u>	<u>CH25H</u>
<u>HSP90AB1</u>	<u>COX4I2</u>	<u>DAB2</u>	<u>BCCIP</u>	<u>TGFBR3</u>	<u>SPHK1</u>	<u>MACF1</u>	<u>HAS2</u>
<u>CYP1B1</u>	<u>PAMR1</u>	<u>SLC25A33</u>	<u>PCOLCE</u>	<u>H2AFJ</u>	<u>SNHG12</u>	<u>NREP</u>	<u>DUSP1</u>
<u>FGF7</u>	<u>ARHGDI B</u>	<u>NIP7</u>	<u>SRSF5</u>	<u>PEBP1</u>	<u>NEDD9</u>	<u>MFAP5</u>	<u>HOPX</u>
<u>PDLIM4</u>	<u>SRPX</u>	<u>CTGF</u>	<u>ENO1</u>	<u>HEYL</u>	<u>CTSB</u>	<u>MT1M</u>	<u>PTGDS</u>
<u>FKBP1A</u>	<u>FOSL1</u>	<u>PNRC1</u>	<u>EGR1</u>	<u>MT-ND6</u>	<u>LAMB1</u>	<u>COX7A2</u>	<u>KLF2</u>
<u>MYC</u>	<u>MGST3</u>	<u>C7</u>	<u>TRMT10C</u>	<u>REXO2</u>	<u>RP11-14N7.2</u>	<u>MSRB3</u>	<u>CXCL1</u>
<u>EIF1</u>	<u>TUBB2A</u>	<u>BIN1</u>	<u>SVEP1</u>	<u>ADD3</u>	<u>GSN</u>	<u>PTX3</u>	<u>PDGFRA</u>
<u>MT-ND4L</u>	<u>COL4A1</u>	<u>PAICS</u>	<u>HNRNPD L</u>	<u>MOXD1</u>	<u>EDF1</u>	<u>LRP1</u>	<u>BTG1</u>
<u>AC090498.1</u>	<u>MESDC1</u>	<u>PTGIS</u>	<u>PPP3CA</u>	<u>CLCF1</u>	<u>GLT8D2</u>	<u>NDUFB7</u>	<u>COL6A2</u>
<u>NOP58</u>	<u>DCAF13</u>	<u>EGFR</u>	<u>BCAM</u>	<u>ARPC3</u>	<u>COMP</u>	<u>S100A16</u>	<u>REL</u>
<u>VEGFA</u>	<u>IGF1</u>	<u>NAMPT</u>	<u>FUS</u>	<u>TNFAIP6</u>	<u>ADGRF5</u>	<u>PTN</u>	<u>ELN</u>
<u>SRSF7</u>	<u>NT5E</u>	<u>TUBB6</u>	<u>C10orf10</u>	<u>SDCBP</u>	<u>CCNL1</u>	<u>TCEAL4</u>	<u>NR4A2</u>
<u>WT1</u>	<u>PTRH2</u>	<u>CYBRD1</u>	<u>EXOSC4</u>	<u>TGFB1I1</u>	<u>HMG2</u>	<u>RRAD</u>	<u>IGFBP2</u>
<u>CALD1</u>	<u>PLBD1</u>	<u>TXNRD1</u>	<u>TXN</u>	<u>BAIAP2</u>	<u>RASL12</u>	<u>IGSF10</u>	<u>S100A10</u>
<u>BTG3</u>	<u>CD82</u>	<u>B4GALT1</u>	<u>TUBB3</u>	<u>PLEKHH2</u>	<u>SORBS2</u>	<u>TUBA1B</u>	<u>FBLN2</u>
<u>MYL6</u>	<u>SH3BP5</u>	<u>CPXM2</u>	<u>SERTAD1</u>	<u>VAMP8</u>	<u>STRAP</u>	<u>MT-ND3</u>	<u>CRABP2</u>
<u>C16orf45</u>	<u>C16orf89</u>	<u>NOTCH3</u>	<u>TPBG</u>	<u>ISYNA1</u>	<u>TIMP2</u>	<u>C1QTNF3</u>	<u>HSPA1B</u>
<u>PDGFRL</u>	<u>HNRNPU</u>	<u>EMILIN2</u>	<u>CCDC109 B</u>	<u>NEGR1</u>	<u>TGFBI</u>	<u>UQCR10</u>	<u>PLK2</u>
<u>LSP1</u>	<u>CYP26B1</u>	<u>GPX3</u>	<u>ABHD5</u>	<u>PCBP1</u>	<u>TNS1</u>	<u>DDX24</u>	<u>ARC</u>
<u>EGFL6</u>	<u>NFE2L2</u>	<u>TNXB</u>	<u>INPP1</u>	<u>STAT3</u>	<u>TMEM204</u>	<u>C9orf16</u>	<u>SFRP2</u>
<u>ATP13A3</u>	<u>XBP1</u>	<u>KRT18</u>	<u>RANBP2</u>	<u>INSIG1</u>	<u>F2R</u>	<u>PDGFRB</u>	<u>HSPA1A</u>
<u>PLAU</u>	<u>KLF3</u>	<u>TINAGL1</u>	<u>PLPP3</u>	<u>IPO7</u>	<u>CTSD</u>	<u>SLC39A14</u>	<u>QSOX1</u>
<u>CCDC80</u>	<u>MYH11</u>	<u>DES</u>	<u>RPF2</u>	<u>CREB5</u>	<u>BRD2</u>	<u>ACTG1</u>	<u>COL14A1</u>
<u>ZFP36L1</u>	<u>FSTL1</u>	<u>POSTN</u>	<u>RBM25</u>	<u>TBX2</u>	<u>EIF3K</u>	<u>JUNB</u>	<u>GADD45 B</u>



<u>HSPA8</u>	<u>SNU13</u>	<u>ITGBL1</u>	<u>SGCA</u>	<u>CCDC47</u>	<u>ZC3H15</u>	<u>STEAP1</u>	<u>HIGD1B</u>
<u>MAT2A</u>	<u>OSR1</u>	<u>SYNCRIP</u>	<u>OSMR</u>	<u>CTSH</u>	<u>SLC3A2</u>	<u>HLA-DRB1</u>	<u>ID2</u>
<u>CHD1</u>	<u>BZW1</u>	<u>TOP1</u>	<u>PROS1</u>	<u>MIDN</u>	<u>KRT8</u>	<u>PSME1</u>	<u>CXCL3</u>
<u>CEBPZ</u>	<u>CPXM1</u>	<u>PLS3</u>	<u>ST3GAL1</u>	<u>SERTAD2</u>	<u>COX6B1</u>	<u>SCN7A</u>	<u>RGS2</u>
<u>PPDPF</u>	<u>STK17A</u>	<u>POLR1C</u>	<u>HNRNPA0</u>	<u>SNRPB</u>	<u>DDR2</u>	<u>C12orf57</u>	<u>NBL1</u>
<u>NPM1</u>	<u>TNFRSF1A</u>	<u>SLC40A1</u>	<u>TPT1</u>	<u>UGP2</u>	<u>C8orf4</u>	<u>ANK2</u>	<u>CXCL2</u>
<u>ATP5G2</u>	<u>GRPEL1</u>	<u>ABL1</u>	<u>CILP</u>	<u>FAM46A</u>	<u>CFL1</u>	<u>ENAH</u>	<u>RGCC</u>
<u>C3</u>	<u>SEPW1</u>	<u>CD34</u>	<u>GABARAP</u>	<u>FABP5</u>	<u>PRRX1</u>	<u>RARRES1</u>	<u>RHOB</u>
<u>EZR</u>	<u>METRNL</u>	<u>TOMM5</u>	<u>TFAM</u>	<u>ACTN1</u>	<u>UBE2N</u>	<u>ANKRD28</u>	<u>EMP1</u>
<u>AMD1</u>	<u>RFK</u>	<u>SCARA5</u>	<u>DDX3Y</u>	<u>CDH11</u>	<u>RPL22L1</u>	<u>HIF1A</u>	<u>FABP4</u>
<u>LBH</u>	<u>KLF4</u>	<u>TNC</u>	<u>ABCA8</u>	<u>TMEM176B</u>	<u>HLA-DPB1</u>	<u>TSKU</u>	<u>ATF3</u>
<u>NXT1</u>	<u>EDNRA</u>	<u>UCK2</u>	<u>RBM39</u>	<u>COX4I1</u>	<u>PDE5A</u>	<u>TLN1</u>	<u>THBD</u>
<u>CHRDL1</u>	<u>ABL2</u>	<u>IGFBP4</u>	<u>SLC16A1</u>	<u>RCAN2</u>	<u>MYL12B</u>	<u>SMOC2</u>	<u>CTSK</u>
<u>LTBP2</u>	<u>EBF2</u>	<u>EIF2S1</u>	<u>H2AFX</u>	<u>ADAMTS16</u>	<u>TSC22D3</u>	<u>GPM6B</u>	<u>G0S2</u>
<u>BDKRB1</u>	<u>NOP56</u>	<u>FBLN1</u>	<u>IGFBP6</u>	<u>SLC19A2</u>	<u>PARK7</u>	<u>COL15A1</u>	<u>PRG4</u>
<u>LRRN4CL</u>	<u>COL8A1</u>	<u>SLC20A1</u>	<u>SOAT1</u>	<u>HLA-DRA</u>	<u>HNRNP H1</u>	<u>FERMT2</u>	<u>SGK1</u>
<u>ETF1</u>	<u>MPZL1</u>	<u>TSPAN3</u>	<u>CYB5R3</u>	<u>MARCKSL1</u>	<u>ATPIF1</u>	<u>PLXDC2</u>	<u>FHL2</u>
<u>CAV1</u>	<u>COTL1</u>	<u>LIMCH1</u>	<u>SEMA6A</u>	<u>HIPK3</u>	<u>ABI3BP</u>	<u>SNAI2</u>	<u>APOE</u>
<u>WDR43</u>	<u>RGS5</u>	<u>SNRPD1</u>	<u>HMGN3</u>	<u>MYH10</u>	<u>TGFBR2</u>	<u>RAB13</u>	<u>BMP5</u>
<u>CBLB</u>	<u>HSP90AA1</u>	<u>CALM1</u>	<u>HSPA9</u>	<u>HAS1</u>	<u>SPCS1</u>	<u>HCFC1R1</u>	<u>NR4A1</u>
<u>IFI16</u>	<u>NIFK</u>	<u>GTPBP4</u>	<u>SYNGR2</u>	<u>CD4</u>	<u>GUCY1A3</u>	<u>MCAM</u>	<u>NFKBIA</u>
<u>ACKR3</u>	<u>CIRBP</u>	<u>DNTTIP2</u>	<u>TAF1D</u>	<u>PLA2G2A</u>	<u>RBBP6</u>	<u>ESAM</u>	<u>JUN</u>
<u>LDHA</u>	<u>ARPC5L</u>	<u>GLIS3</u>	<u>SPARC</u>	<u>FLNB</u>	<u>COX7A1</u>	<u>TACC1</u>	<u>CTSC</u>
<u>EGR3</u>	<u>BAZ1A</u>	<u>DDX5</u>	<u>EIF5</u>	<u>PITPNB</u>	<u>IL33</u>	<u>MRC2</u>	<u>GEM</u>
<u>KLF9</u>	<u>SERBP1</u>	<u>CFI</u>	<u>CCT2</u>	<u>FOSB</u>	<u>WDR83OS</u>	<u>MSN</u>	<u>PTGS2</u>
<u>ITGA1</u>	<u>A2M</u>	<u>PERP</u>	<u>HMGAI</u>	<u>RDH10</u>	<u>ATP5D</u>	<u>NDUFB10</u>	<u>CFB</u>
<u>PLAUR</u>	<u>TSHZ2</u>	<u>EIF3J</u>	<u>CRIM1</u>	<u>ACTN4</u>	<u>PODN</u>	<u>TMEM70</u>	<u>C11orf96</u>
<u>RPL41</u>	<u>TUBB4B</u>	<u>GSPT1</u>	<u>NME1</u>	<u>APP</u>	<u>PAG1</u>	<u>WFDC1</u>	<u>CNN1</u>
<u>ATP1A1</u>	<u>TUBA1C</u>	<u>STEAP2</u>	<u>PNPLA8</u>	<u>COX8A</u>	<u>SPINT2</u>	<u>ILK</u>	<u>TNFAIP3</u>
<u>CALM2</u>	<u>CD248</u>	<u>NAA50</u>	<u>EIF5B</u>	<u>VAT1</u>	<u>VIMP</u>	<u>NEXN</u>	<u>VCAN</u>

<u>DCN</u>	<u>DNAJB1</u>	<u>IL6ST</u>	<u>USP36</u>	<u>EIF4A1</u>	<u>ACTG2</u>	<u>HMGNI</u>	<u>ADAMTS</u> <u>4</u>
<u>SFRP1</u>	<u>COL4A2</u>	<u>FAM198</u> <u>B</u>	<u>SPTSSA</u>	<u>UOCRB</u>	<u>SOSTM1</u>	<u>LXN</u>	<u>LMCD1</u>
<u>GNL3</u>	<u>TMEM17</u> <u>6A</u>	<u>RIOK1</u>	<u>VASN</u>	<u>MT-ND2</u>	<u>HTRA3</u>	<u>MIR22H</u> <u>G</u>	<u>SERPIN</u> <u>A3</u>
<u>RSL1D1</u>	<u>MLLT11</u>	<u>TRIO</u>	<u>UOQR11</u>	<u>SF1</u>	<u>TRAPPC</u> <u>1</u>	<u>LMNA</u>	<u>WISP2</u>
<u>YWHAG</u>	<u>MT-ND1</u>	<u>NUFIP2</u>	<u>ELOVL5</u>	<u>KPNA2</u>	<u>SNX9</u>	<u>TNFAIP2</u>	<u>IFI27</u>
<u>PFDN2</u>	<u>CPZ</u>	<u>ANGPTL</u> <u>4</u>	<u>DUSP6</u>	<u>CDC42EP</u> <u>2</u>	<u>GNG11</u>	<u>GAS7</u>	<u>COL3A1</u>
<u>ZNF593</u>	<u>SEMA3C</u>	<u>HSPH1</u>	<u>TNFRSF1</u> <u>2A</u>	<u>WWTR1</u>	<u>HLA-B</u>	<u>SOCS3</u>	
<u>UGDH</u>	<u>RBMS1</u>	<u>OAF</u>	<u>ANXA1</u>	<u>ROBO2</u>	<u>FOSL2</u>	<u>MAFF</u>	
<u>MT-CO3</u>	<u>CD55</u>	<u>TXLNG</u>	<u>DDX3X</u>	<u>AKAP12</u>	<u>GUCY1B</u> <u>3</u>	<u>CCDC71</u> <u>L</u>	
<u>ADAMTS1</u> <u>5</u>	<u>MT-ND5</u>	<u>SELM</u>	<u>SELK</u>	<u>LPL</u>	<u>ZFAS1</u>	<u>PDK4</u>	
<u>NOLC1</u>	<u>HRH1</u>	<u>MRT04</u>	<u>RERG</u>	<u>CTNNAL1</u>	<u>NPNT</u>	<u>MALAT1</u>	
<u>DNAJA1</u>	<u>ITGA5</u>	<u>TPM1</u>	<u>DCLK1</u>	<u>CD9</u>	<u>PDPN</u>	<u>HSPE1</u>	
<u>MTRNR2L</u> <u>12</u>	<u>MT1G</u>	<u>CXCL8</u>	<u>DKK1</u>	<u>RGS16</u>	<u>CCL2</u>	<u>AKR1C1</u>	

2342

2343 \* Derived from(41).

2344

2345

2346 **Table S18, related to Suppl. Fig. 8. Overview of Non-GLP Study CRL 20229915 performed in**  
2347 **cynomolgus monkeys with ALE.F02.**

<b><u>Study type and duration of dosing</u></b>	<b><u>Species, origin, number of animals</u></b>	<b><u>Animal ID</u></b>	<b><u>Doses (mg/kg/day)</u></b>	<b><u>Administration</u></b>
<b><u>Single dose, 42 days</u></b>	<b><u>Cynomolgus monkey (Vietnam)</u></b> <b><u>1 male/group</u></b>	<b><u>2001</u></b>	<b><u>0.3mg/kg</u></b>	<b><u>IV bolus</u></b>
		<b><u>2002</u></b>	<b><u>3mg/kg</u></b>	<b><u>IV bolus</u></b>
		<b><u>2003</u></b>	<b><u>15mg/kg</u></b>	<b><u>IV bolus</u></b>
<b><u>Repeat dose, 28 days, 4 doses applied weekly</u></b>	<b><u>Cynomolgus monkey (Vietnam)</u></b> <b><u>2 males/group</u></b>	<b><u>2004</u></b>	<b><u>60mg/kg</u></b>	<b><u>IV infusion (30 min)</u></b>
		<b><u>2005</u></b>		
		<b><u>2006</u></b> <b><u>2007</u></b>	<b><u>150mg/kg</u></b>	<b><u>IV infusion (30 min)</u></b>

2348  
2349  
2350

2351

2352

2353 **The following Excel files are available online:**

2354

2355 **Data file S1. Raw data from figures.**

2356 **Data file S2, related to Figure 6. CLDN1 interaction partners identified by mass spectrometry in**

2357 **anti-CLDN1 mAb- or Control mAb-treated Huh7 cells.**

2358

2359